This is a non-peer reviewed preprint submitted to Science of the Total Environment.

Graphical Abstract

Apportioning sources of chemicals of emerging concern along an urban river with inverse modelling

Kajetan Chrapkiewicz, Alex G. Lipp, Leon P. Barron, Richard Barnes, Gareth G. Roberts

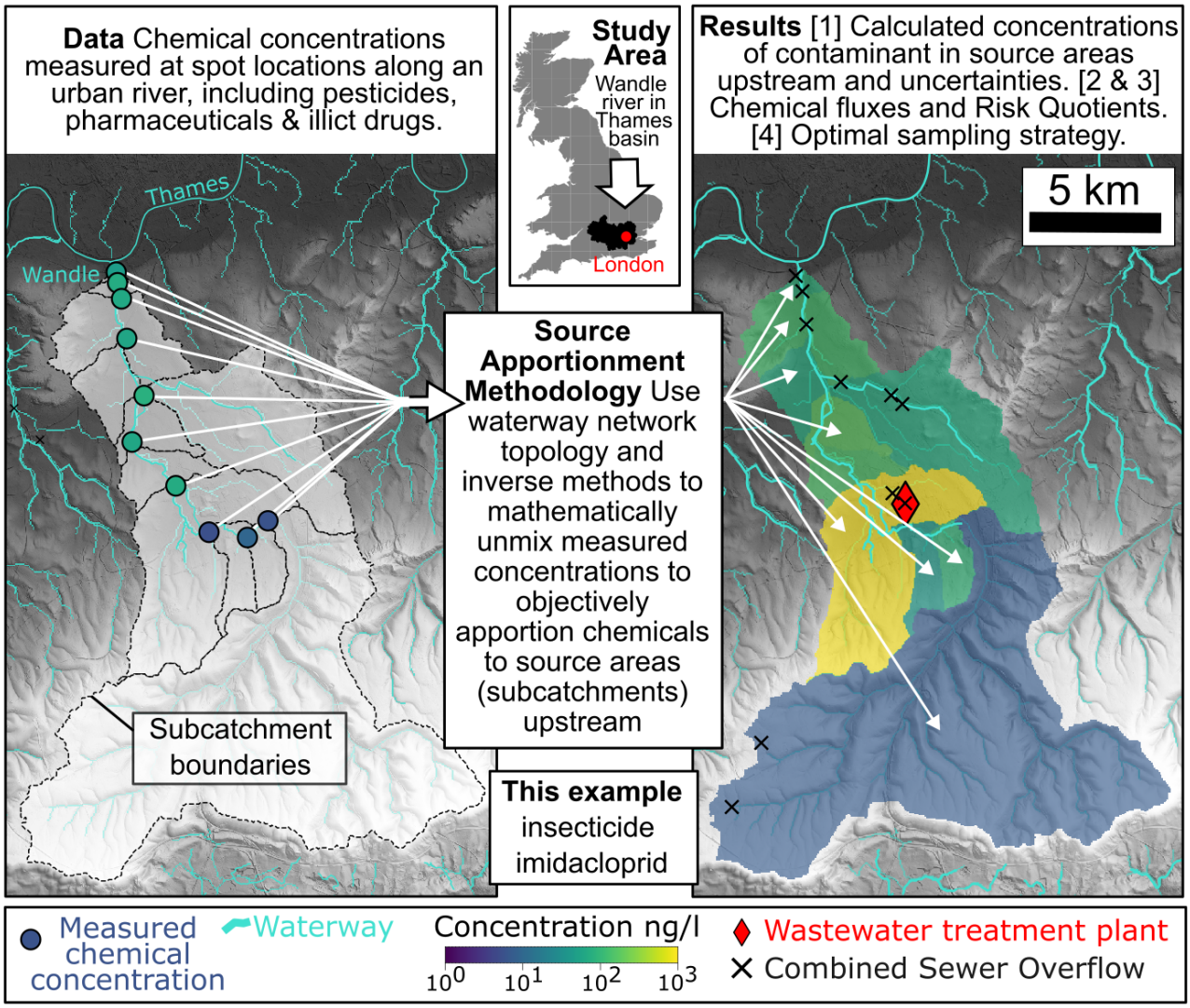

Highlights

Apportioning sources of chemicals of emerging concern along an urban river with inverse modelling

Kajetan Chrapkiewicz, Alex G. Lipp, Leon P. Barron, Richard Barnes, Gareth G. Roberts

- Sources of 13 chemicals are apportioned to treated and untreated wastewater effluent.
- Use of inverse methods to identify locations and magnitudes of sources is demonstrated.
- Waterway topology is combined with downstream contaminant concentrations to identify sources.
- Illicit drugs and salicylic acid have multiple sources from untreated wastewater.
- Highest risk quotients are associated with subcatchment with treatment facility.
- Source apportionment could be improved by sampling strategies guided by waterway topology.

Apportioning sources of chemicals of emerging concern along an urban river with inverse modelling

Kajetan Chrapkiewicz[a,*], Alex G. Lipp[b], Leon P. Barron[c], Richard Barnes[d], Gareth G. Roberts[a,*]

[a]*Department of Earth Science and Engineering, Imperial College London, South Kensington Campus, London, SW7 2AZ, UK*
[b]*Merton College, University of Oxford, Merton Street, Oxford, OX1 4JD, Oxfordshire, UK*
[c]*MRC Centre for Environment and Health, Environment Research Group, School of Public Health, Imperial College London, Wood Lane, London, W12 0BZ, UK*
[d]*Lawrence Berkeley National Laboratory, Wang Hall, Berkeley, CA 94720, USA*

Abstract

Concentrations of chemicals in river water provide crucial information for assessing environmental exposure to fertilisers and insecticides, heavy metals, illicit drugs, pathogens, pharmaceuticals, plastics and perfluorinated substances among others. However, using concentrations measured along waterways to identify sources of contaminants and predict their fate is complicated by downstream mixing. In this study, spot measurements of ecotoxicologically relevant chemicals collected along the Wandle, a rare urban chalk stream that flows into south London, UK, are combined with drainage network topology to objectively calculate locations and concentrations of contaminant sources using an inverse modelling approach. Mixing is assumed to be conservative, and the location of sources and their concentrations are treated as unknowns to be identified. Calculated source concentrations of thirteen chemicals, which range from below detection limit (a few ng/l) up to 1 μg/l, are used to predict concentrations of chemicals downstream. Contaminant fluxes are estimated by combining results with flow gauge measurements. Predicted concentrations and estimates of *probable no-effect* values indicate that chemical risk quotients are *high* for insecticides imidacloprid and acetamiprid, and above *negligible* for the pharmaceutical diclofenac among others. Principal component analysis revealed signatures of two distinct chemical mixtures. First, pharmaceuticals and insecticides were associated with a subcatchment containing a known point source of treated wastewater—the Beddington wastewater treatment plant. Second, illicit drugs and salicylic acid are associated with multiple sources, interpreted as markers of input from untreated sewage including CSOs, misconnections, runoff and direct disposal throughout the catchment. Finally, a simple algorithmic approach that incorporates network topology is developed to design sampling campaigns to improve resolution of source apportionment. Inverse modelling of contaminant measurements could provide objective means to apportion sources in waterways from spot samples in catchments on a large scale.

Keywords: pharmaceutical and illicit drugs, contaminants of emerging concern, water pollution, inverse modelling, mixing, source apportionment, Thames drainage basin

*Corresponding Author
Email addresses: k.chrapkiewicz17@imperial.ac.uk (Kajetan Chrapkiewicz), gareth.roberts@imperial.ac.uk (Gareth G. Roberts)

1. Introduction

Central to effective management of chemical contaminants in waterways (e.g. fertilisers, heavy metals, illicit drugs, pathogens, perfluorinated substances, pharmaceuticals and plastics) is identifying their upstream sources and predicting their effects downstream. However, rivers efficiently mix material they carry downstream, which provides both an opportunity and concomitant challenges.

The opportunity arises because the composition of a few water samples extracted along waterways provide data to efficiently characterise potentially large and diverse environments upstream (e.g. Weltje, 1997; Lipp et al., 2020, 2021; Carraro et al., 2020). To take advantage of this opportunity, two challenges must be addressed. The first challenge is measuring concentrations of the diverse suite of contaminants, which may also have ecotoxicological relevance. Fortunately, new high-throughput direct-injection liquid chromatography mass spectrometry methods have demonstrated that hundreds of such chemicals, including contaminants of emerging concern, can now be measured in water samples extracted from natural waterways (Egli et al., 2023). The demonstrated rapidity of such methods means that it is now practical to determine concentrations of hundreds of chemicals from thousands of spot samples annually.

The second challenge concerns how to interpret the observations of concentrations collected along a waterway. From a theoretical perspective, the challenge is understanding how measured concentrations can be used to identify locations and concentrations of sources upstream. Multiple, known and unknown, point or diffuse, sources, and mixing of material as it is carried downstream have to be disentangled from the spot measurements. In this paper, inverse methodologies are used to objectively disentangle ('unmix') spot measurements of contaminant concentrations for source apportionment. A similar strategy has been used to establish sources of environmental-DNA in water samples and geologically relevant elements in fluvial sediments (Carraro et al., 2020; Lipp et al., 2020, 2021). As far as we are aware, it has not been used to identify sources of contaminants arising from urban consumption, which may have multiple influx routes. Once such estimates exist it is straightforward to estimate concentrations of contaminants throughout waterway networks, and to generate quantitative estimates of chemical fluxes and associated risks, potentially even at larger scales.

This approach is demonstrated in a case study of the Wandle catchment, a tributary of the Thames in south London (Fig. 1; also see Fig. S1 of the Supporting Information). The Wandle is a polluted urban river, and one of only a handful of chalk streams globally. Its network topology is nearly all natural, determined principally by topography (Fig. 1). In 2022, two monitored reaches of the Wandle, upstream at Carshalton and downstream of Croydon, were given 'poor' and 'moderate' ecological status, respectively[1]. For the downstream reach, of the 16 proposed 'reasons for not achieving good ecological status', eight were related to pollution. Wastewater and urban runoff have been suggested by the Environment Agency (the environmental regulatory agency for England) as the principal sources of contaminants in the river. The Beddington wastewater treatment plant (WWTP) discharges into the Wandle (Fig. 1c).

Egli et al. (2023) measured a suite of contaminant concentrations across London, including the River Wandle in 2019–2021, which have been used in this study (see Fig. 1 & S2). Phar-

[1] `https://environment.data.gov.uk/catchment-planning/OperationalCatchment/3514`

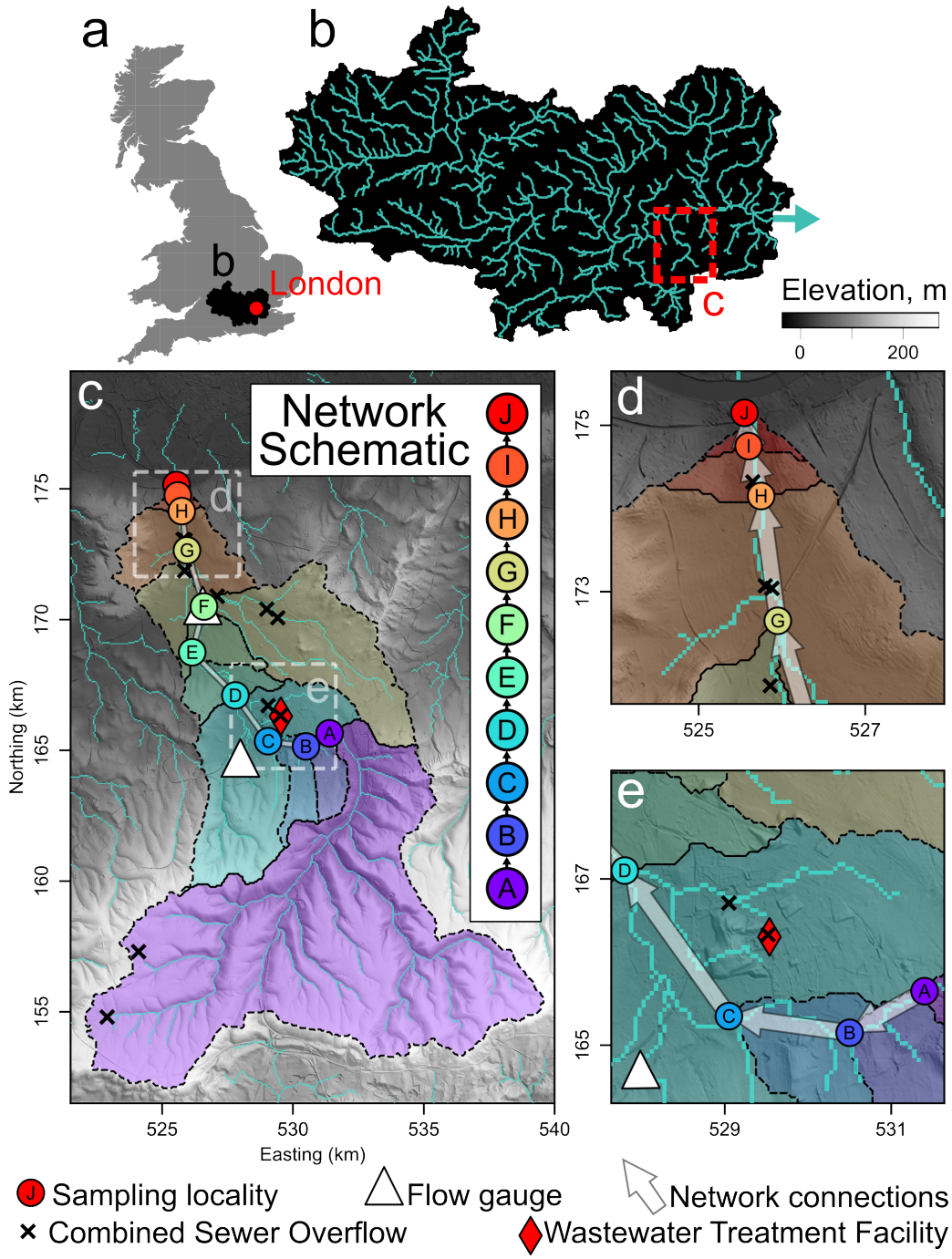

Figure 1: **Study area.** (a–b) Study area (red dashed polygon) with respect to the UK, London and Thames basin (b); rivers and basin outline are from Hydrosheds. (c) Wandle catchment. Topography from 10-m resolution LIDAR digital elevation model (UK-CEH) used for visualisation. Turquoise lines = rivers with upstream area > 1 km^2. Circles = 10 localities where water samples were collected and used to predict composition of upstream source regions. Coloured regions = unique subcatchments corresponding to each locality; these colours are used consistently throughout the paper. White triangles = flow gauges, the one closest to locality F was used to calculate flux. x = CSOs that were active at any time during the sample collection period. Red diamond = Beddington wastewater treatment plant. Inset shows network schematic. (d–e) Zoom into most densely sampled subcatchments.

maceuticals and illicit drugs were observed to have accumulated in the Wandle such that they exceeded *predicted no-effect concentrations* (PNEC) reported in the NORMAN Network Ecotoxicology Database[2]. Contaminants, including the insecticide imidacloprid, were observed at concentrations that constitute a high environmental risk. Development of effective mitigation strategies would be aided if the exact sources of the contaminants could be identified. Whilst potential sources have been proposed, the exact location and magnitude of these sources remain unconstrained. The central question we address in this study is this: Given existing samples, can the sources of pollutants be identified objectively?

Mechanistic approaches to predicting pollutant transport in waterways tend to assume that concentrations can be determined downstream by solving partial differential equations or via a mass-balance approach (see e.g. Cox, 2003, and references therein). A general advection-diffusion formation to predict the rate of change of concentrations can be expressed, $\partial C/\partial t = -v\nabla C + \kappa\nabla^2 C + S(x,t)$, where v sets the velocity at which contaminants advect downstream, κ is diffusivity, S is a source term, x is space (e.g. distance along a river) and t is time (e.g. Aster et al., 2005). The partial differential equation can be modified to incorporate hydrological models (via the advective velocity and diffusivity terms), and transformation of chemicals downstream (via, addition of terms representing in-stream biogeochemical processes). Such approaches are widely used but require initial source data for calibration to be specified. When such an approach is used, pollutant sources are manually inserted into the model, or they are generated from land-use models (e.g., in the SAGIS decision support tool; Comber et al., 2013). As such, using this approach to identify sources of contaminants, especially those unknown *a priori*, can be fraught.

Quantitative approaches to source apportionment have tended to focus on multi-variate and/or statistical approaches (e.g. Weltje, 1997; Zhou et al., 2023; Chen et al., 2023). These studies often seek theoretical end-member sources of pollutants that can then be related, by inference or by including additional data (e.g. satellite imagery), to actual sources of pollution. Alternative approaches assume end-members have known geochemical or contaminant compositions *a priori*, and the proportions of these are varied to fit observations (e.g. Christophersen et al., 1990; Collins et al., 2020). In contrast, in this study, a methodology that can objectively apportion contaminant measurements to sources without assuming their composition, concentration or location *a priori* is explored. Inverse modelling using network topology has been demonstrated as a useful approach for doing so (e.g. Milledge et al., 2012; Lipp et al., 2021; Barnes and Lipp, sub).

In this contribution, inverse modelling of measured concentrations is used, for the first time, to directly solve for actual locations and concentrations of contaminant sources from observations downstream. The approach uses the topology of waterway networks, a simple theory of contaminant mixing downstream and optimisation theory that seeks to identify sources that predict concentrations downstream that best-fit observations (i.e. measured chemical concentrations; Barnes and Lipp, sub).

Data and methodologies are first described. The inversion strategy for recovering the sources of thirteen chemicals in the Wandle catchment is then demonstrated. Principal component analysis is then used to explore how the spatial distribution of contaminant sources for this set of chemicals can be greatly simplified. Once armed with source concentrations, chemical exposure throughout the drainage basin can be calculated. The results from inverse modelling are used

[2] `https://www.norman-network.com/nds/ecotox`

to calculate contaminant fluxes and risk quotients. The results emphasise the need to consider the topology of waterway networks when choosing sampling localities. Thus, in the second part of this paper, an objective approach to designing sampling campaigns, optimised to identify the provenance of contaminants and quantify associated fluxes of chemicals downstream, is developed.

2. Data & Methods

2.1. Selection of chemical data for analysis

The chemical data used in this study are described in detail by Egli et al. (2023). In summary, they collected 390 samples from waterways across Greater London in 2019–2021. Using novel direct-injection liquid chromatography mass spectrometry methods they produced 10,029 measurements of 66 unique contaminants of emerging concern including pharmaceutical and illicit drugs, which, alongside rainfall, river flow rate, and CSO event duration monitoring data, provide contextual information for this study (see Fig. S3–6; see also Munro et al., 2019). This study is focused on the Wandle catchment where $N = 33$ samples were collected during two campaigns in two consecutive years (2020–2021; Fig. 1 & 2). Each campaign spanned approximately two months in autumn or winter. All sampling localities were upstream of the Thames tidal reach. Summary statistics for the 66 chemicals measured along the Wandle are shown in Fig. S3. The 'lower limit of detection' (LLOD), later referred to as the detection limit, is 3 ng/l.

For the remainder of this paper, we focus on investigating thirteen contaminants of emerging concern (CECs) in the Wandle (Fig. 2a & S7-S19). They include the contaminants with the highest concentrations (see Fig. S3) and a selection of other pharmaceuticals and illicit drugs chosen for their potential for significant risk, or so that results from inverting chemicals with different solid-water partition coefficients, PNEC values and concentrations can be assessed. These chemicals provide a diverse suite of tracers for investigating multiple sources, pathways and fates of contaminants in waterway networks. The contaminants investigated are carbamazepine (pharmaceutical used to treat e.g. epilepsy, peripheral neuropathy and bipolar disorder), salicylic acid (used in e.g. skincare products), tramadol (painkiller), diclofenac (anti-inflammatory), venlafaxine (antidepressant), imidacloprid and acetamiprid (insecticides), cocaine and its metabolite benzoylecgonine, and trimethoprim, clarithromycin, azithromycin and sulfamethoxazole (antibiotics). Concentrations for all chemicals studied, including repeat measurements at individual localities (replicates), are shown in Fig. 2a.

2.2. Variance of measured concentrations

The inverse approach used assumes that the concentration at each sample site is fixed in time, and thus well suited for identifying sources of chronic pollution. Additionally, a pollutant is assumed to be well mixed across the channel. To explore whether measured concentrations, c, from the Wandle catchment accord with these assumptions, a nested analysis of variance (ANOVA) for all sample concentrations is performed. Each contaminant is assessed independently. Inter- (i.e. between localities) and intra-site (i.e. within locality) variance is calculated for the thirteen contaminants measured at the ten localities sampled in 2020–2021 (Fig. 2b). The inter-site variance reflects the systematic spatial variability of contaminant concentrations introduced by, say, different sources distributed across the catchment. The intra-site variance reflects variability of contaminant concentration at the same site in time, introduced by, say, inefficient mixing of the contaminant or temporally variable sources.

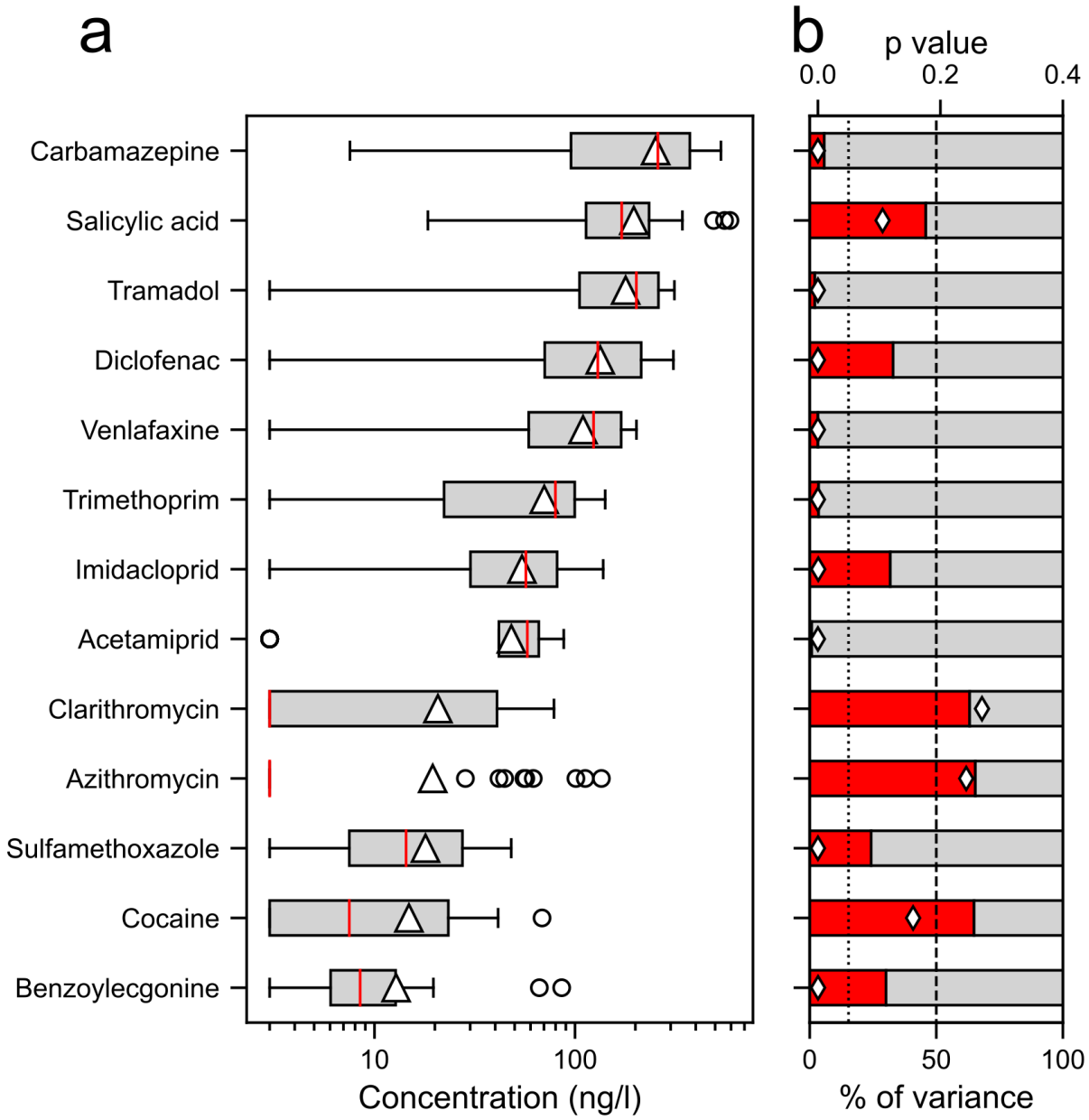

Figure 2: **Analysis of variance of chemicals in Wandle catchment.** (a) Concentration of chemicals at localities A–J including all replicates (see Fig. 1). Note that the lower limit of detection (LLOD) = 3 ng/l. Triangle = mean. Red vertical line = median. Box encloses 25^{th} to 75^{th} percentiles. Whiskers = $\pm 1.5\times$ the inter-quartile range. Circles = outliers, i.e. greater or less than values indicated by whiskers. Note: median for azithromycin equals LLOD, as it was not detected in more than half of the samples. (b) Analysis of Variance (ANOVA). p-values = white diamonds). Dotted line = p-value of 0.05. Red/gray bars = intra-/inter-site variances normalised to 100%. Dashed line (50%) indicates equal intra-site and inter-site variance.

Samples collected at different dates but located within 100 m of each other were considered to be replicates and grouped into localities A–J using the DBSCAN algorithm in the sklearn.cluster Python library (Fig. 1; see also Fig. S7–S19). The results of the clustering were then quality-checked by visual inspection. The following analysis of variance incorporates all samples at the $n = 10$ (A–J) localities, where the ith locality contains n_i samples. As concentration data is log-normal, log-variance is explored. Variation of contaminant concentration within each locality (intra-site variation) is

$$v_w^i = \sum_{j=1}^{n_i} (\log c_j - \log \bar{c}_i)^2, \tag{1}$$

where j is the sample index unique to each locality, c_j is the concentration of individual samples within the locality and $\bar{c}_i$ is the mean concentration of all samples at the locality,

$$\bar{c}_i = \exp\left(\frac{1}{n_i} \sum_{j=1}^{n_i} \log c_j\right) \tag{2}$$

and is equal to the geometric mean of the concentrations $\left(\prod_{j=1}^{n_i} c_j\right)^{1/n_i}$. Similarly, the standard deviation at ith locality is defined as

$$\sigma_{c_i} = \exp \sqrt{\frac{1}{n_i} \sum_{j=1}^{n_i} (\log c_j - \log \bar{c}_i)^2}. \tag{3}$$

Variation incorporating all samples at all localities is

$$v_w = \sum_{i=1}^{n} v_w^i = \sum_{i=1}^{n} \sum_{j=1}^{n_i} (\log c_j - \log \bar{c}_i)^2. \tag{4}$$

Variation between localities (inter-site variation) is,

$$v_b = \sum_{i=1}^{n} (\log \bar{c}_i - \log \bar{c})^2. \tag{5}$$

where $\bar{c}$ is the grand mean of all samples at all localities

$$\bar{c} = \exp\left(\frac{1}{N} \sum_{j=1}^{N} \log c_j\right). \tag{6}$$

The ratio of (arithmetic) mean variation within a locality (intra-site) and between localities (inter-site) can thus be expressed as

$$\frac{\sum_{i=1}^{n} v_w^i}{n \cdot v_b}, \tag{7}$$

and is shown on Fig. 2b. The length of the red and grey bars in this figure show within-locality (intra-site) and between-localities (inter-site) variance, respectively. The dashed line on this panel indicates equal variance. If calculated p-values, indicated by the white diamonds, are

> 0.05 (dotted line) the null hypothesis—the difference in intra- and inter-site variance is not statistically significant—cannot be rejected. An interpretation of these results is that the concentrations of chemicals such as imidacloprid and benzoylecgonine can be considered as being controlled by chronic, temporally invariant, pollutant sources that are distributed inhomogeneously across the catchment. In contrast, concentrations of chemicals such as clarithromycin and azithromycin may be controlled by local effects or temporally variable sources.

In the source apportionment calculations that follow, mean location of replicates at each locality A-J, their geometric mean concentration and the corresponding standard deviation (Eq. 2 & 3, respectively) are used.

2.3. Drainage network and sample localities

A digital drainage network for the study area was generated using established flow routing techniques (Fig. 1). First, flow directions of waterways were calculated with LandLab package (Hobley et al., 2017) by applying the D8 algorithm (O'Callaghan and Mark, 1984) to the Center for Ecology and Hydrology's Integrated Hydrological Digital Terrain Model, which has a horizontal resolution $\sim$ 50 m (Morris and Flavin, 1994). Overland flow was defined for grid cells with upstream drainage areas > 1 km^2. Calculated drainage compares favourably to independently mapped waterways (Ordnance Survey, Environment Agency) and high-resolution LIDAR data[3]. Localities were then automatically snapped to the nearest node on the digital drainage network. The resultant map was manually checked for mislocations. Only locality F required a small manual relocation from an adjacent tributary onto the main channel.

2.4. Predicting chemical concentrations downstream from known sources

A simple approach, using only the topology of a drainage network, is used to solve the forward problem, i.e. predict pollutant concentrations downstream given a set of sources upstream (see Barnes and Lipp sub). Our forward modelling strategy assumes that chemical concentrations downstream are at steady state and well-mixed. It purposefully does not incorporate travel times of chemicals along rivers, nor decay or other chemical transformation.

Concentration d at a given point downstream is calculated based on contaminant concentrations c_i and fluxes q_i (kg/s) of its N upstream sources such that

$$d = \frac{1}{Q}\sum_{i=1}^{N} q_i c_i \quad \text{where} \quad Q = \sum_{i=1}^{N} q_i. \tag{8}$$

Q is a total flux of the river. Note that the units of d and c_i must be the same (e.g. ng/l, kg/m^3), but are otherwise arbitrary. This simple forward model can predict concentrations for all points along the drainage network. However, measurements used to validate predicted concentrations are typically available only at select locations (e.g. Fig. 1). Consequently, it is often adequate to calculate d only at the locations where the measurements are available and thus reduce the computational costs.

The approach introduced in Barnes and Lipp (sub) is used to predict contaminant concentrations $d_1, d_2, \ldots, d_N$ at N localities $x_1, x_2, \ldots, x_N$ of spot samples along the drainage network. The method uses a graph representation of the nested samples based on their connectivity

[3] `https://environment.data.gov.uk/dataset/ce8fe7e7-bed0-4889-8825-19b042e128d2`

within the drainage network. A topological network (a directed acyclic graph) of unique sub-catchments is generated from the sample-set (see e.g. inset in Fig. 1c). Each node on the network corresponds to a sub-catchment defined by a sample site. Each subcatchment, which encloses the drainage area between adjacent samples, is unique i.e. does not overlap with any other subcatchment. Each subcatchment (node) is described by three parameters: unique upstream area A (m^2), run-off ϕ ($kg/s/m^2$), here defined as a mass flux per unit upstream area, and concentration (kg/m^3). For each subcatchment, average run-off can be combined with its drainage area to calculate the flux, $q_i = A_i\phi_i$. In this study, run-offs are assumed identical for all the subcatchments so, effectively, the fluxes depend only on the subcatchment areas.

For each (ith) locality, the set $\mathbb{U}_i$ is associated with all its upstream subcatchments. For example, for subcatchment D the set $\mathbb{U}_i = \{\mathsf{D}, \mathsf{C}, \mathsf{B}, \mathsf{A}\}$. The forward operator can then be expressed in discrete form as

$$d_i = \frac{1}{\sum_{j\in\mathbb{U}_i} q_j} \sum_{j\in\mathbb{U}_i} c_j q_j. \tag{9}$$

When upstream basins are nested, the forward model (Eq. 9), is solved in topological order, building the above expression for each node upstream to downstream (see inset in Fig. 1c).

2.5. Inverse Method

In general, measured concentrations of contaminants in source regions are sparse or unavailable. This data limitation makes predicting the composition of drainage networks using only a *forward* modelling strategy fraught. Instead, in this study sparse downstream samples are inverted to determine source concentrations upstream. This approach seeks to identify sub-catchment concentrations that predict (via Eq. 9) concentrations downstream that minimise misfit to spot measurements (Fig. 1). The inverse method introduced by Barnes and Lipp (sub), which uses the graph based forward model described above, is used.

More formally, this approach seeks to identify the vector of source concentrations, $\mathbf{c}$ ($= c_1, c_2, \ldots, c_n$), that best fits the vector of measured chemical concentrations downstream $\mathbf{d}^{\text{obs}}$ ($= d_1^{\text{obs}}, d_2^{\text{obs}}, \ldots, d_n^{\text{obs}}$). The inverse model seeks to minimise the cumulative misfit between $\mathbf{d}^{\text{obs}}$ and the vector of predicted concentrations at the same localities, $\mathbf{d}^{\text{pred}}$ ($= d_1^{\text{pred}}, d_2^{\text{pred}}, \ldots, d_n^{\text{pred}}$), calculated using the forward model (Eq. 9). Formally,

$$\min \sum_{i\in N} \text{misfit}\left(\mathbf{d}^{\text{obs}}, \mathbf{d}^{\text{pred}}\right), \tag{10}$$

is sought. Since concentration data can span many orders of magnitude, and because efficient convex optimisation is desirable, the following misfit function is defined

$$\text{misfit}\left(\mathbf{d}^{\text{obs}}, \mathbf{d}^{\text{pred}}\right) = \max\left(\frac{\mathbf{d}^{\text{obs}}}{\mathbf{d}^{\text{pred}}}, \frac{\mathbf{d}^{\text{pred}}}{\mathbf{d}^{\text{obs}}}\right). \tag{11}$$

2.5.1. Regularisation

Measurements are likely to contain noise and analytical uncertainties and the forward model is a simplification of reality. Thus regularised solutions for each contaminant are sought. Deviations of $\mathbf{c}$ from the (geometric) mean of observed concentrations (at the sample sites), $\bar{\mathbf{d}}$, are penalised, where

$$\bar{\mathbf{d}} = \left(\prod_{i=1}^{n} \mathbf{d}^{\text{obs}}\right)^{1/n}. \tag{12}$$

Thus, the optimisation algorithm works to solve the following

$$\min_{\text{w.r.t. } \mathbf{c}} \left\{ \sum_{i \in N} \max \left(\frac{\mathbf{d}^{\text{obs}}}{\mathbf{d}^{\text{pred}}}, \frac{\mathbf{d}^{\text{pred}}}{\mathbf{d}^{\text{obs}}} \right) + \lambda \sum_{i \in N} \max \left(\frac{\bar{\mathbf{d}}}{\mathbf{c}}, \frac{\mathbf{c}}{\bar{\mathbf{d}}} \right) \right\}, \tag{13}$$

by seeking optimal $\mathbf{c}$. Regularisation is controlled by the value of λ. The optimal model is the one that minimises the terms within the braces in Eq. 13. The optimal values of λ are identified for each chemical via a systematic sweep of values in a series of inverse models (see e.g. Fig. S20-32c). Each inverse model solves for source concentrations by minimising misfit to the mean values of measured concentrations at localities A–J, which are assumed to be free of noise. Optimal values for each chemical are identified as those that yield maximum curvature when data misfit (first term in braces in Eq. 13) is compared to model misfit (second term in braces in Eq. 13; see Parker, 1994). Solutions to Eq. 13 are sought using *embedded conic solvers* within the `cvxpy` Python package (Domahidi et al., 2013; O'Donoghue et al., 2016).

2.5.2. Uncertainty Propagation

The impact of measurement uncertainties on predicted concentrations are assessed via Monte Carlo experimentation as follows. A log-normal distribution of uncertainties, unique to each observation, with the mean and standard deviation defined in Eq. 2 & 3 is assumed for each contaminant from which $n = 10^4$ 'data' vectors are drawn randomly, effectively adding noise to measured concentrations. Regularisation parameters (per contaminant) are held constant in all iterations of the Monte Carlo experiment, so that mean, median, and standard deviation of the ensemble of final models are straightforward to interpret. Maps of mean model output and standard deviations from the Monte Carlo experiments are shown. Median values are calculated to assess skewness of the distribution (e.g. Shapiro and Ritzwoller, 2002). Results from inverting imidacloprid and benzoylecgonine concentrations are shown in Fig. 3. Results for all chemicals investigated and a summary of calculated concentrations and uncertainties is shown in Fig. S20–32.

2.6. Environmental risk assessment

For each chemical, s, and each subcatchment, i, risk quotients were calculated such that $R_i^s = c_i^s / p_s$. p_s indicates PNEC values from the NORMAN ecotoxicological database, with the following values (ng/l) acetamiprid: 24, azithromycin: 19, carbamazepine: 2000, cocaine: 2456, diclofenac: 50, imidacloprid: 13, salicylic acid: 18,000, sulfamethoxazole: 600, tramadol: 8653, trimethoprim: 120,000, venlafaxine: 880. As an example, if the concentration of an arbitrary chemical in a subcatchment $c_i^s = 10$ ng/l and it has an associated PNEC value of 2 ng/l, its risk quotient (dropping the indices) $R = 5$. Following Egli et al. (2023) and Palma et al. (2014), risks were defined as *high* if $R > 10$, *medium* if $10 \geq R \geq 1$, *low* if $1 \geq R \geq 0.1$, and *insignificant* if $R < 0.1$. See Fig. S33 for calculated concentrations, c_i, and uncertainties, σ_c, used to calculate R and uncertainties shown in Fig. 4. The results are discussed below.

2.7. Estimating chemical fluxes downstream

With estimates of both source concentrations and river discharge it is straightforward to calculate chemical fluxes, q (kg/s), for each subcatchment. Here, the mass flux of a chemical from a subcatchment is estimated using the product of water discharge, f (m^3/s), and volumetric density (concentration) of the chemical, c (kg/m^3),

$$q = f \cdot c. \tag{14}$$

Uncertainties in concentrations and water discharge can be propagated to calculate uncertainties in chemical flux,

$$\sigma_q = \sqrt{\left(\frac{\partial q}{\partial c}\sigma_c\right)^2 + \left(\frac{\partial q}{\partial f}\sigma_f\right)^2} = \sqrt{(f\sigma_c)^2 + (c\sigma_f)^2}, \tag{15}$$

where c and σ_c are the respective mean and standard deviation of concentrations extracted from the ensemble of models generated by Monte Carlo experimentation. f and σ_f are mean and standard deviation of water discharge. Errors are assumed to be independent (Taylor, 1997). The values have not been corrected for smoothing due to regularisation.

To estimate water discharge measurements made between 2019 and 2020 (overlapping with chemical sampling) at the "Wandle at South Wimbledon" gauge station (UK-CEH's National River Flow Archive: ID: 39003) are used. Calculated mean discharge and standard deviation are $f = 1.84$ and $\sigma_f = 0.15$ m^3/s, respectively. Average unit (per m^2) runoff, $\mathcal{O}(10^{-8}$ m/s), is estimated by normalising measured discharge by the drainage area upstream of the gauge station (176 km^2). Note that this measurement, which was extracted from the digitised drainage network, substantially exceeds effective drainage area estimated by UK-CEH (54 km^2). The consequences of changing the run-off are assessed later in the manuscript. Finally, water discharge at the localities A–J is calculated by multiplying average runoff by the unique catchment area upstream of each locality. Calculated fluxes of imidacloprid and benzoylecgonine are shown in Fig. 5a–d. Calculated fluxes for all chemicals are summarised in Fig. 5e, and the results are discussed below.

2.8. Principal Component Analysis of source concentrations

In this study sources of thirteen chemical contaminants are mapped. Whilst exploring the spatial distribution of sources of each chemical individually is important, it may also be useful to identify common patterns between multiple chemicals. Such patterns may, for instance, reflect a smaller number of underlying contaminating processes or sources manifest in measured concentrations. Identifying such underlying processes may allow for more efficient mitigation. One way to assess similarities and dissimilarities in the variance of calculated concentrations is via principal component analysis (PCA).

PCA is used to find eigenvectors of the covariance matrix of calculated subcatchment concentrations of chemicals. The inverse models introduced in the previous section recovers concentrations of n chemicals in m subcatchments. These results provide an $m \times n$ matrix of concentrations with m rows corresponding to the number of subcatchments and n columns corresponding to the basis vectors (the chemical concentrations). For stability, PCA requires $m > n$ (i.e., the matrix needs to have enough rows to be at least square) so some variables must be excluded. Acetamiprid, trimethoprim, clarithromycin, and azithromycin are excluded, excluding different chemicals does not materially change the conclusions so long as the two groups of chemicals, discussed in the results section below, are well represented.

To perform the PCA, first, the matrix of concentrations is recast using the centred log-ratio (clr) transformation (Aitchinson, 1983). The transformation calculates the logarithm of the ratio of a concentration to the geometric mean of all concentrations within the compositional data set. This transform addresses the 'closure effect', whereby the components of a compositional dataset are constrained to sum to a constant (the case for all data with units ppm, ppb, %, etc.). PCA is performed using the Python `scikit` library `sklearn.decomposition.PCA` (Pedregosa et al., 2011). The resulting principal components (eigenvectors of the covariance matrix) are each a linear combination of basis vectors (chemicals). The contribution of a given

principal component and its projection onto an original basis vector are referred to as its score and loading, respectively. By changing the basis of the data matrix each subcatchment can now be presented in terms of principal components, or the score for each component can be mapped in space (e.g. Fig. 6c).

2.9. Identifying 'optimal' sampling sites

In general, sources of contaminants in waterways are unknown. In this study an objective source apportionment method is used to invert observations at sample sites to recover sources upstream. It is therefore desirable to identify where in a catchment samples should be taken such that recovered sources are most informative. Such a goal is especially important in cases where finite resources mean that it is only possible to gather a limited number of samples. A variety of methods for objectively identifying sampling sites on drainage networks have previously been proposed which seek to optimise sampling for different purposes (e.g. Dixon et al., 1999; Carraro et al., 2021; Singhal et al., 2023). For our specific purposes however, sources are apportioned into n approximately equal area subcatchments. This allows unbiased coverage of a catchment where contaminant sources could, theoretically, be anywhere with equal probability. This approach, when provided with a target catchment size, A, identifies sample localities required to divide the network into subcatchments no greater in area than A. The scheme developed here is parameterised using topography extracted from a digital elevation model so that optimal sampling localities in a natural drainage network can be identified.

First, a topologically ordered (from downstream to upstream) list of nodes extracted from a digital drainage network is generated. Each node on the network corresponds to a pixel (cell) in the underlying DEM. The algorithm removes all nodes with upstream areas smaller than the target (equal) area, and creates a new list from the remaining nodes. The algorithm iterates across the list of nodes from upstream to downstream. Upstream area is calculated for each node. Nodes with areas that meet the target are saved as sampling sites, and the corresponding upstream nodes are deleted from the list. Once all nodes in the network have been visited, a list of sample sites is produced that provides approximately equal-area coverage across the network. The algorithm is provided and described in detail here: `zenodo.org/records/7311352`.

3. Results

3.1. Inverse modelling for source concentrations

3.1.1. Validating the method by inverting synthetic data

The capability of the inverse model to apportion chemicals to sources upstream is tested by first inverting synthetic data (see Fig. S34). In a series of experiments known concentrations of an arbitrary contaminant were inserted into subcatchments and the regularisation parameter was varied systematically such that $\lambda = 10^{-2}$, 10^{-4} or 10^{-6}. In the simple scenarios examined, the 'true' concentration of the contaminant in single subcatchments was set to be arbitrarily high (1000 ng/l), and it is arbitrarily low (1 ng/l) in all other subcatchments. For example, setting the concentration in subcatchment D to be very high compared to other subcatchments could represent a simplified example of pollution from a single point-source in subcatchment D, for example the Beddington wastewater treatment plant. These known 'source' concentrations were used to calculate concentrations at localities A–J downstream using the forward model (Eq. 9).

Calculated concentrations at localities A–J were then inverted to recover source concentrations (Eq. 13). For clarity, the only inputs into the inverse models are the drainage network, the

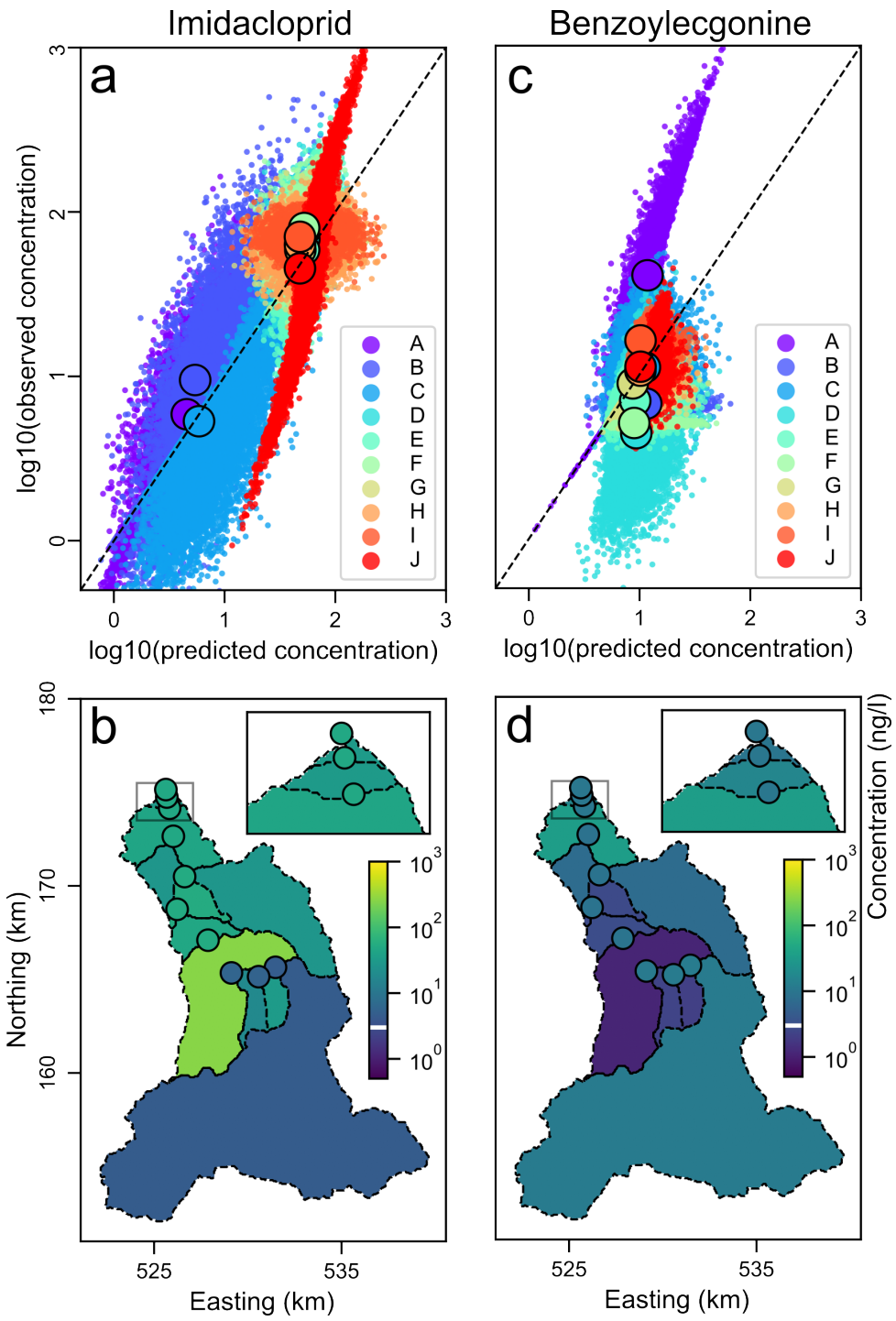

Figure 3: **Objective source apportionment for insecticide imidacloprid and cocaine's metabolite benzoylecgonine.** (a) Small circles = observed vs. predicted downstream concentrations at sample localities A–J (see Fig. 1) from Monte Carlo experiment incorporating 10^4 inverse models of measured concentrations randomly perturbed within their uncertainties unique to each observation; large circles = mean misfit for each locality. Dashed line = 1:1 correlation. Downstream predictions were calculated from the results of apportionment (i.e. predicted upstream concentrations) by solving the forward problem. (b) Mean predicted upstream concentrations in each subcatchment for optimal regularisation. Coloured circles = mean observed concentrations at sample localities. White line on colour bar = detection limit. (c–d) Results for benzoylecgonine. See Fig. S22 & S27 for extended results and Fig. S20–S32 for all the chemicals inverted in this study.

synthetic concentrations of the contaminant at the ten localities, and the value of the regularisation parameter, λ. In other words, the original 'known' *source* concentrations are discarded. Instead, they are recovered by inverting the concentration 'measurements' at localities A–J.

When $\lambda = 0$ (i.e., no regularisation) predicted source concentrations match the 'known' true concentrations perfectly (within machine precision). When λ is increased calculated concentrations more closely align with average concentration of the ten localities, as expected. Peak concentrations were always correctly located in subcatchment D for all values of λ tested. These results indicate that source apportionment from inversion of the real chemical observations in this catchment can be used to quantify the locations and concentrations of actual sources of contaminants.

An important concern is that noise might negatively impact recoverability of source concentrations from measurements downstream. Noise might be introduced by analytical error or as a consequence of physical or chemical processes not incorporated into the forward model (e.g. rivers that are not well-mixed across a channel), for instance. Fig. S35 shows the results from 10^4 inversions of synthetic data generated by the procedure described in the previous paragraph plus added random noise. In each of these experiments noise was added to the (initially noise-free) chemical concentrations at localities A–J shown in Fig. S34. Noise was added commensurate with the range of values at each locality determined by imidacloprid field data. The results indicate that concentration measurements at localities can be reliably inverted for source concentrations, and their uncertainties estimated, even in the presence of realistic uncertainties.

Results from varying the location of the source of the arbitrary contaminant are shown in Fig. S36–37. The *resolution matrices* shown in these figures demonstrate that inverse modelling of real chemical data could be expected to recover the locations and concentrations of contaminants in source areas. They also demonstrate that increasing noise and regularisation 'smears' calculated concentrations between nearby subcatchments, as expected. The results also indicate that source apportionment is sensitive to subcatchment run-off rates.

3.1.2. Inverting measured chemical concentrations

Fig. 3a–b shows the results from inverting concentrations of the pesticide imidacloprid measured at localities A–J (Fig. 1). In these models regularisation parameter $\lambda = 10^{-1.7}$, which sits at the location of maximum curvature in the plot of data misfit vs. model roughness (see Sect. 2.6; Fig. S20-32c). Fig. 3a shows a comparison of observed and predicted concentrations at the sample sites for all 10^4 iterations of the Monte Carlo experiment, mean values for each subcatchment are also shown. These results indicate that the inverse model generates good fits to the data. Resultant source apportionment is shown in panel (b). Alternative presentation of fits to data, source apportionment and uncertainties are shown in Supporting Information. The results emphasise the importance of subcatchment D as a source of imidacloprid. In D the median source concentration across all models is more than an order of magnitude higher than in all other subcatchments. Inverse modelling of synthetic data discussed in the previous section (i.e. a model with a single subcatchment with high concentrations) reveals a very similar spatial pattern of recovered concentrations with artificially increased values in subcatchments B–C and E–F for high values of λ (see Fig. S34–35). As a result, a portion of the relatively higher calculated concentrations for adjacent subcatchments, i.e. B–C and E–H could be attributed to regularisation. The results are insensitive to the LLOD values tested (Fig. S39–41).

Inverse modelling of benzoylecgonine, a metabolite of cocaine, is shown in Fig. 3c–d. The same modelling strategy used to invert imidacloprid was followed (with $\lambda = 10^{-2.7}$; Fig. S22c).

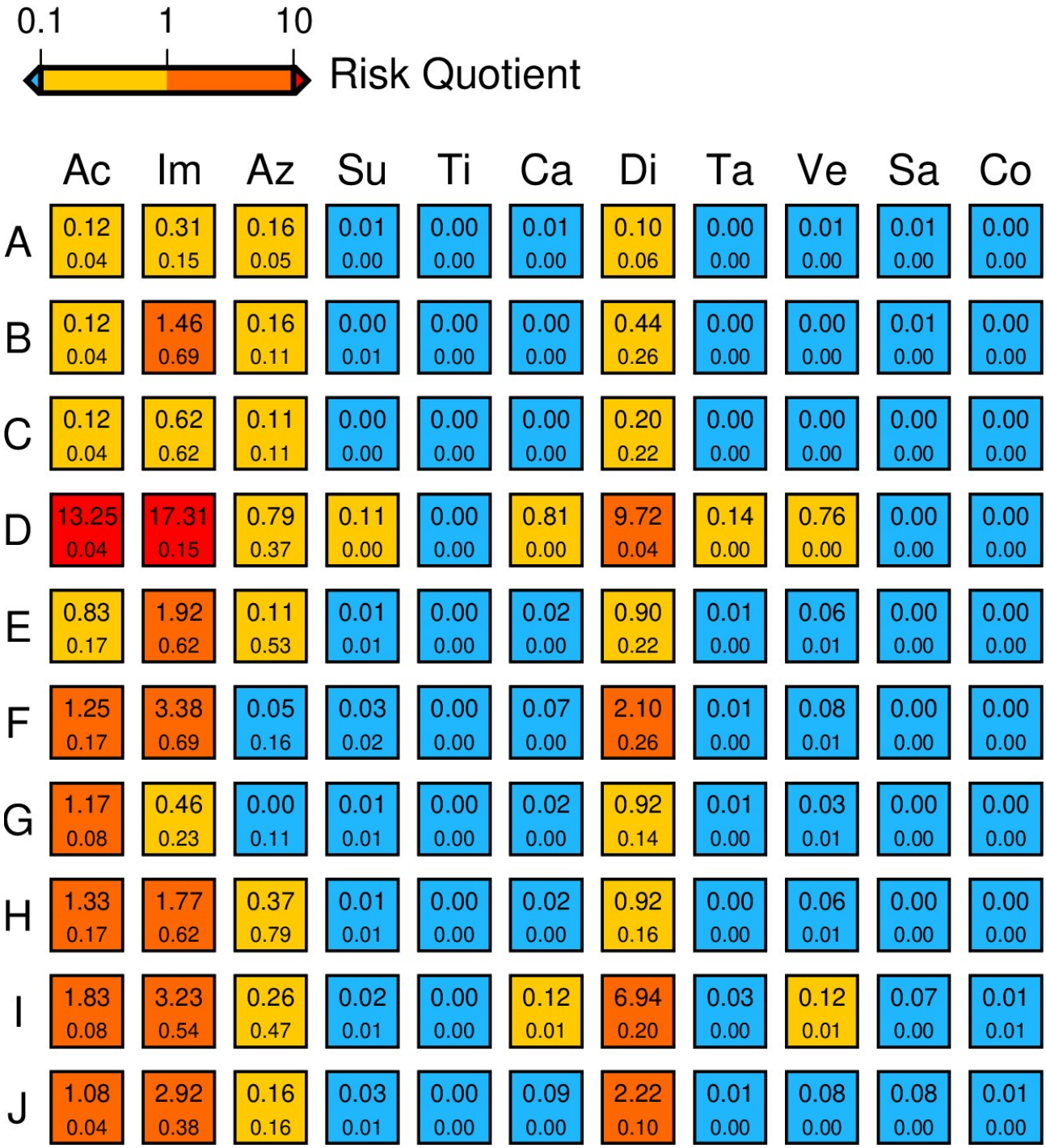

Figure 4: **Predicted risk quotients for calculated subcatchment contaminant concentrations.** A–J: subcatchments (see Fig. 1). Abbreviations—Ac: acetamiprid, Im: imidacloprid, Az: azithromycin, Su: sulfamethoxazole, Ti: trimethoprim, Ca: carbamazepine, Di: diclofenac, Ta: tramadol, Ve: venlafaxine, Sa: salicylic acid, Co: cocaine. Risk quotients—red: high, orange: medium, yellow: low, blue: insignificant (see scale bar and body text for details). Large/small numbering = risk quotient/uncertainty. See Fig. S33 for calculated concentrations and uncertainties.

In contrast with imidacloprid, calculated concentrations of benzoylecgonine in mid-reach subcatchments (B–F) of the Wandle are low. Cocaine and benzoylecgonine are generally very well removed in wastewater treatment (Munro et al., 2019). Calculated concentrations are highest in subcatchments upstream (A) and downstream (G–J), which do not include WWTPs. Predicted concentrations of benzoylecgonine are the most poorly fitting of all the chemicals inverted. Residual misfit between observed and theoretical concentrations of benzoylecgonine is highest at localities A and D (see Fig. S22a). Encouragingly, calculated concentrations at other localities more closely match observations. Results for cocaine and its metabolite benzoylecgonine are similar, as expected for chemicals with expected similar pathways (cf. Fig. 3c–d and Fig. S25).

One explanation for the relatively high residual misfit in subcatchments A and D is that data uncertainty is actually larger than that indicated by the spread of concentrations measured at these localities. Another, more likely, explanation is that actual fluxes from neighbouring basins are not (cannot) be predicted accurately by the simple forward model, which does not consider temporally variable sources. This issue is explored by first noting that there is a theoretical limit on observed downstream concentrations given the prescribed forward model.

Consider a two component model, i.e. two measured concentrations d_1 (upstream) and d_2 (downstream) with associated unique subcatchments with concentrations c_1 and c_2, and fluxes q_1 and q_2. Downstream concentrations measured at the sample locations will be $d_1 = c_1$ and $d_2 = (c_1q_1 + c_2q_2)/(q_1 + q_2)$, thus

$$c_2 = d_2 \left(\frac{q_1 + q_2}{q_2} \right) - d_1 \left(\frac{q_1}{q_2} \right). \tag{16}$$

As concentrations and fluxes must be ≥ 0, $d_2(q_1+q_2)/q_1 \geq d_1$, which places limits on the possible values of concentrations that can be predicted. For example, for equal fluxes, $d_2 \geq d_1/2$, i.e., concentrations at locality d_2 cannot be less than half the concentration at d_1. More generally:

$$\frac{d_{i+1}}{d_i} \geq \frac{\Sigma_{j=1}^{i} q_j}{\Sigma_{j=1}^{i+1} q_j}. \tag{17}$$

If these inequalities are not satisfied it could indicate that the forward model is not appropriate, i.e. processes other than conservative mixing are important or that calculated fluxes are incorrect. Subcatchments with similar, low, concentrations, e.g. A and B or I and J, tend not to satisfy the inequality. Nonetheless, about half of the subcatchments have calculated downstream concentrations that do satisfy it. For instance, high calculated concentrations of most chemicals in subcatchment D almost always satisfy the inequality in all iterations of the Monte Carlo experiment. In other words, $d_\mathsf{D}/d_\mathsf{C}$ is usually $> (q_\mathsf{A} + q_\mathsf{B} + q_\mathsf{C})/(q_\mathsf{A} + q_\mathsf{B} + q_\mathsf{C} + q_\mathsf{D})$. These results emphasise the importance of regularising the inverse model, which utilises a simple forward model that does not include complex hydrology or chemical transformations, say.

The results summarised above demonstrate that the forward model can effectively identify and quantify sources of chronic pollution. They also suggest that for chemicals with rapidly fluctuating concentrations, such as those related to Combined Sewer Overflows (CSOs)—the primary source of benzoylecgonine in waterways as noted by Munro et al. (2019); Rapp-Wright et al. (2022)—it may be necessary to incorporate time-varying effects to better explain the observed data. Enhancing the temporal resolution of sampling campaigns would be one way to better track the dynamic patterns of such contaminants.

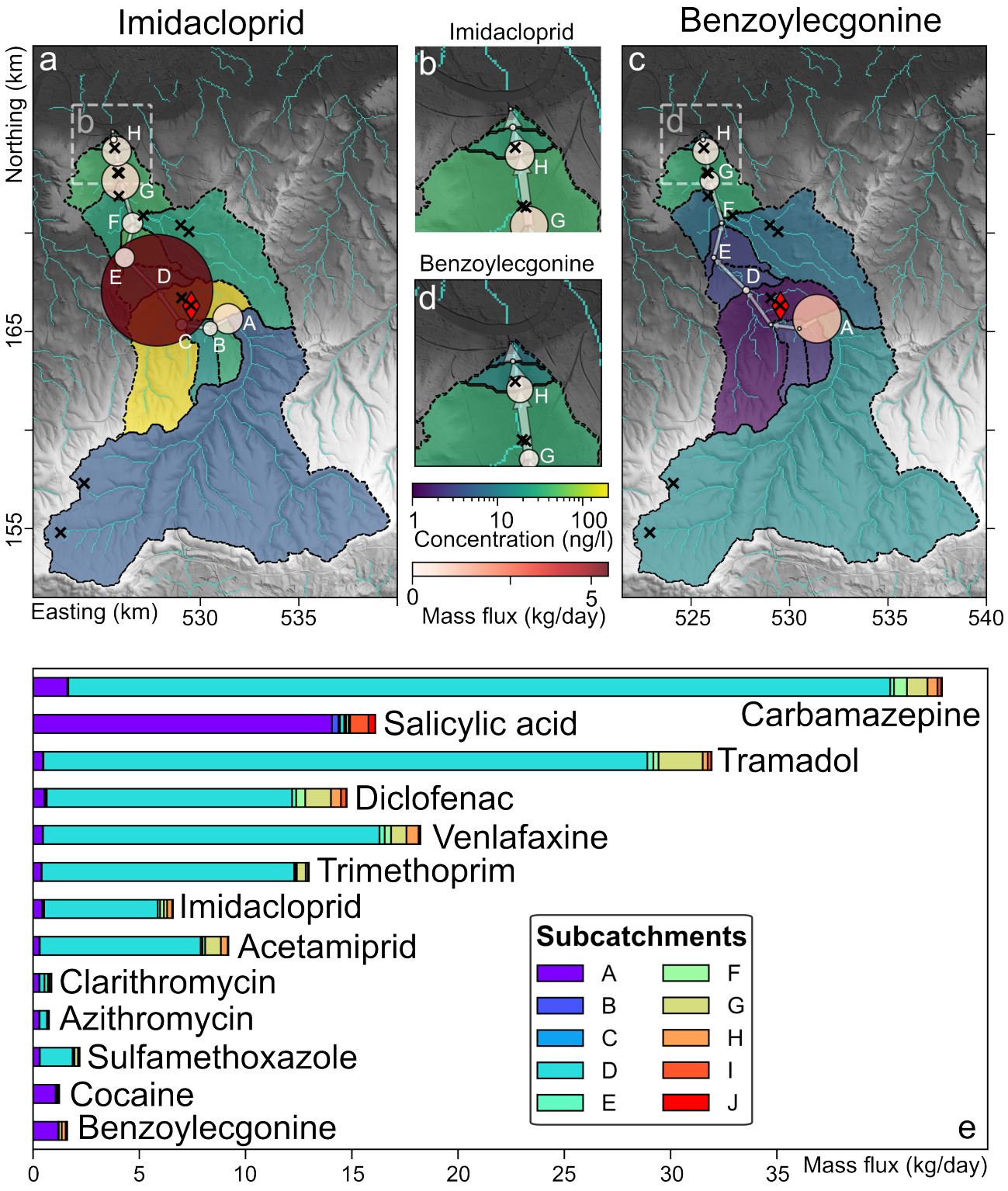

Figure 5: **Calculated fluxes of contaminants from Wandle subcatchments.** (a–d) Coloured regions = subcatchments A–J (source areas; see Fig. 3) coloured by calculated concentrations of insecticide imidacloprid and cocaine's metabolite benzoylecgonine. Circles = fluxes from individual subcatchments (circle area is proportional to flux). (a & d) Concentrations and fluxes close to Thames confluence. (e) Bar heights = cumulative mass fluxes (kg/day) of all chemicals inverted in this study; colours = contributions from each subcatchment (see key and Fig. 1). Note dominant sources of high chemical flux: subcatchment D (e.g. carbamazepine, tramadol, diclofenac, venlafaxine, trimethoprim, acetamiprid) and subcatchment A (e.g. salicylic acid). Calculated concentrations for all contaminants are shown in Fig. S20–32 and summarised in Fig. S33.

Misfit between observed and predicted concentration at localities A and D appears to arise from from two sources. First, added noise, which can generate small unrealistic relative changes in concentration downstream (such that the inequality is not satisfied). Second, accurately constraining fluxes (q; i.e. effective drainage areas) is crucial to reducing uncertainty. Decreasing the run-off from subcatchment A reduces the residual misfit between observed and theoretical concentrations at sampling localities A–J (Fig. S36–S37 & S42).

Results from inverse modelling of all other chemicals are shown in Fig. S20–32 and summarised in Fig. S33. The source apportionment calculations indicate that subcatchment D is a dominant source of insecticides (imidacloprid and acetamiprid) in the Wandle. Similarly this subcatchment is a dominant source of the pharmaceuticals sulfamethoxazole, trimethoprim, carbamazepine, diclofenac, tramadol, and venlafaxine. In contrast calculated concentrations of the antibiotics azithromycin and clarithromycin, salicylic acid, cocaine and it metabolite benzoylecgonine are relatively low in subcatchment D. Instead, they tend to be higher close to the Wandle's confluence with the Thames. There are seven known CSO outlets in subcatchments downstream of D, which could be sources of untreated wastewater explaining the high concentrations in these subcatchments. These results indicate that different contaminants in the Wandle catchment are derived from distinct sources upstream. However, they also emphasise that subcatchment D is the dominant source for a large number of contaminants. This catchment includes the Beddington wastewater treatment plant. These results indicate that the locations of suspected point sources can be independently recovered just from downstream observations.

3.2. Chemical risks and fluxes

Fig. 4 shows calculated risk quotients for the water added from each subcatchment. Most subcatchments have *low* to *medium* risk quotients for the insecticides acetamiprid and imidacloprid, the antibiotic azithromycin, and anti-inflammatory diclofenac. Subcatchment D has *high* risk quotients for both insecticides, and medium (close to high) risk quotients for diclofenac. It also has low to medium risk quotients for sulfamethoxazole, carbamazepine, tramadol and venlafaxine. The predicted quotients are broadly consistent with Egli et al. (2023) who reported highest values for imidacloprid (maximum = 10.6), diclofenac (6.2), acetamiprid (3.3). The predicted values must be interpreted with some caution given that mean subcatchment concentrations are sought. Chemical risks could be significantly higher at specific localities (e.g. individual tributaries or ponds) within the subcatchments as well as closer to point sources.

Fig. 5a–d shows the calculated fluxes of imidacloprid and benzoylecgonine from subcatchments A–J. Imidacloprid flux is dominated by subcatchment D. In contrast, efflux of benzoylecgonine from subcatchment D is low, whereas subcatchments A and G–J have relatively high fluxes. Fig. 5e shows calculated fluxes for all chemicals and subcatchments examined. It demonstrates that subcatchment D dominates the flux of carbamazepine, tramadol, diclofenac, venlafaxine, trimethoprim, imidacloprid, acetamiprid and sulfamethoxazole in the Wandle. In contrast, subcatchment A is an important source of salicylic acid, cocaine and benzoylecgonine. In fact, calculated fluxes indicate that subcatchments A and E–J are important sources of most chemicals, although for subcatchment A this is in part related simply to its larger size relative to other subcatchments.

3.3. Principal component analysis

Fig. 6 shows the results of the PCA of calculated contaminant concentrations, used to establish relationships between sources of chemicals in the Wandle catchment. Panel (a) shows the

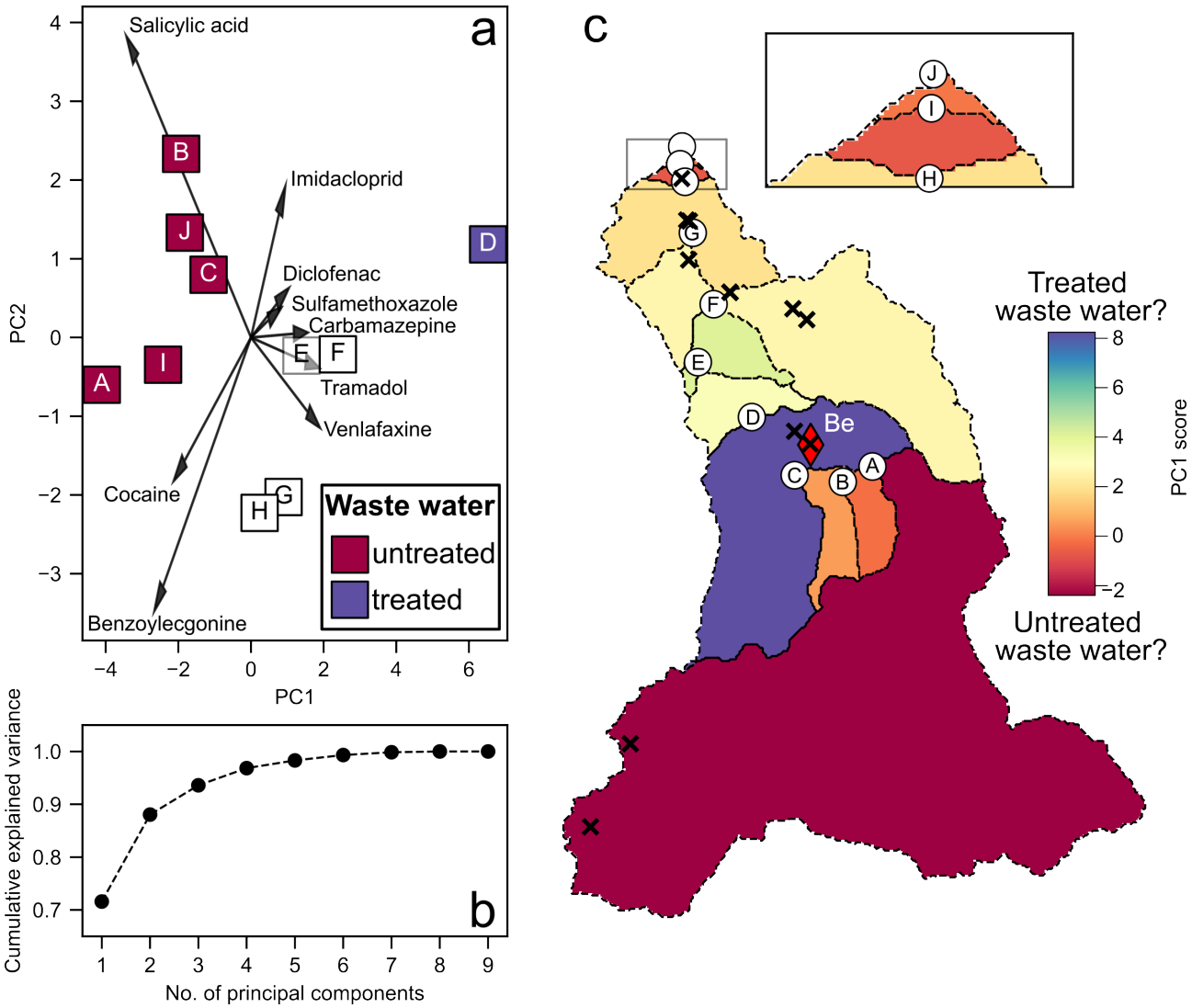

Figure 6: **Principal component analysis of source (subcatchment) contaminant concentrations in the Wandle.** (a) Biplot showing chemical loading of the first two principal components explaining >85% of variance of subcatchment contaminant concentrations. Colours indicate interpreted dominant pollutant pathway in each subcatchment. (b) Cumulative variance as a function of number of principal components. (c) Map showing scores for the first principal component in each subcatchment (see Fig. 1). Inset shows zoom at confluence with Thames river. White labeled circles = sample localities; x = CSOs, red diamond labeled Be = Beddington WWTP.

first two principal components of nine chemicals and the subcatchments. $> 70\%$ of the variance is explained by the first component (PC1), $> 85\%$ is explained by the first two components. As expected, cocaine and its metabolite benzoylecgonine have similar loadings on these two components (see vectors in panel a). Salicylic acid has a similarly negative loading on the first principal component. In contrast, the pharmaceuticals (including pain medications, antibiotics and insecticides) have positive loadings on the first principal component. Subcatchment D is significantly positively loaded onto the first principal component. In contrast, other subcatchments are negatively loaded, or close to zero. As the first principal component contains the majority of the variability in the dataset it is visualised spatially in panel c. This map shows the loadings on the first principal component for each subcatchment. These results emphasise that the contaminant composition of subcatchment D is distinct from the other subcatchments.

These results are interpreted as indicating the presence of two primary pathways for chemical contaminants into the Wandle. The contaminant load from subcatchment D is fundamentally distinct from the contaminant load from any other subcatchment. Positive loadings on the first principal component are interpreted as representing the 'fingerprint' of treated waste water. These results could be explained by the presence of the Beddington WWTP in subcatchment D. In contrast, subcatchments with negative loadings on PC1, i.e., A, B, C, I, J, are interpreted as having a distinct contaminant pathway. This source is interpreted as corresponding to *untreated* wastewater due to the presence of illicit drugs, which are present in wastewater and treated if they reach wastewater facilities (Munro et al., 2019). These results are broadly consistent with hierarchical cluster analysis of contaminants in rivers across London, which emphasises commonalities between contaminant concentrations measured downstream of WWTPs, and commonalities of concentrations measured in catchments without WWTPs (Egli et al., 2023). Untreated wastewater could be entering the river via sewerage misconnections, combined sewer overflow events (CSOs), runoff or perhaps via direct dumping. CSOs may have been active in some of the subcatchments during the period of sampling (see Fig. S4–S6), although specific discharge dates are not available. Subcatchments E, F, G, H were not found to be compositionally distinct sources of any contaminants.

3.4. Optimal sampling strategies

Finally, optimisation of source recovery in future sampling campaigns is examined (see Sect. 2.9). Fig. 7 shows the results from a suite of inverse models solved using different distributions of sampling localities (white circles) for an arbitrary (well mixed, conservative) contaminant. The yellow crosses indicate point sources of the contaminant throughout the Wandle catchment (e.g. CSO), which are constant in each test. Concentrations at sampling localities are calculated using the forward model (Eq. 9). Panel (a) shows the results from the first test in which 'measured' concentrations at the actual sampling localities used in this study were inverted (see e.g. Fig. 1). Panels (b–d) show the results from inverting an increasingly high number of samples located so that subcatchments upstream have an equal area. These results indicate that sources of contaminants could be more precisely, and objectively, identified using a sampling strategy optimised to determine contaminant concentrations in equal-area subcatchments. In other words, sampling campaigns that seek to determine sources of chemicals, especially those that are unknown or suspect, should incorporate knowledge of network topology when deciding where to collect samples for chemical analyses.

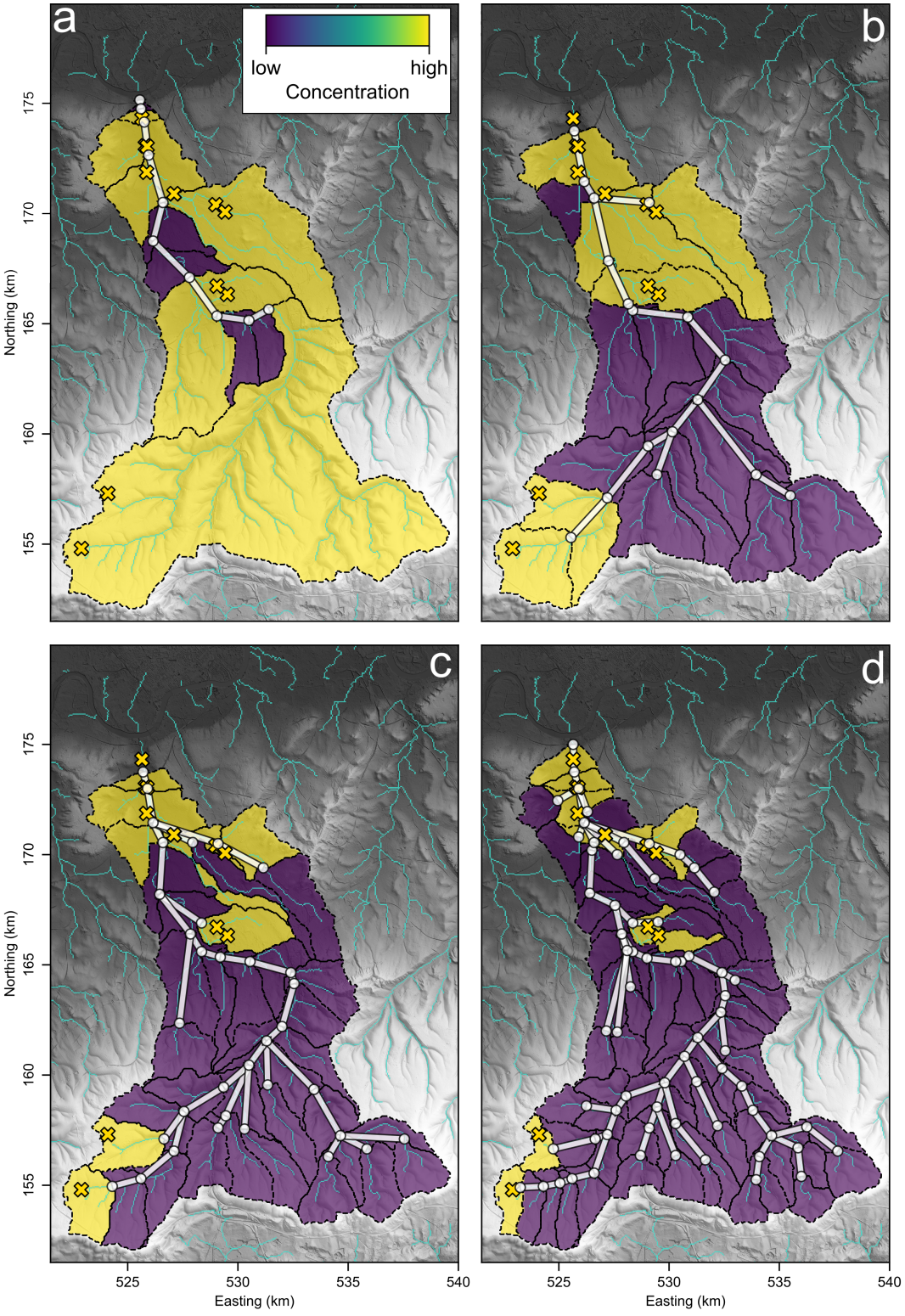

Figure 7: **Improving precision of source apportionment.** (a) Apportionment using actual sampling localities from this study (see Fig. 1). (b–d) Apportionment using sampling localities distributed so that unique subcatchments have equal area. (b) 17 samples; 5 km^2. (c) 34 samples, 2 km^2. (d) 66 samples, 1 km^2. Yellow crosses = locations of synthetic point sources of contaminants (e.g. note that they are located at actual CSO events). White circles = sample sites; white lines = network connecting sample sites. Turquoise curves = drainage network; Coloured regions with dashed outlines = subcatchments unique to each sample, coloured by calculated source concentration.

4. Discussion

4.1. An objective approach to determining contaminant provenance

A principal finding from this study is that spot measurements of contaminant concentrations in water can be combined with the topology of waterway networks to invert for sources of chemicals. We emphasise that this approach is objective and that it solves for actual sources of contaminants (rather than theoretical end-members, say) without recourse to additional information (e.g. satellite imagery, hydrodynamic variables). Ecotoxicologically relevant chemicals in the Wandle catchment, including insecticides, pharmaceuticals and illicit drugs, can be apportioned to sources upstream with no prior knowledge of provenance. The results indicate that conservative mixing, assumed in this study, has provided enough complexity to accurately predict concentrations of most contaminants downstream (e.g. Fig. 3a). In other words, complex hydrological modelling or chemical transformation may not always be required to reliably predict concentrations of contaminants in waterways downstream. However, the inverse scheme developed has sufficient flexibility such that more complex forward models (e.g. allowing for chemical decay) could be straightforwardly incorporated if necessary.

4.2. Contaminant sources in the River Wandle

Calculated source apportionment and chemical fluxes for the Wandle emphasise the importance of subcatchment D as a source of insecticides and most pharmaceuticals investigated. Efflux from the Beddington WWTP appears to be the most likely source of these chemicals. In other words it would appear that these chemicals, directed to this sewer network terminus from the Beddington WWTP catchment (incorporating Croydon, Carshalton, Coulsdon, Caterham, and Warlingham), can evade treatment and exit the plant at concentrations that are likely to have adverse ecological impacts (Fig. 3 & 4). These results are consistent with independent chemical analysis of treated and untreated effluent from other areas (Du et al., 2014; Munro et al., 2019; Golovko et al., 2021; Rapp-Wright et al., 2022). An obvious implication of this finding is that reducing contaminant concentrations in subcatchment D could be expected to significantly reduce exposure to many chemicals downstream.

In contrast, sources of illicit drugs and salicylic acid are not dominated by a single subcatchment. They appear to have sources across multiple catchments. Consider that the first principal component of calculated source concentrations divides the Wandle catchment into two groups of subcatchments of concern, one is dominated by subcatchment D (and by inference the Beddington WWTP), and the other by more dispersed entry (e.g. CSO spills, sewer leaks, runoff, direct dumping). Reported rainfall and river flow rates were low during the acquisition of chemical measurements at localities A–J. A tentative comparison with more recent, and more complete, data suggests that CSO discharges may also have been low then (see Fig. S5–S6). However, information about dry weather discharges, and time-series of CSO spills during the 2019-2021 sampling period, is not available. A denser or more strategically-sited sampling campaign could help determine the source(s) of these chemicals. Options for improving source apportionment are explored in Sect. 4.4.

4.3. Environmental risks

Each of the chemicals inverted has distinct properties and uses, which can influence their environmental impact and ecotoxicological relevance. The potential risks associated with water entering the Wandle from each sub-catchment is explored. These risks are not the same as those calculated for the water in the main channel, which is an integrated signal of all upstream

areas. For example, if all of the water entering the channel in a particular subcatchment derives from a single tributary the risks calculated here correspond to the risks for the water in that tributary. Alternatively, if the subcatchment contributes water via surface run-off, these risks would correspond to that surface run-off. Correspondingly, risks in individual subcatchments could be higher than the main channel if they are subsequently diluted.

Estimated mean concentrations for some chemicals in source areas exceed toxicity thresholds indicated by PNEC. Calculated concentrations of acetamiprid and imidacloprid, for instance, exceed PNEC in most subcatchments. The respective calculated concentrations of acetamiprid and imidacloprid are more than 10 and 17 times PNEC in subcatchment D. Calculated risk quotients for these chemicals are *high* (Fig. 4). This result is primarily a concern for non-target insects. Imidacloprid is known to be highly toxic for invertebrates resulting in its ban for agricultural use since 2018. Its more recent appearance in river water has been interpreted as an indication that medication from companion animals (e.g. dog worming) is finding its way into waterways (Egli et al., 2023). Pharmaceuticals and illicit drugs are also of emerging concern due to potential effects on aquatic life and human health. Calculated concentrations of diclofenac exceed PNEC values in subcatchments D–J. They are almost ten, seven and two times PNEC in subcatchments D, I, and F and J, respectively. In fact, calculated risk quotients for diclofenac in all subcatchments are above *insignificant*. The recreational drug cocaine and its metabolite benzoylecgonine are monitored for their societal implications and potential environmental impact. They are also known to be highly toxic to Bacillariophyta and Chlorophyta phytoplankton (Chia et al., 2021). Calculated concentrations of cocaine and its metabolite benzoylecgonine are highest in subcatchment I, but still far lower than PNEC (Fig. 4). Calculated fluxes are the same order of magnitude (several kg/day) as estimates from the Po river in Milan (cf. Fig. 3 and Zuccato et al., 2005).

4.4. Optimal sampling strategies

The chemical concentrations inverted in this study are from a legacy dataset that was not collected with inverse source apportionment in mind. Future sampling strategies could be optimised for the source apportionment methods presented here. For example, our analysis has identified subcatchment A as a potential source of illicit drugs into the Wandle. Unfortunately, this particular subcatchment covers a large area. As such, ascribing sources to a specific pollutant pathway, for example a specific CSO or a misconnection, is severely limited by the distribution of sampling downstream.

Fig. 7 demonstrates how sampling strategies that prioritise equal-area apportionment (see Sect. 2.9) could yield better assessments of chemical concentrations in sources areas, with increasingly large numbers of samples. This approach is explored using the example of CSOs as potential point sources of an arbitrary, conservative and well-mixed, contaminant. The yellow crosses in Fig. 7 indicate the locations of CSOs in the Wandle catchment. Subcatchments are coloured yellow if they contain a CSO. Panel (a) shows the actual sample set used in this study. Note that most sub-catchments contain CSOs and therefore performing source apportionment on this dataset would struggle to uniquely identify them as a potential source of a contaminant. However, panels (b–d) indicate that by increasing the number of samples, and distributing them across the catchment such that they have approximately equal upstream area, locations of individual point sources can be better distinguished. Optimal sampling combined with the inverse approach developed in this study could provide practical means to identify and quantify contaminant sources throughout drainage networks.

5. Conclusion

Contaminant concentrations measured in waterways provide crucial information about pollutant sources upstream. Such information is central to mitigating contaminant risks for ecology and human health. To utilise such information it is necessary to first apportion the contaminant observations downstream to sources upstream. In this study, an inverse modelling strategy is applied for the first time to an urban river—the River Wandle, a tributary of the Thames, UK—to recover sources of thirteen chemical contaminants (including insecticides, pharmaceuticals and illicit drugs) measured along its drainage network.

Contaminant transport is assumed to be conservative and chemicals are assumed to be well mixed downstream. Source concentrations are assumed to not change as a function of time. These assumptions are tested by analysing the inter- and intra-site variance of measured concentrations and by inverting measurements from along the river for source concentrations. The recoverability of concentrations in the Wandle's source areas is demonstrated by first inverting synthetic data. The concentrations of the thirteen contaminants, measured at ten localities along the Wandle in 2020–2021, are then inverted. The inverse approach demonstrates how data and model uncertainties can be incorporated into source apportionment. Two distinct chemical contaminant pathways into the Wandle are identified. The first pathway corresponds to discharge of treated water from a subcatchment that contains the Beddington wastewater treatment plant. This plant appears to be the dominant source of the pharmaceuticals and insecticides measured in this study (e.g. imidacloprid, tramadol). The second pathway is more dispersed, indicating multiple points of entry for cocaine and its metabolite benzoylecgonine and some pharmaceuticals (e.g. salicylic acid) into the Wandle catchment. We tentatively suggest that this second pathway corresponds to untreated wastewater from sewerage misconnections, combined sewer overflow events, runoff or perhaps direct dumping.

Calculated sources are combined with estimates of *predicted no-effect concentrations* to estimate risk from contaminants throughout the Wandle. The results indicate that environments in source areas are at risk from a diverse suite of pharmaceuticals. We stress that the estimates of risk are mean values across entire subcatchments and that risks could be considerably higher or lower for tributaries within the subcatchments investigated. By combining recovered source concentrations with river discharge data the mass fluxes of all studied chemicals are calculated. To improve the resolution of the recovered sources, more samples are required. An objective method to identify potential future sample sites would better characterise pollutant sources in the Wandle, and other catchments. Combining optimal sampling strategies and inverse modelling of measured contaminant concentrations could identify the location and concentrations of contaminant sources in a wide variety of waterways globally.

Acknowledgements

We thank the Natural Environment Research Council for funding this work (NE/X010805/1).

Code and Data availability

Code to perform the source apportionment calculations (the inverse model) is available from `https://github.com/AlexLipp/faster-unmixer`. Code to identify localities that provide equal area sampling of a drainage network are available at `zenodo.org/records/7311352`. A high-level Python code providing a framework for the data analysis is available from

https://github.com/kmch/SourceApp. LIDAR digital elevation data used is available from https://environment.data.gov.uk/dataset/ce8fe7e7-bed0-4889-8825-19b042e128d2. Hydrosheds drainage data is available from https://www.hydrosheds.org. CSO event data is available from https://www.thameswater.co.uk, sublink: /about-us/performance/river-health/storm-discharge-data#annual-edm-reports. Environment Agency data for the Wandle catchment can be accessed at https://environment.data.gov.uk/catchment-planning/OperationalCatchment/3514. Weather data was accessed at http://nw3weather.co.uk/. The NORMAN ecotoxicology database that contains *predicted no-effect concentrations* of chemicals can be accessed at https://www.norman-network.com/nds/ecotox.

References

Aitchinson, J. (1983). Principal component analysis of compositional data. *Biometrika*, 70(1):57–65.

Aster, R. C., Borchers, B., and Thurber, C. H. (2005). *Parameter Estimation and Inverse Problems*. Elsevier, 1st edition.

Barnes, R. and Lipp, A. G. (sub.). Identifying tracer and pollutant sources in drainage networks from point concentration observations using an efficient convex unmixing scheme. *Submitted to Water Resources Research*.

Carraro, L., Mächler, E., Wüthrich, R., and Altermatt, F. (2020). Environmental DNA allows upscaling spatial patterns of biodiversity in freshwater ecosystems. *Nature Communications*, 11(1):3585.

Carraro, L., Stauffer, J. B., and Altermatt, F. (2021). How to design optimal edna sampling strategies for biomonitoring in river networks. *Environmental DNA*, 3(1):157–172.

Chen, K., meng Liu, Q., hua Peng, W., Liu, Y., and tao Wang, Z. (2023). Source apportionment of river water pollution in a typical agricultural city of Anhui Province, eastern China using multivariate statistical techniques with APCS–MLR. *Water Science and Engineering*, 16(2):165–174.

Chia, M. A., Lorenzi, A. S., Ameh, I., Dauda, S., Cordeiro-Araújo, M. K., Agee, J. T., Okpanachi, I. Y., and Adesalu, A. T. (2021). Susceptibility of phytoplankton to the increasing presence of active pharmaceutical ingredients (APIs) in the aquatic environment: A review. *Aquatic Toxicology*, 234:105809.

Christophersen, N., Neal, C., Hooper, R. P., Vogt, R. D., and Andersen, S. (1990). Modelling streamwater chemistry as a mixture of soilwater end-members — a step towards second-generation acidification models. *Journal of Hydrology*, 116(1):307–320.

Collins, A. L., Blackwell, M., Boeckx, P., Chivers, C.-A., Emelko, M., Evrard, O., Foster, I., Gellis, A., Gholami, H., Granger, S., Harris, P., Horowitz, A. J., Laceby, J. P., Martinez-Carreras, N., Minella, J., Mol, L., Nosrati, K., Pulley, S., Silins, U., da Silva, Y. J., Stone, M., Tiecher, T., Upadhayay, H. R., and Zhang, Y. (2020). Sediment source fingerprinting: benchmarking recent outputs, remaining challenges and emerging themes. *J Soil Sediments*, 20:4160–4193.

Comber, S. D. W., Smith, R., Daldorph, P., Gardner, M. J., Constantino, C., and Ellor, B. (2013). Development of a chemical source apportionment decision support framework for catchment management. *Environmental Science & Technology*, 47(17):9824–9832.

Cox, B. A. (2003). A review of currently available in-stream water-quality models and their applicability for simulating dissolved oxygen in lowland rivers. *Sci Total Environ.*, 314–316.

Dixon, W., Smyth, G. K., and Chiswell, B. (1999). Optimized selection of river sampling sites. *Water Research*, 33(4):971–978.

Domahidi, A., Chu, E., and Boyd, S. (2013). ECOS: An SOCP Solver for Embedded Systems. *2013 European Control Conference (ECC)*.

Du, B., Price, A. E., Scott, W. C., Kristofco, L. A., Ramirez, A. J., Chambliss, C. K., Yelderman, J. C., and Brooks, B. W. (2014). Comparison of contaminants of emerging concern removal, discharge, and water quality hazards among centralized and on-site wastewater treatment system effluents receiving common wastewater influent. *Science of The Total Environment*, 466-467:976–984.

Egli, M., Rapp-Wright, H., Oloyede, O., Francis, W., Preston-Allen, R., Friedman, S., Woodward, G., Piel, F. B., and Barron, L. P. (2023). A One-Health environmental risk assessment of contaminants of emerging concern in London's waterways throughout the SARS-CoV-2 pandemic. *Environment International*, 180(108210):108210.

Golovko, O., Örn, S., Sörengård, M., Frieberg, K., Nassazzi, W., Lai, F. Y., and Ahrens, L. (2021). Occurrence and removal of chemicals of emerging concern in wastewater treatment plants and their impact on receiving water systems. *Science of The Total Environment*, 754:142122.

Hobley, D. E. J., Adams, J. M., Nudurupati, S. S., Hutton, E. W. H., Gasparini, N. M., Istanbulluoglu, E., and Tucker, G. E. (2017). Creative computing with Landlab: An open-source toolkit for building, coupling, and exploring two-dimensional numerical models of Earth-surface dynamics. *Earth Surface Dynamics*, 5(1):21–46.

Lipp, A. G., Roberts, G. G., Whittaker, A. C., Gowing, C. J. B., and Fernandes, V. M. (2020). River Sediment Geochemistry as a Conservative Mixture of Source Regions: Observations and Predictions From the Cairngorms, UK. *Journal of Geophysical Research: Earth Surface*, 125(12).

Lipp, A. G., Roberts, G. G., Whittaker, A. C., and others (2021). Source region geochemistry from unmixing downstream sedimentary elemental compositions. *Geochem. Explor. Environ. Analy.*

Milledge, D. G., Lane, S. N., Heathwaite, A. L., and Reaney, S. M. (2012). A monte carlo approach to the inverse problem of diffuse pollution risk in agricultural catchments. *Science of The Total Environment*, 433:434–449.

Morris, D. G. and Flavin, R. W. (1994). Sub-set of the UK 50 m by 50 m hydrological digital terrain model grids. *NERC, Institute of Hydrology, Wallingford*.

Munro, K., Martins, C. P. B., Loewenthal, M., Comber, S., Cowan, D. A., Pereira, L., and Barron, L. P. (2019). Evaluation of combined sewer overflow impacts on short-term pharmaceutical and illicit drug occurrence in a heavily urbanised tidal river catchment (London, UK). *Science of the Total Environment*, 657:1099–1111.

O'Callaghan, J. F. and Mark, D. M. (1984). The extraction of drainage networks from digital elevation data. *Computer Vision, Graphics, and Image Processing*, 28(3):323–344.

O'Donoghue, B., Chu, E., Parikh, N., and Boyd, S. (2016). Conic Optimization via Operator Splitting and Homogeneous Self-Dual Embedding. *J Optim Theory Appl*, 169.

Palma, P., Köck-Schulmeyer, M., Alvarenga, P., Ledo, L., Barbosa, I., López de Alda, M., and Barceló, D. (2014). Risk assessment of pesticides detected in surface water of the alqueva reservoir (guadiana basin, southern of portugal). *Science of The Total Environment*, 488–489:208–219.

Parker, R. L. (1994). *Geophysical Inverse Theory*, volume 1. Princeton University Press.

Pedregosa, F., Varoquaux, G., Gramfort, A., Michel, V., Thirion, B., Grisel, O., Blondel, M., Prettenhofer, P., Weiss, R., Dubourg, V., Vanderplas, J., Passos, A., Cournapeau, D., Brucher, M., Perrot, M., and Duchesnay, E. (2011). Scikit-learn: Machine learning in Python. *Journal of Machine Learning Research*, 12:2825–2830.

Rapp-Wright, H., Regan, F., White, B., and Barron, L. P. (2022). A year-long study of the occurrence and risk of over 140 contaminants of emerging concern in wastewater influent, effluent and receiving waters in the republic of ireland. *Sci. Total Environ.*, page 160379.

Shapiro, N. and Ritzwoller, M. (2002). Monte-Carlo inversion for a global shear-velocity model of the crust and upper mantle. *Geophysical Journal International*, 151(1):88–105.

Singhal, A., Jaseem, M., Divya, Sarker, S., Prajapati, P., Singh, A., and Jha, S. K. (2023). Identifying potential locations of hydrologic monitoring stations based on topographical and hydrological information. *Water Resources Management*.

Taylor, J. R. (1997). *An introduction to error analysis: the study of uncertainties in physical measurements*. University Science Books, 2 edition.

Weltje, G. J. (1997). End-member modeling of compositional data: Numerical-statistical algorithms for solving the explicit mixing problem. *Math. Geol.*, 29:503–549.

Zhou, G., Chen, S., Li, A., Xu, C., Jing, G., Chen, Q., Hu, Y., Tang, S., Lv, M., and Xiao, K. (2023). Pollution source apportionment of river tributary based on pmf receptor model and water quality remote sensing in xinjian river, china. *Water*, 15(1).

Zuccato, E., Chiabrando, C., Castiglioni, S., Calamari, D., Bagnati, R., Schiarea, S., and Fanelli, R. (2005). Cocaine in surface waters: a new evidence-based tool to monitor community drug abuse. *Environmental Health*, 4:14.

Submitted to Science of The Total Environment

Supporting Information for "Apportioning sources of chemicals of emerging concern along an urban river with inverse modelling"

Kajetan Chrapkiewicz[1,*], Alex G. Lipp[2], Leon P. Barron[3], Richard Barnes[4], and Gareth G. Roberts[1,*]

[1]*Department of Earth Sciences and Engineering, Imperial College London, London, UK*
[*]*Corresponding authors: k.chrapkiewicz17@imperial.ac.uk, gareth.roberts@imperial.ac.uk*
[2]*Merton College, University of Oxford, Oxford, UK*
[3]*MRC Centre for Environment and Health, Imperial College London, UK*
[4]*Lawrence Berkeley National Laboratory, USA*

Introduction
This document contains 42 additional figures referred to in the body text and figure captions of the main manuscript.

Fig. 1–2 provide additional information about sampling localities in the context of the Thames basin and the schedule of sampling at localities A–J along the Wandle tributary (see Fig. 1 of main manuscript).

Fig. 3 summarises concentrations for all chemicals measured by Egli et al. (2023), which provide the data used in this study and contextual information. Note that the 13 chemicals inverted in this study (indicated by red arrows in Fig. 3) include those with highest concentrations and a selection of other pharmaceuticals and illicit drugs chosen for their potential for significant risk, or so that we can assess results from inverting chemicals with different affinities and concentrations.

Fig. 4 summarises combined sewer overflow events in the Wandle catchment during the years of the sampling campaigns (2020-2021) recorded in the Events Duration Monitor (EDM) Annual Return reports of Thames Water. Unfortunately, no data on specific discharge date and times are available for this period.

Fig. 5 shows the correlation between the rainfall (measured by a single weather station in North London) and a number of all starts of CSO discharges recorded by Event Duration Monitoring by Thames Water company. Note that, the EDM service started in April 2022 and does not cover the period of our sampling campaigns.

Fig. 6 shows rainfall and flow rate during the the period of the sampling campaigns in 2020 and 2021 (top and bottom panel, respectively). It suggests that few, if any at all, CSOs have been recorded in our dataset. The most likely dates seem to be 27-10-2020 and 28-11-2021, potentially

also 13-11-2021.

Fig. 7-19 show the spatio-temporal distribution of measured concentrations of acetamiprid, azithromycin, carbamazepine, clarithromycin, cocaine, diclofenac, salicylic acid, sulfamethoxazole, tramadol, trimethoprim and venlafaxine in the Wandle catchment.

Fig. 20-32 show source apportionment and uncertainties from inverse modelling of the chemical data shown in Fig. 7-19. Results for imidacloprid and benzoylecgonine are summarised in Fig. 3 of the main manuscript.

Fig. 33 summarises calculated (source) concentrations in subcatchments A–J and associated uncertainties. These values were used to estimate risk quotients shown in Fig. 4 of the main manuscript.

Fig. 34 shows the results from inverse modelling of synthetic 'data' to test the recovery of source concentrations from perfect data (i.e. when downstream concentrations are entirely determined by the forward model, see main manuscript). It also shows the role regularisation plays in determining calculated source concentrations. In this example, the 'true' concentration in subcatchment D (between localities C and D) is set to be arbitrarily high (1000 ng/l), concentrations in all other catchments are arbitrarily low (1 ng/l). The forward model then uses these concentrations to calculate concentrations at localities A–J. As expected, calculated concentrations at localities A–C are very low, whereas concentrations are highest at locality D, and thence decrease downstream. Inversion of this noise-free 'data' gives a perfect recovery of source concentrations provided that regularisation is switched off ($\lambda = 0$). High concentrations in subcatchment D, and low concentrations in basins upstream are accurately predicted for all values of regularisation parameter λ tested. In contrast, as this figure shows, increasing its value (and hence the 'strength' of regularisation) systematically smears predicted source concentrations downstream.

Fig. 35 shows results of tests that seek to establish impact of noisy data on source apportionment. Noise commensurate with intra-site (within locality) variance of imidacloprid field data are randomly added to the 'true' concentrations determined by the forward model shown in Fig. 34 of this document. 10^4 noisy data sets are thus inverted and their results are summarised in this figure. Note that peak amplitude in source areas (subcatchment D) is slightly under-recovered, which we attribute to the finite number of inversions incorporated into the Monte Carlo experiment. These results indicate that concentration measurements at localities downstream can be reliably inverted for source concentrations, and their uncertainties estimated, even in the presence of realistic uncertainties.

Fig. 36–37 show resolution matrices generated by inverting noise-free and noisy synthetic data, respectively. The resolution matrix $\mathbf{R}$ provides a quantitative measure of the inverse model's ability to resolve model parameters, i.e. subcatchment concentrations, c_i (Aster et al., 2005). We define $\mathbf{R}\mathbf{c}_{\text{true}} = \mathbf{c}$, where $\mathbf{c}$ and $\mathbf{c}_{\text{true}}$ are the respective vectors of true and recovered subcatchment concentration. Each column of the matrix represents a calculated subcatchment concentration in the solution of the inverse model. A perfectly resolved model (i.e. a model in which calculated concentrations are equal to true concentrations) would result in a diagonal matrix. Off-diagonal elements with values $R_i \neq 1$ indicate 'cross-talk' between subcatchments, where a perturbation to

concentrations in one subcatchment influences calculated values in another. The magnitude of the off-diagonal elements provides insight into interdependence among subcatchments in the inversion process. Resolution matrices are calculated by performing a series of spike tests similar to the ones shown in Fig. 34 and 35. Each spike test involved setting concentration in a single subcatchment to 1000 ng/l, whilst keeping all others constant (at 10 ng/l). The resultant concentrations at localities downstream were then inverted to assess resolution of recovered source concentrations (see body text of main manuscript for extended description of these experiments). Note, 1000 ng/l and 10 ng/l values in the plots correspond to 1 and 0 values in the mathematical definition of $\mathbf{R}$.

Results are shown for three different values of the regularisation parameter: $\lambda = 10^{-6}, 10^{-4}$ and 10^{-2}. In the case of noise-free data and variable fluxes (top panel of Fig. 36), perturbation of the most upstream subcatchment A introduces artefacts in all other basins downstream. High concentration in subcatchment A causes the inverse model to erroneously assign increased concentrations in all other basins (first column of the top-right matrix). The error decreases with weaker regularisation. Similar, but much more subtle effects, can be observed for other subcatchments. For instance, subcatchment D exhibits the second-largest artefacts after A, despite having a smaller area than G. Interestingly, the true spike in I is 'recovered' in H rather than in its true position. Note that in all cases the largest errors are found in the most downstream subcatchments I–J.

We also investigated the impact of effective subcatchment area (export rates) on inverse modelling results. Equal fluxes from each subcatchment are simulated by setting the export rate of a given subcatchment to the reciprocal of its area. The lower row of panels in Fig. 36 show that, in this case, errors are close to zero in all basins for regularisation parameter values smaller than or equal to 10^{-4}. For the highest values tested, residual misfit is smaller than in the case of variable export rates except for the most downstream subcatchments G–J. The more downstream the subcatchment, the more it affects its immediate downstream neighbour and the less it impacts those further away. For example, subcatchment A (weakly) affects all basins and H (strongly) affects I but not J. When noise is added commensurate with imidacloprid field data, smearing of calculated concentrations is observed up- and downstream when subcatchment fluxes are not equal (top panel of Fig. 37). Concentrations in subcatchments D, G and H are best recovered, however underrecovery is present in each case. Unlike the noise-free case, the strongest regularisation suppresses the high-amplitude artifacts in most downstream subcatchments, however it introduces small errors upstream.

In summary, inverse modelling of synthetic data indicates that inverting real chemical data could be expected to recover the locations and concentrations of contaminants in source areas, and that increasing noise and regularisation 'smears' calculated concentrations between nearby subcatchments, as expected. The results also indicate that source apportionment is sensitive to subcatchment export rates.

Fig. 38 shows results from inverse modeling of imidacloprid using different values of regularisation parameter λ. The regularisation methodology and results are discussed in the main manuscript.

Fig. 39-41 show results from inverse modelling of data with different assumed lower limits of detection (LLOD) for imidacloprid. Changing the LLOD affects the data uncertainty of the most

upstream samples (A–C), which results in spread of the recovered models that increases with decreasing LLOD values. Remarkably, the peak concentrations (subcatchment D) remain approximately the same across all test cases.

Fig. 42 shows results from inverse modelling of benzoylecgonine data with export rate in subcatchment A reduced by a factor of 100. These results demonstrate that reducing export rate from subcatchment A can yield very low residual misfit in this case.

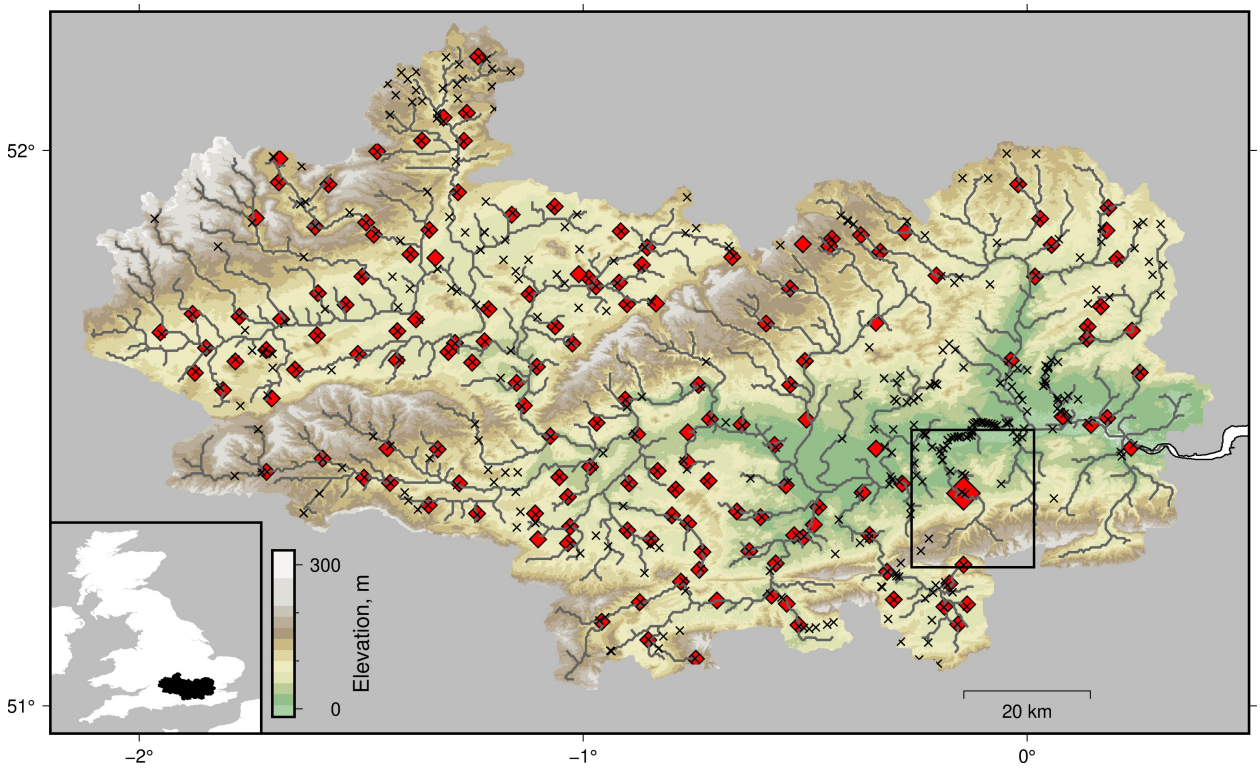

Figure 1: **Thames drainage basin study area.** Red diamonds = 153 Thames Water waste water treatment facilities (WWTP). Large red diamond = Beddington WWTP. x = Combined Sewer Overflows that were active at any time between 17 April 2022 and 14 November 2023 (see body text of main manuscript for details). Black box atop main panel shows location of maps in subsequent figures. Rivers and basin outline are from Hydrosheds. Inset map shows location of Thames basin.

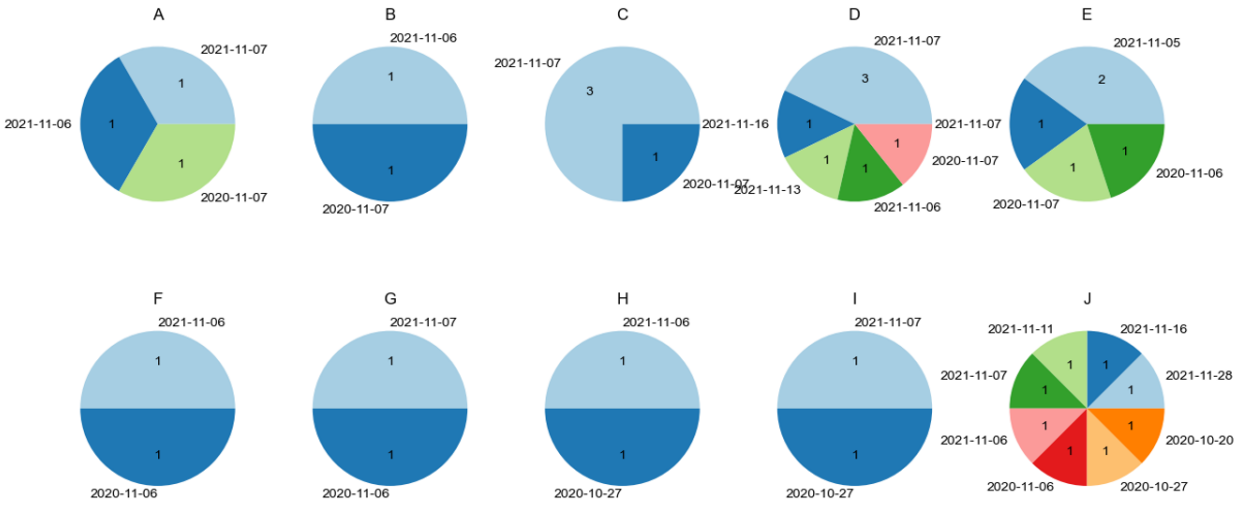

Figure 2: **Sampling history for each locality (A–J) of the Wandle dataset** (see Fig. 1 of main manuscript). Numbers within segments indicate number of samples acquired on one day. Note that all localities were sampled in 2020 and 2021.

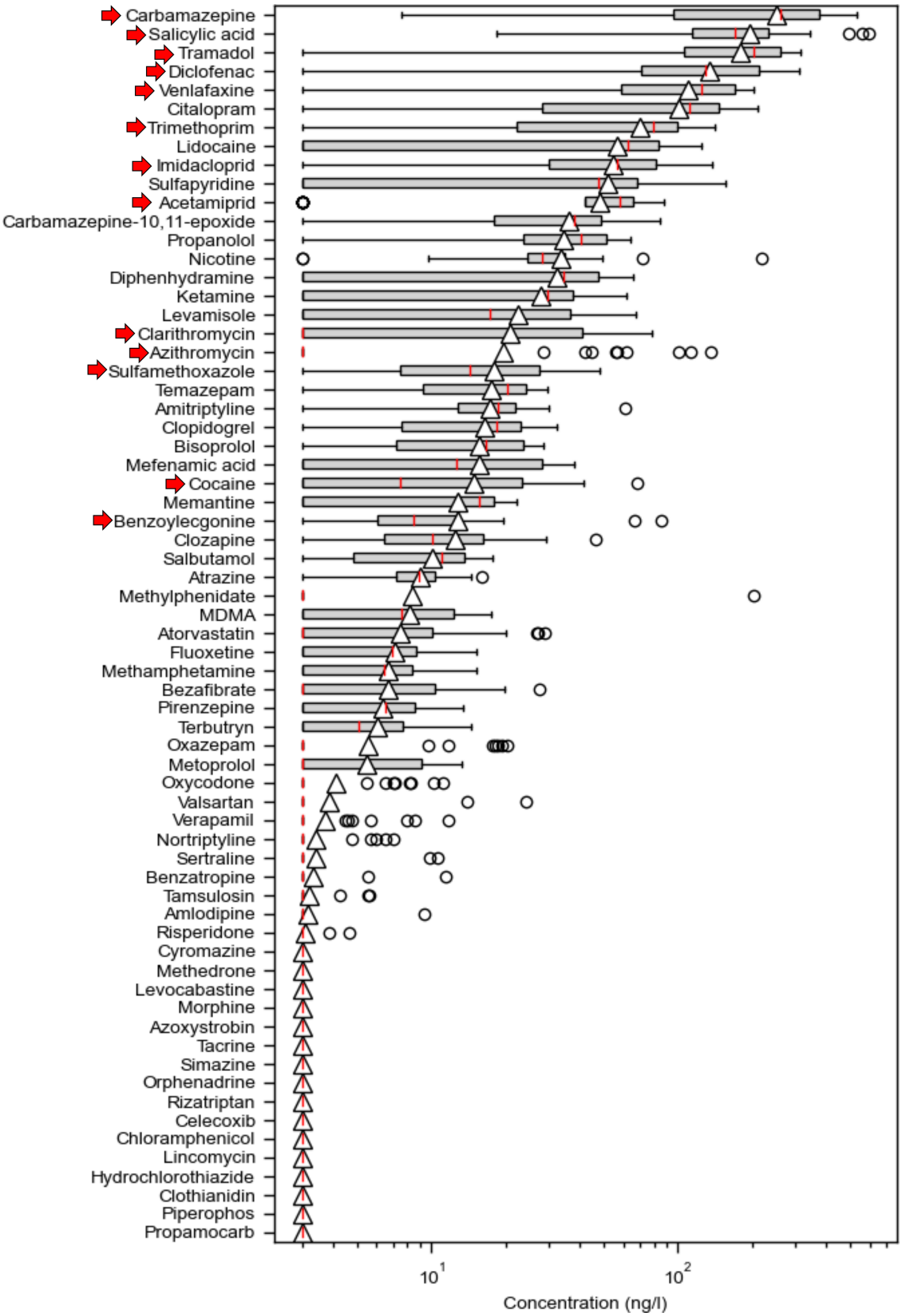

Figure 3: **Concentrations for all chemicals analysed in Egli et al. (2023).** Red arrows = chemicals inverted for source apportionment in this study. See Fig. 2a in main manuscript for extended caption.

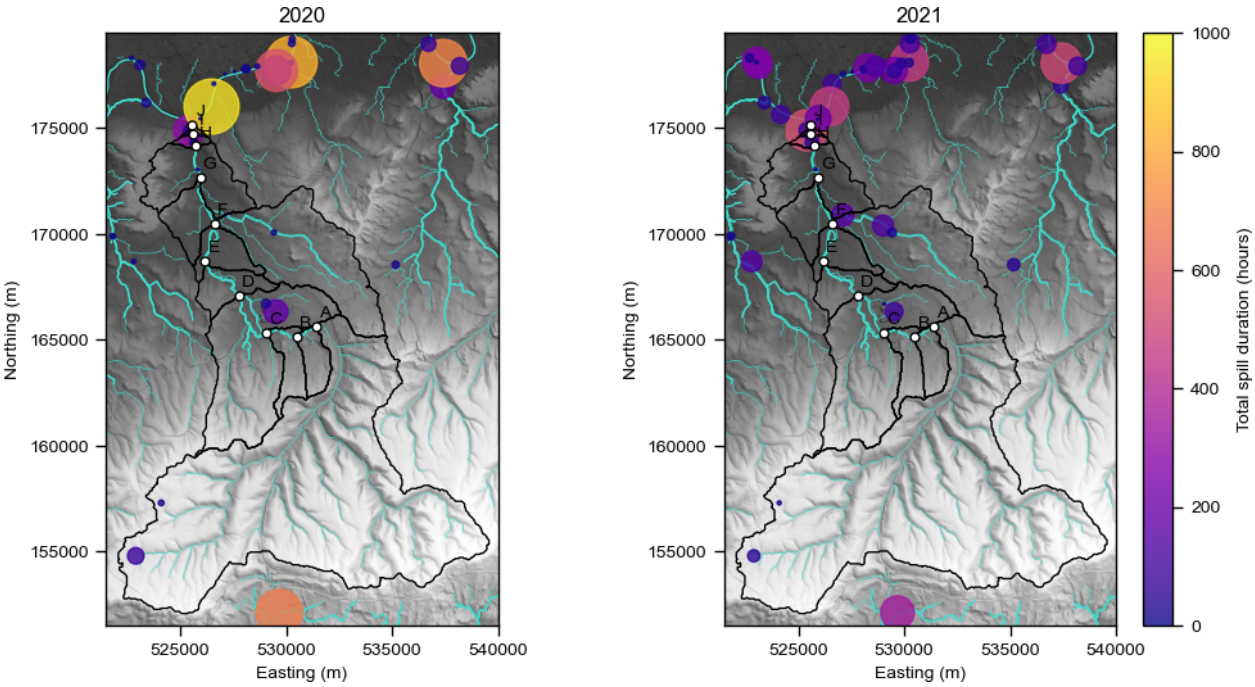

Figure 4: **Combined sewer overflows in 2020 (left) and 2021 (right) from the event duration monitoring Annual Return reports of Thames Water**. Accessed 22-11-2023.

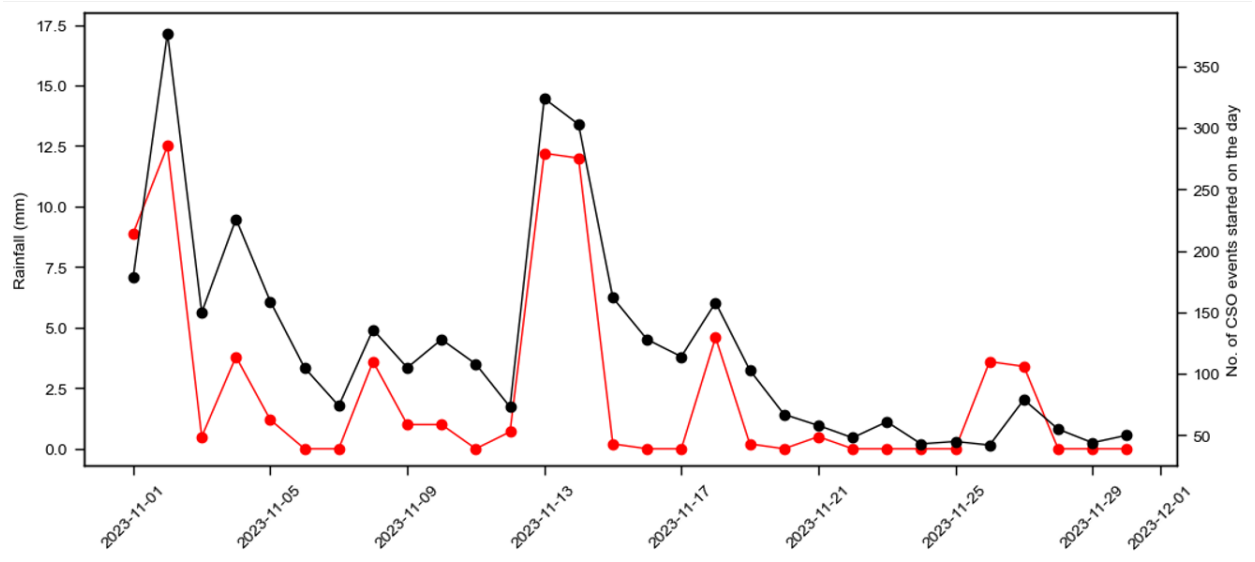

Figure 5: **Combined sewer overflows (black) in 2023 from the real-time event duration monitoring of Thames Water** overlain on daily rainfall data (red) from a semi-professional weather station (http://nw3weather.co.uk/) in Hampstead Heath, London (lat= 51.556, lon=−0.155). Both datasets were accessed on 28-12-2023.

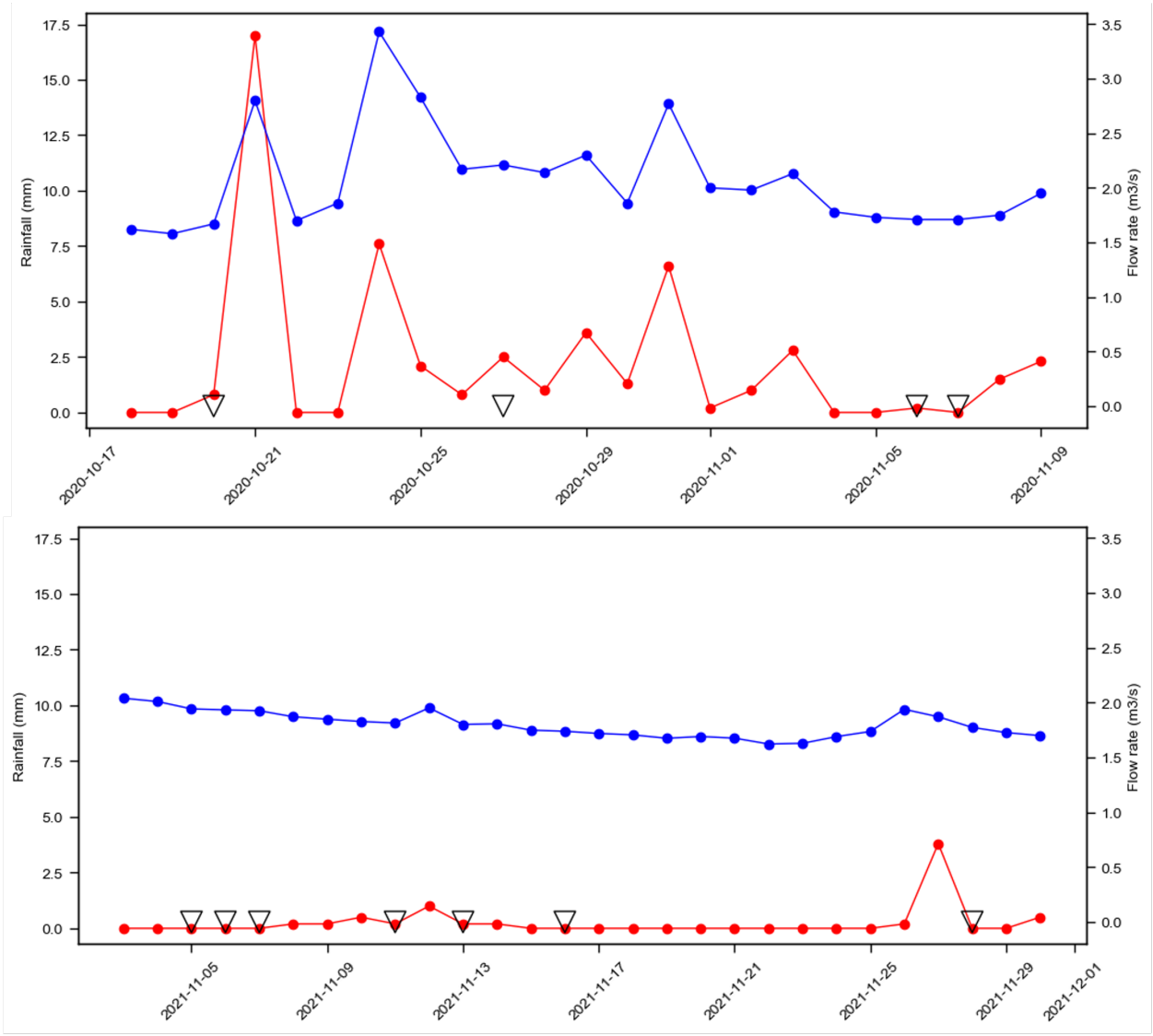

Figure 6: **Rainfall (red) and flow-rate (blue) during the sampling campaigns**. The sampling days are marked with white triangles. Source of the rainfall data same as in Fig. 5. The daily flow-rate data comes from the UK-CEH's gauge station no. 39003 (see Fig. 1 of the main manuscript). Both datasets were accessed on 28-12-2023.

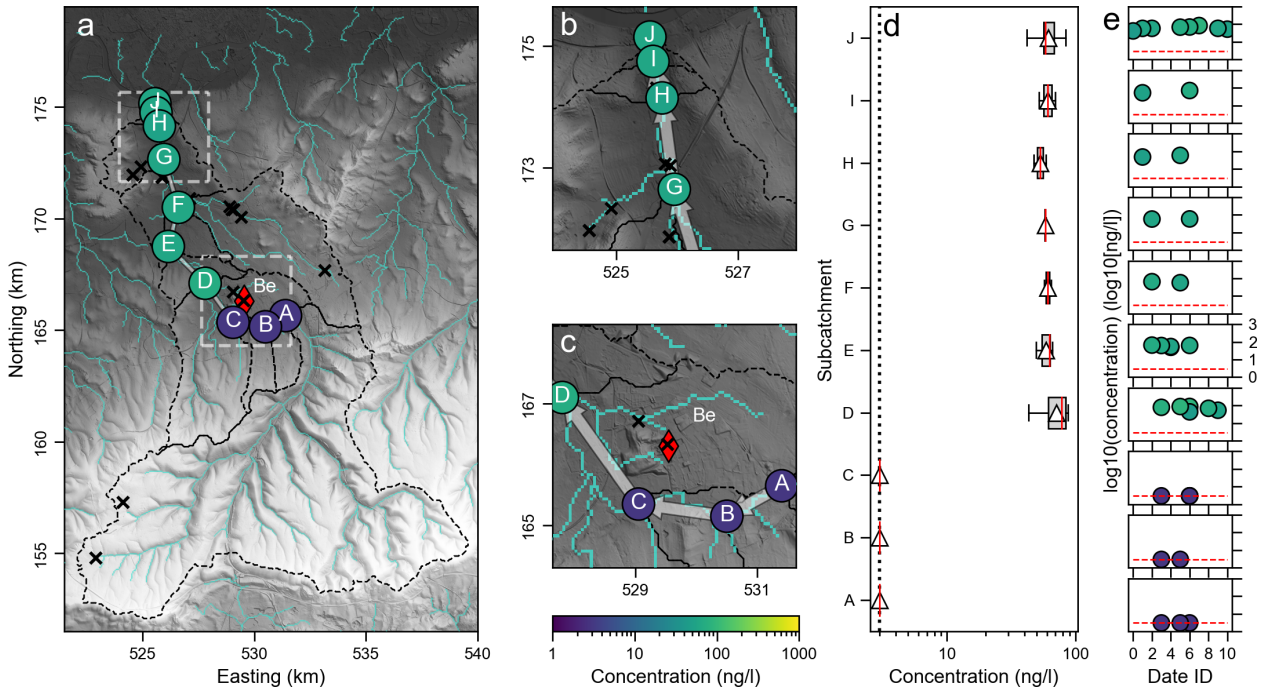

Figure 7: **Measured acetamiprid concentrations along the Wandle river.** (a) Turquoise curves = drainage network. Circles = mean chemical concentrations at localities indicated by circles labelled A–J, coloured by concentration. Thin dashed contours = upstream drainage areas unique to each sampling locality. Gray scale = hill-shaded digital elevation model. Thick dashed squares = location of maps shown in panels b and c. Red diamond = Beddington (Be) WWTP. x = CSOs. (b-c) Sampling localities and drainage network at confluence with Thames and around the Beddington WWTP. (d) Concentrations of samples at each locality: triangles = mean values; red line = median; box encloses 25th to 75th percentiles; whiskers = full range; circles = outliers. (e) Concentration for individual samples at each locality; sample dates (Date ID) are as follows, 0: 2020-10-20, 1: 2020-10-27, 2: 2020-11-06, 3: 2020-11-07, 4: 2021-11-05, 5: 2021-11-06, 6: 2021-11-07, 7: 2021-11-11, 8: 2021-11-13, 9: 2021-11-16, 10: 2021-11-28.

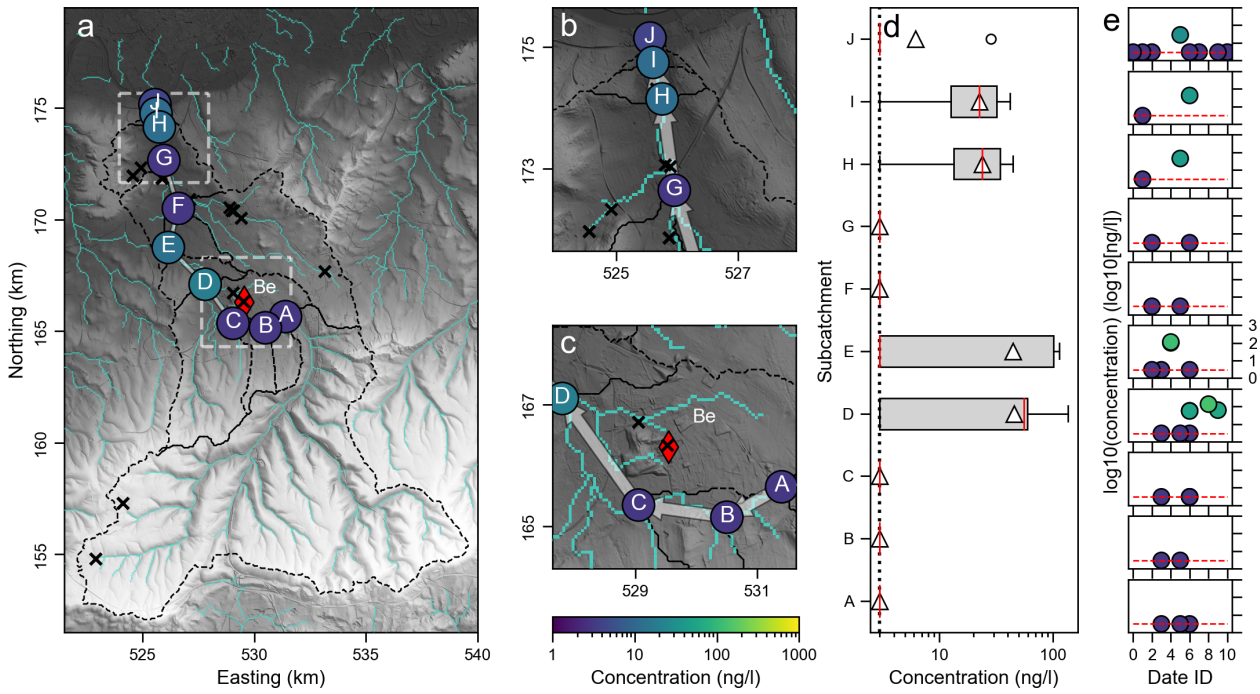

Figure 8: **Measured azithromycin concentrations.** See Fig. 7 for extended caption.

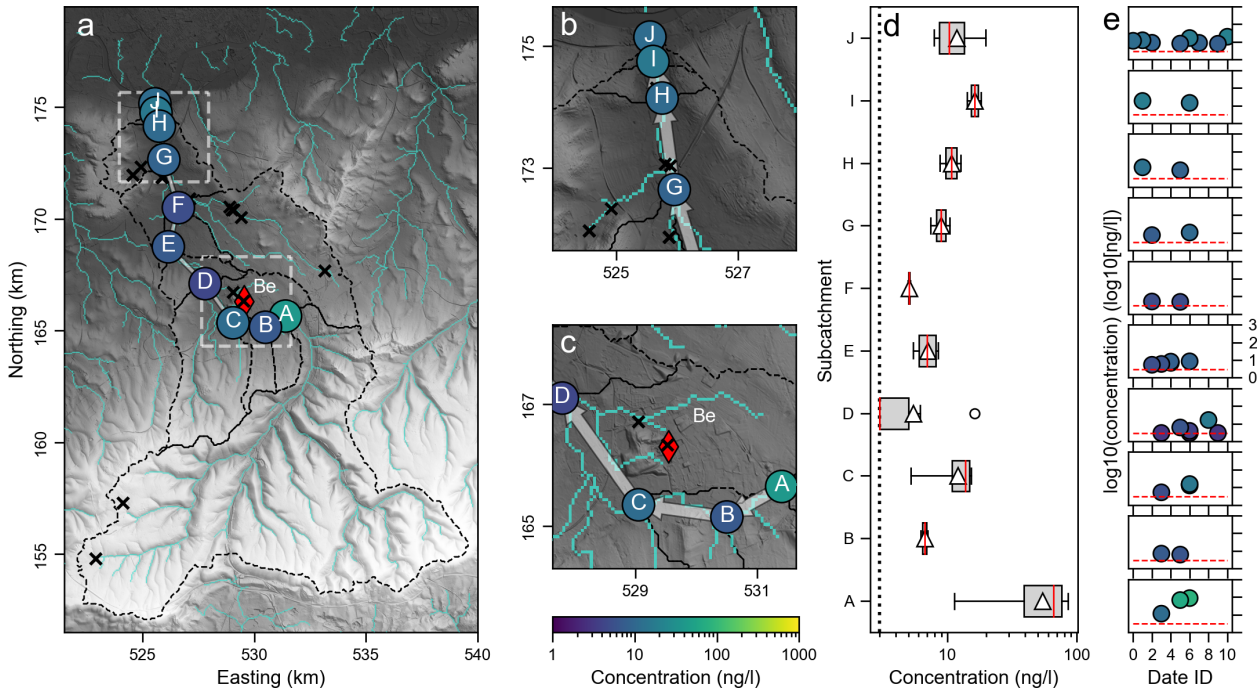

Figure 9: **Measured benzoylecgonine concentrations.** See Fig. 7 for extended caption.

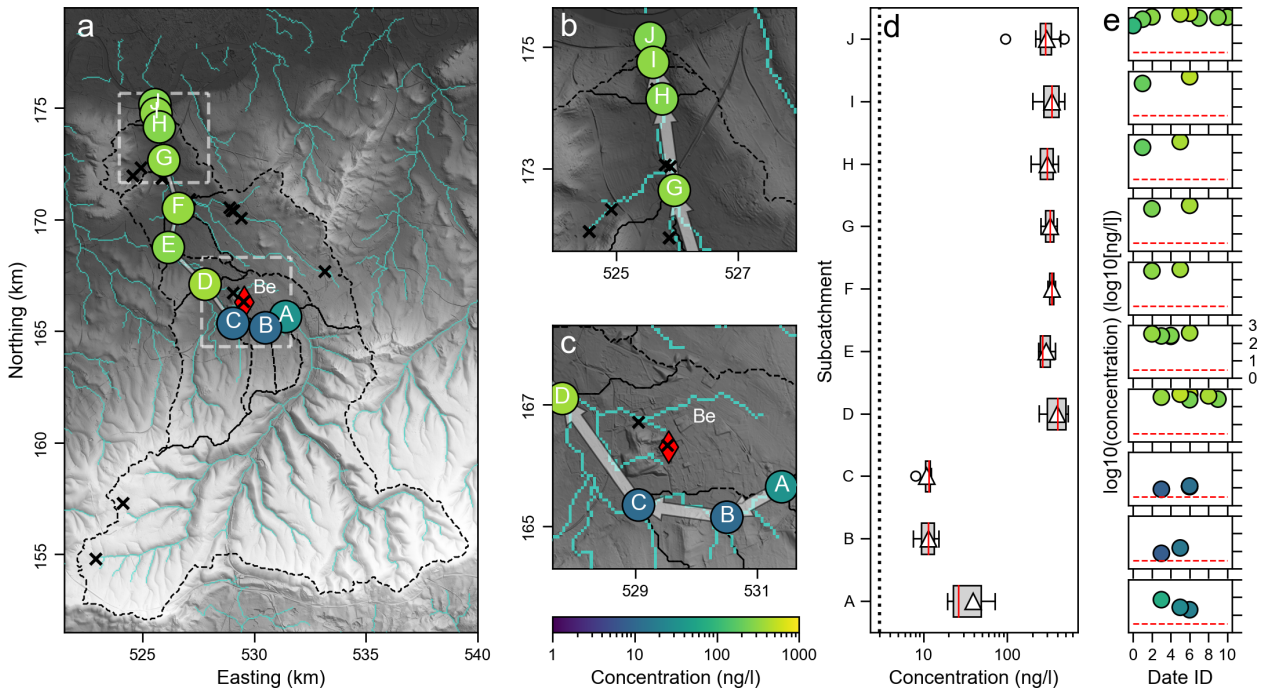

Figure 10: **Measured carbamazepine concentrations.** See Fig. 7 for extended caption.

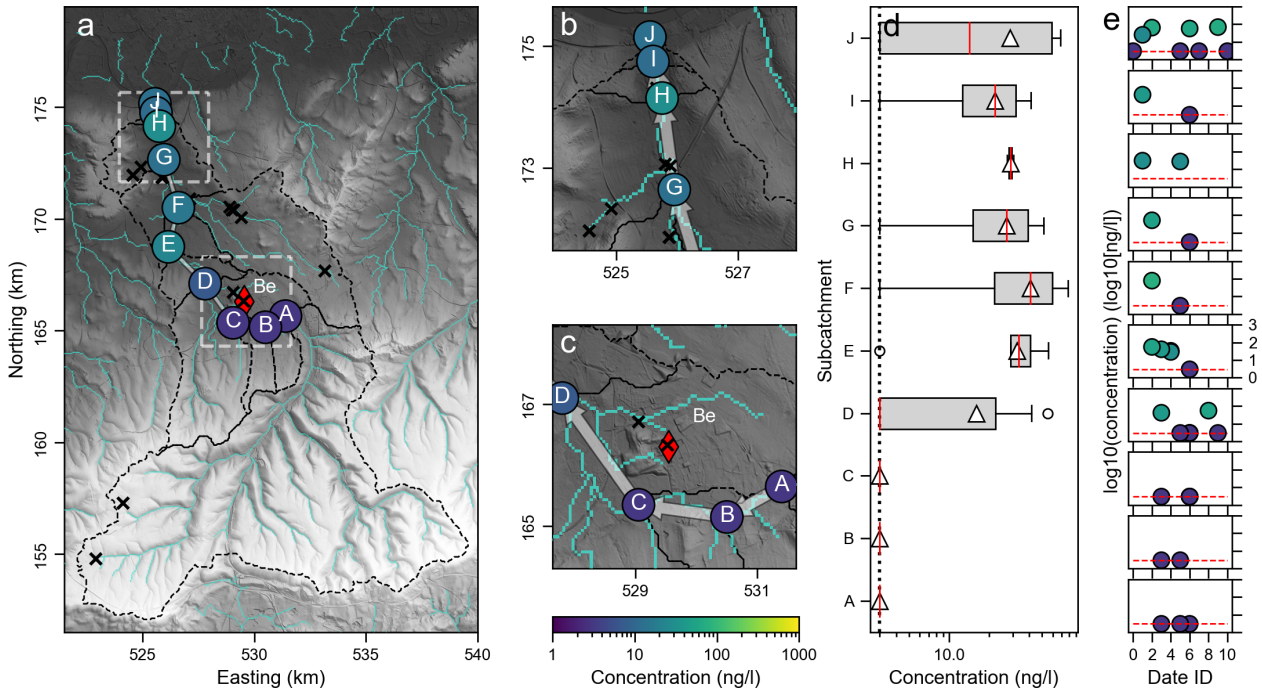

Figure 11: **Measured clarithromycin concentrations.** See Fig. 7 for extended caption.

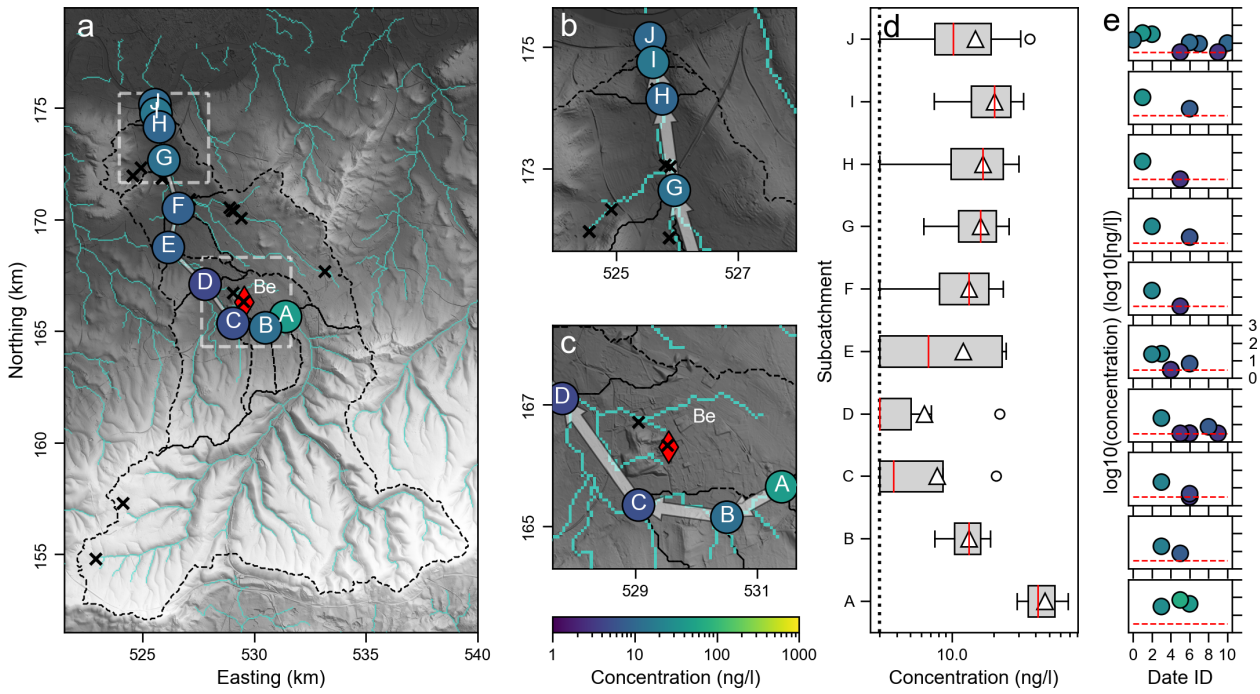

Figure 12: **Measured cocaine concentrations.** See Fig. 7 for extended caption.

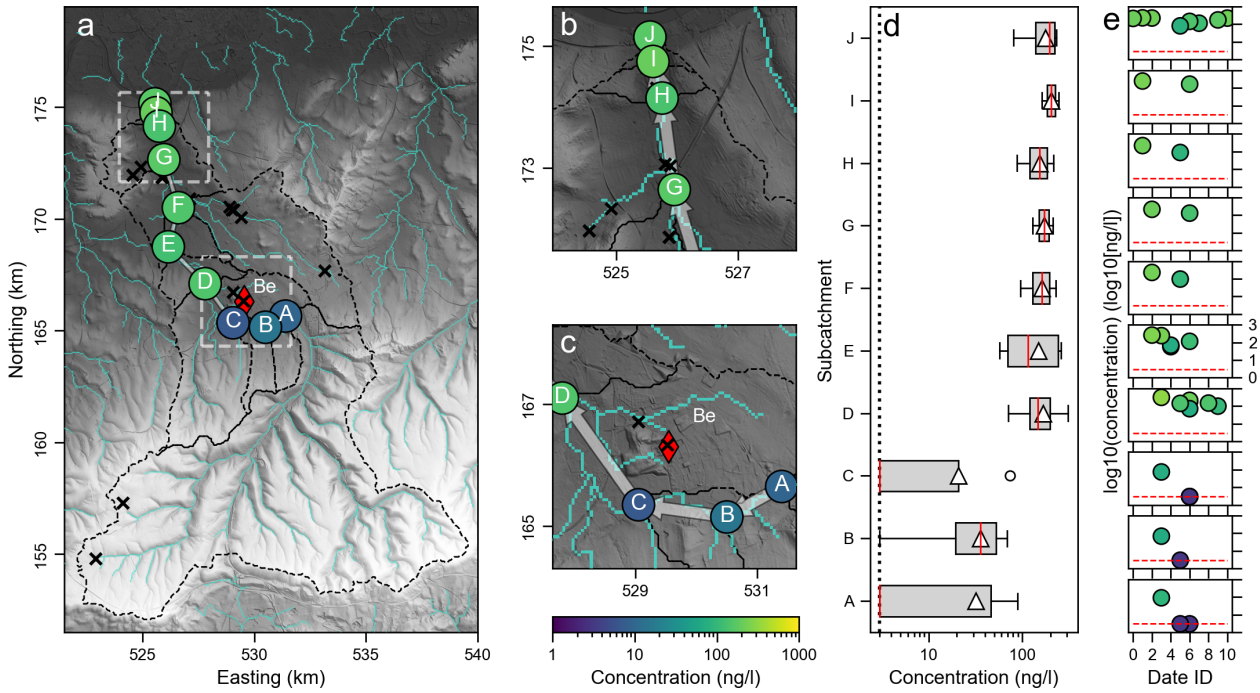

Figure 13: **Measured diclofenac concentrations.** See Fig. 7 for extended caption.

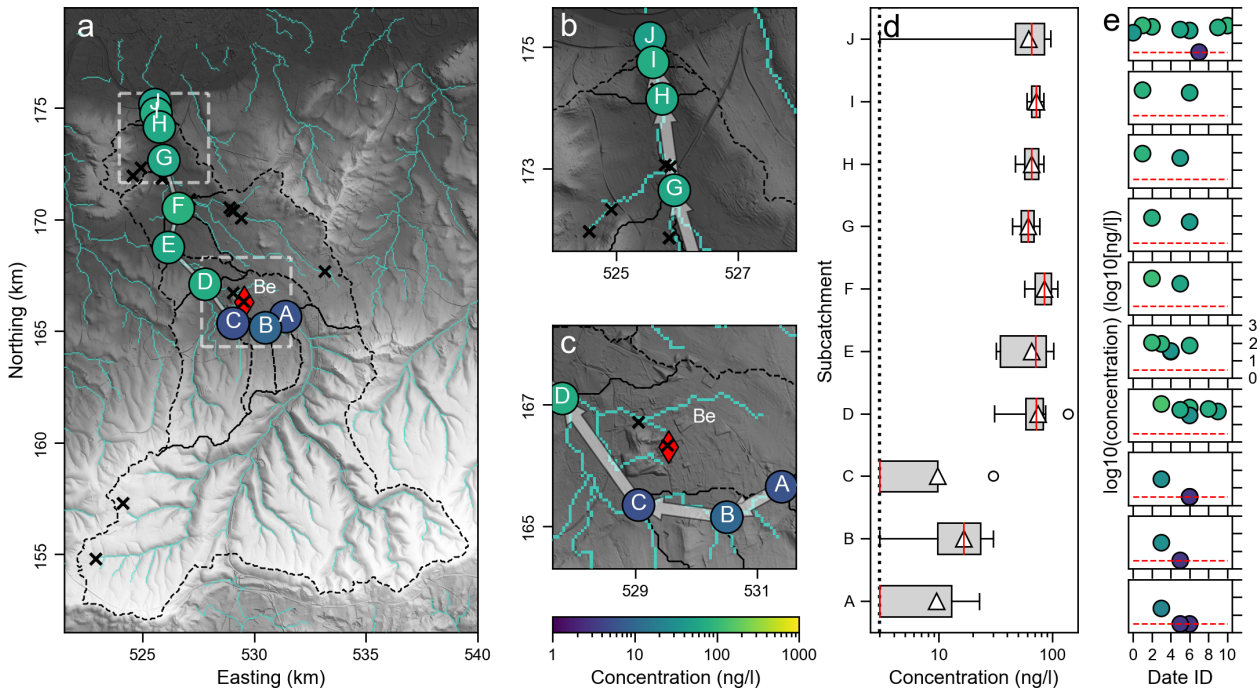

Figure 14: **Measured imidacloprid concentrations.** See Fig. 7 for extended caption.

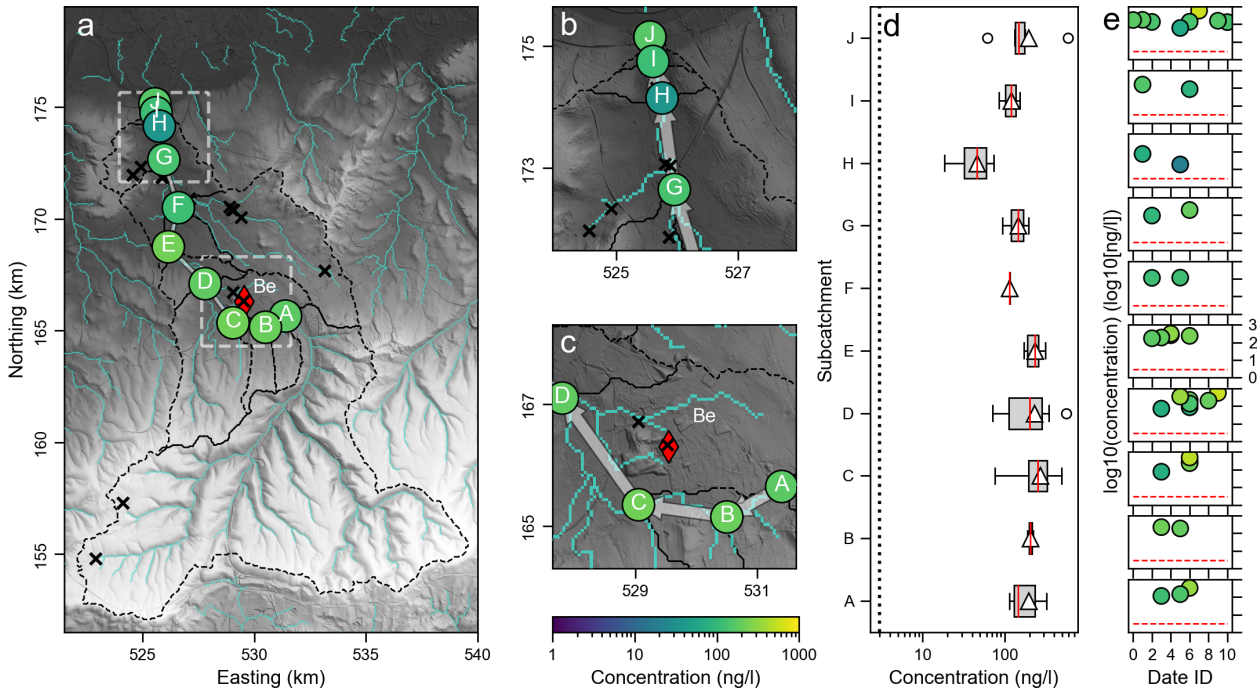

Figure 15: **Measured salicylic acid concentrations.** See Fig. 7 for extended caption.

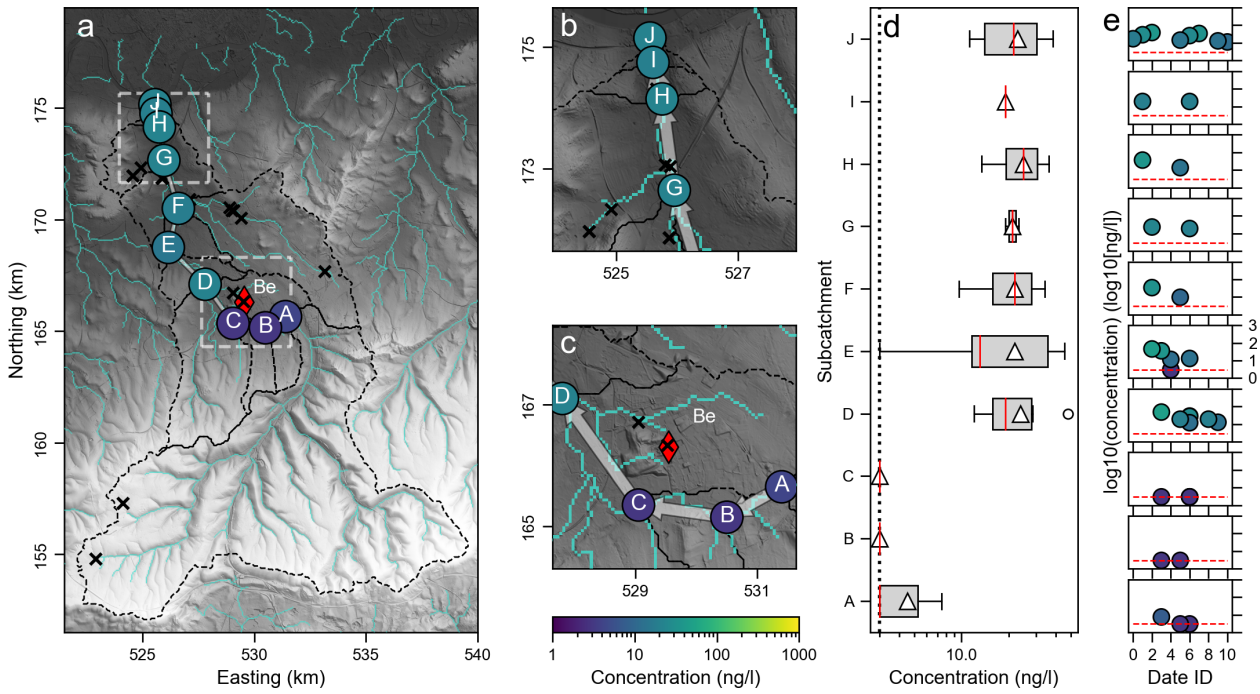

Figure 16: **Measured sulfamethoxazole concentrations.** See Fig. 7 for extended caption.

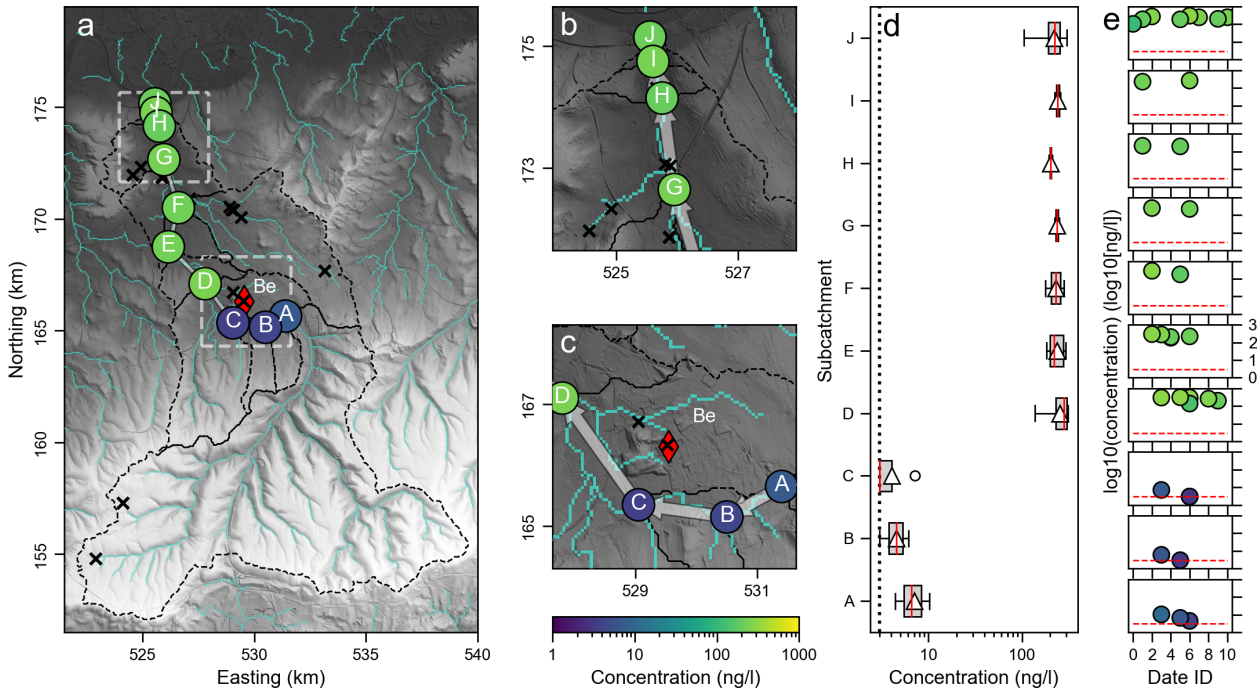

Figure 17: **Measured tramadol concentrations.** See Fig. 7 for extended caption.

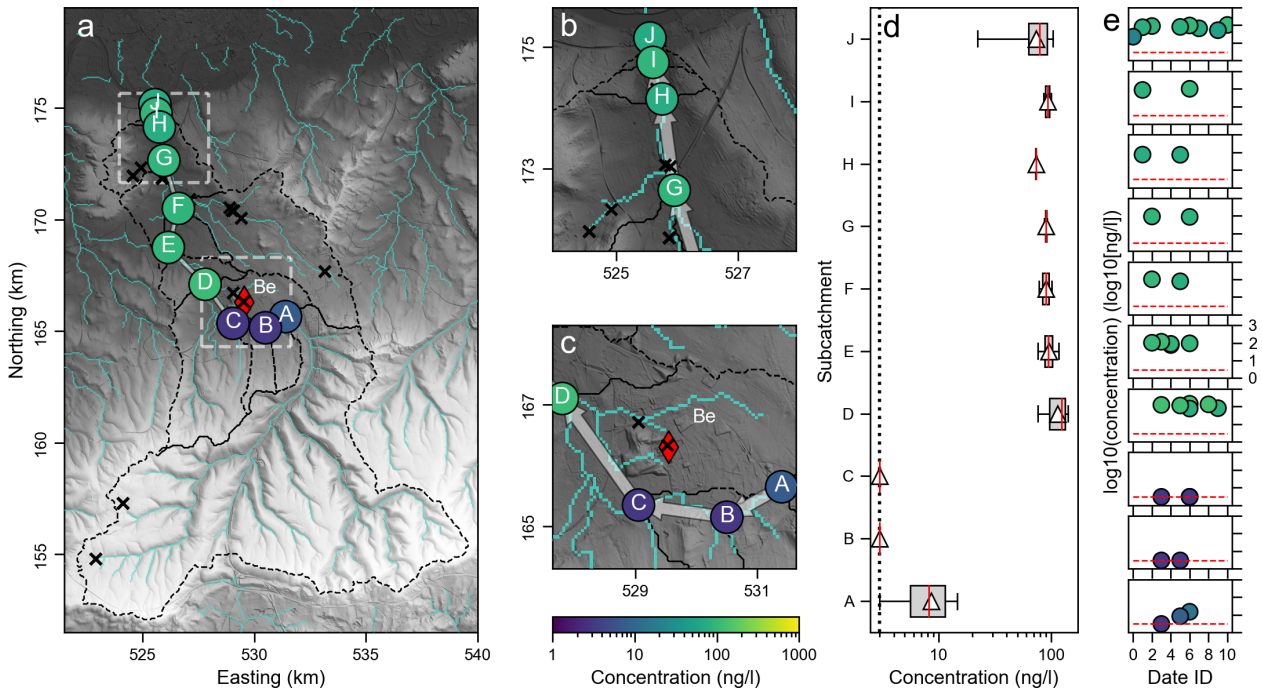

Figure 18: **Measured trimethoprim concentrations.** See Fig. 7 for extended caption.

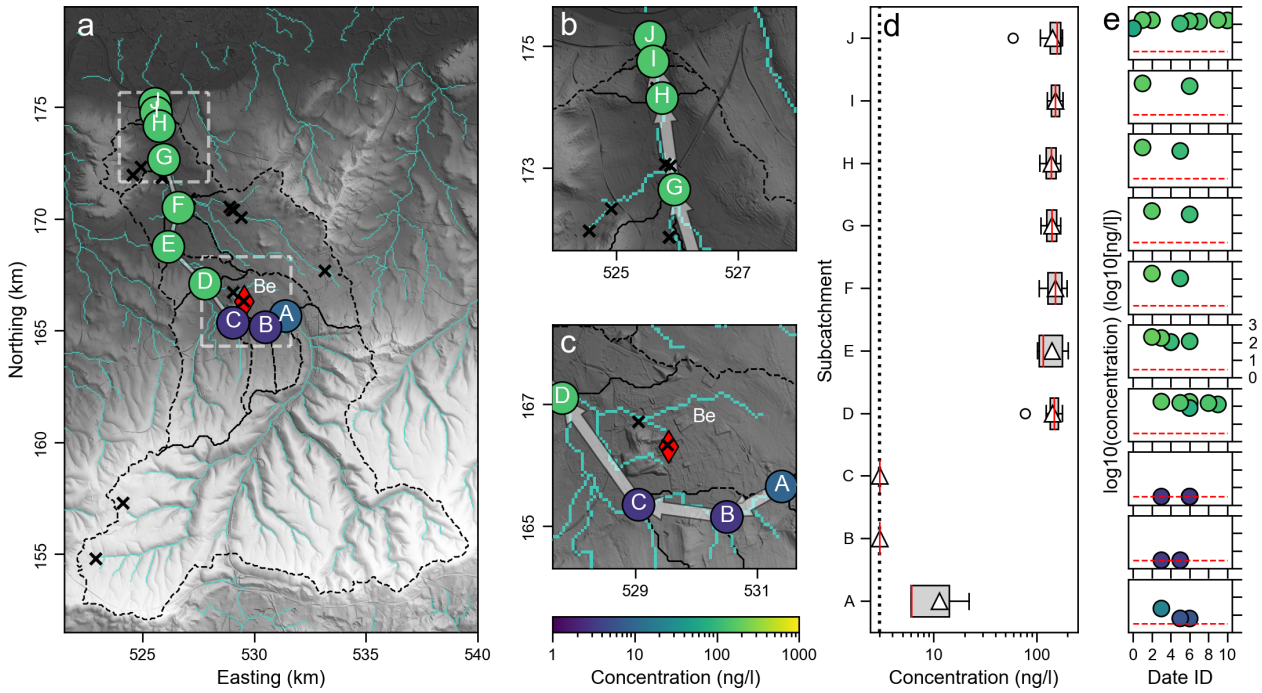

Figure 19: **Measured venlafaxine concentrations.** See Fig. 7 for extended caption.

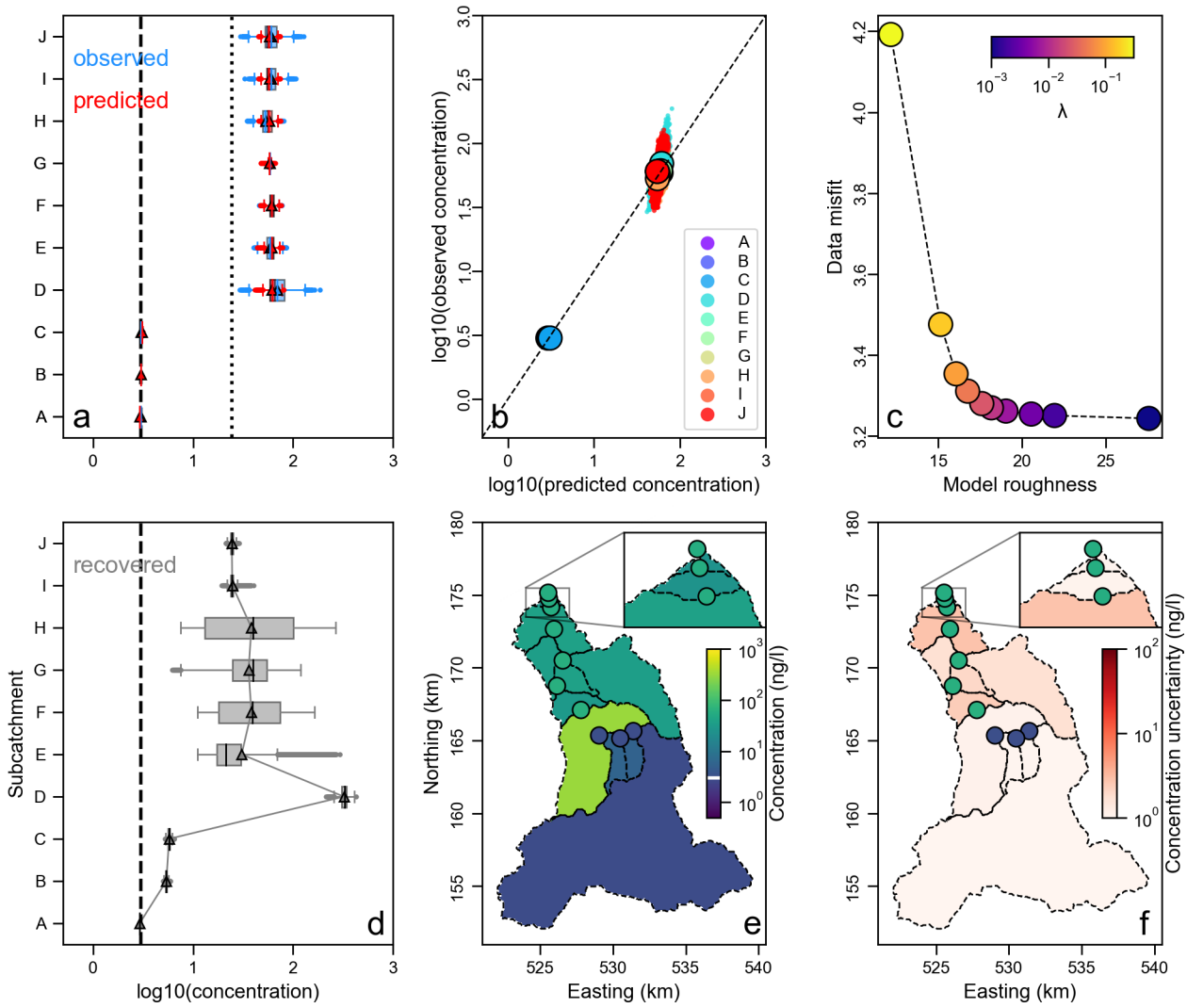

Figure 20: **Objective source apportionment of acetamiprid.** (a) Blue = observed chemical concentrations at sample sites A–J (see Fig. 7); triangles = mean values; boxes enclose 25$^{\text{th}}$ to 75$^{\text{th}}$ percentile; whiskers = full range; circles = outliers; dashed black line = detection limit (LLOD); dotted black line = geometric mean of observed concentrations. Red = downstream concentrations at sample localities A–J predicted from upstream source concentrations that best-fit the observations by solving the forward problem (see body text of main manuscript for details). (b) Observed vs. predicted concentrations at sample localities (coloured points) from Monte Carlo inversion incorporating uncertainties in measured concentrations; coloured circles = mean misfit for each sample. Dashed line = 1:1 correlation. (c) Trade-off between the model roughness and data misfit due to regularisation (colours). (d) Predicted concentrations in each subcatchment for optimal regularisation ($\lambda = 10^{-1.7}$; see panel c; symbols are as for panel a). Dashed black line = detection limit (LLOD). (e) Mean predicted concentrations in each subcatchment for optimal regularisation. Coloured circles = mean observed concentrations at sample localities. (f) Standard deviations of predicted source concentrations (see body text for details). White line on colour bar = detection limit.

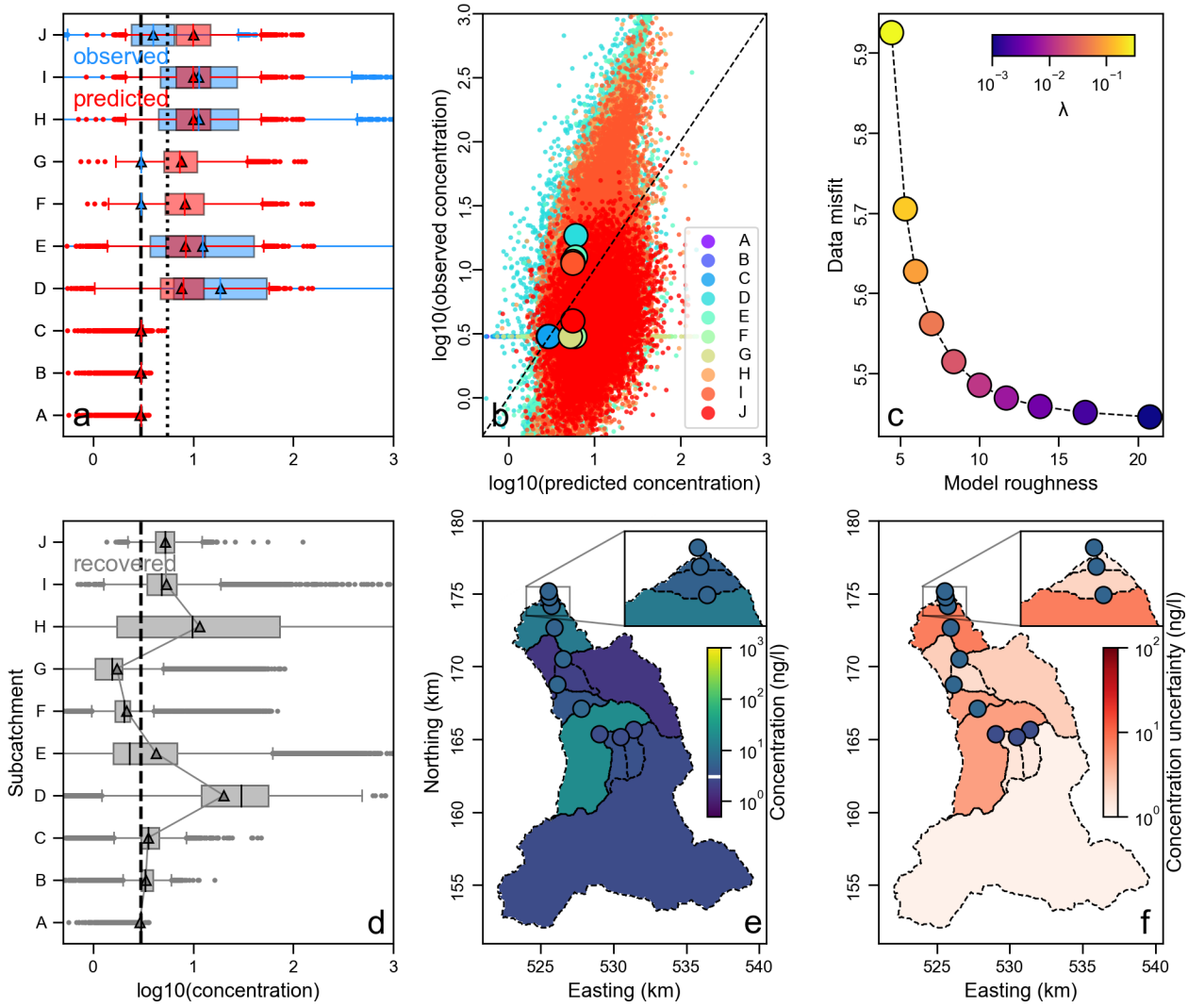

Figure 21: **Objective source apportionment of azithromycin.** See caption of Fig. 20 for extended caption and Fig. 8 for description of data. Optimal $\lambda = 10^{-1.7}$.

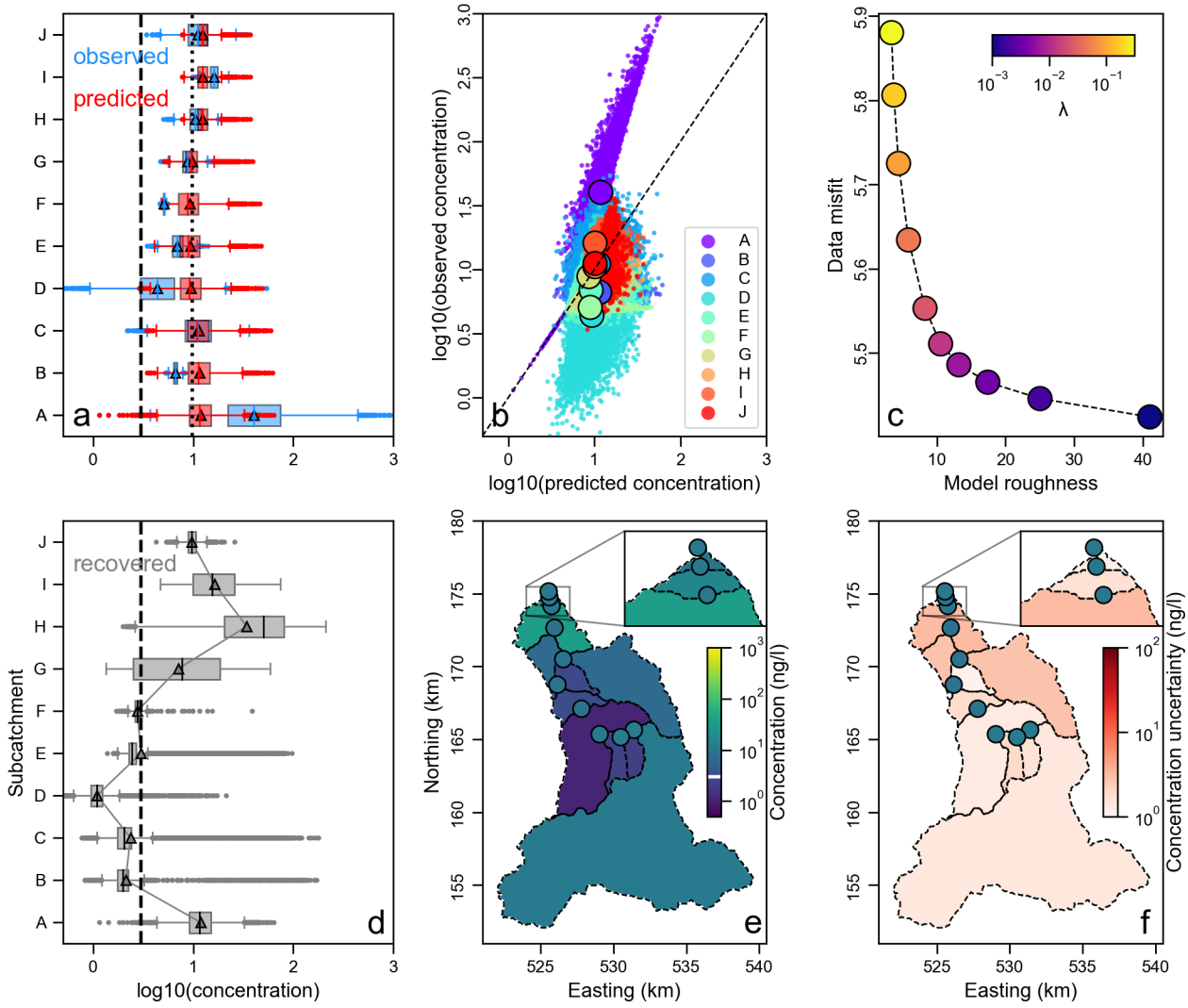

Figure 22: **Objective source apportionment of benzoylecgonine.** See caption of Fig. 20 for extended caption and Fig. 9 for description of data. Optimal $\lambda = 10^{-2.2}$.

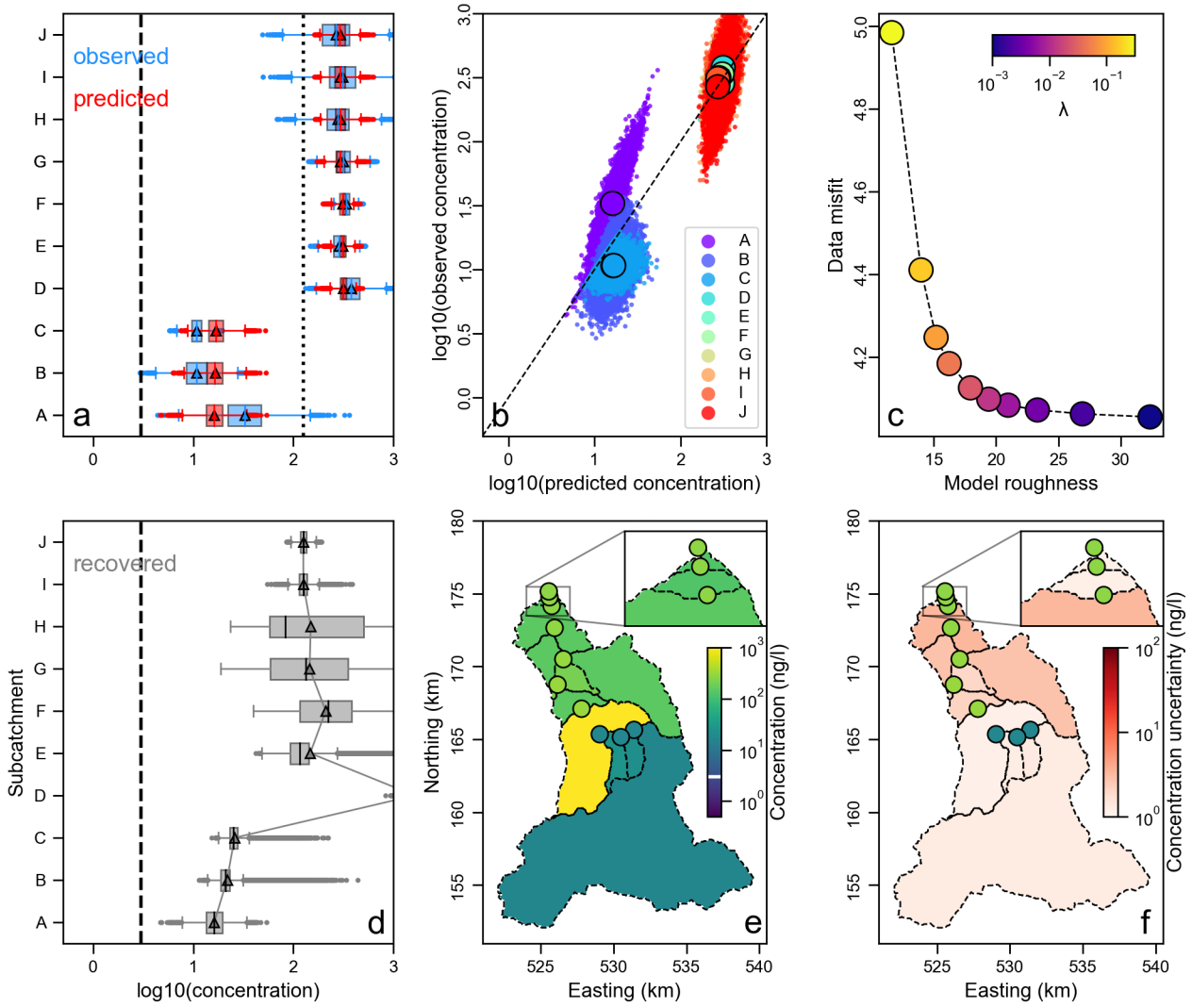

Figure 23: **Objective source apportionment of carbamazepine.** See caption of Fig. 20 for extended caption and Fig. 10 for description of data. Optimal $\lambda = 10^{-1.7}$.

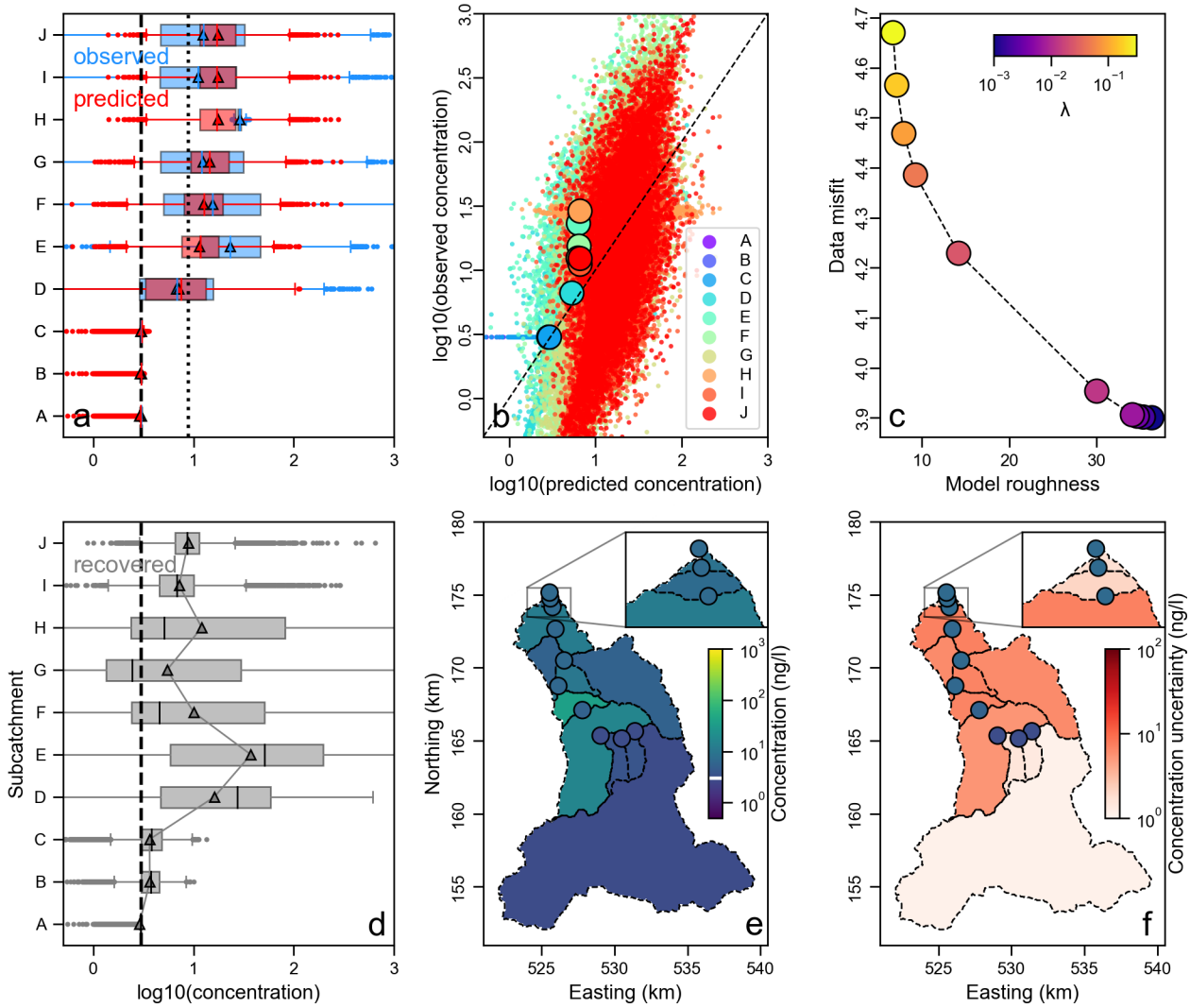

Figure 24: **Objective source apportionment of clarithromycin.** See caption of Fig. 20 for extended caption and Fig. 11 for description of data. Optimal $\lambda = 10^{-1.7}$.

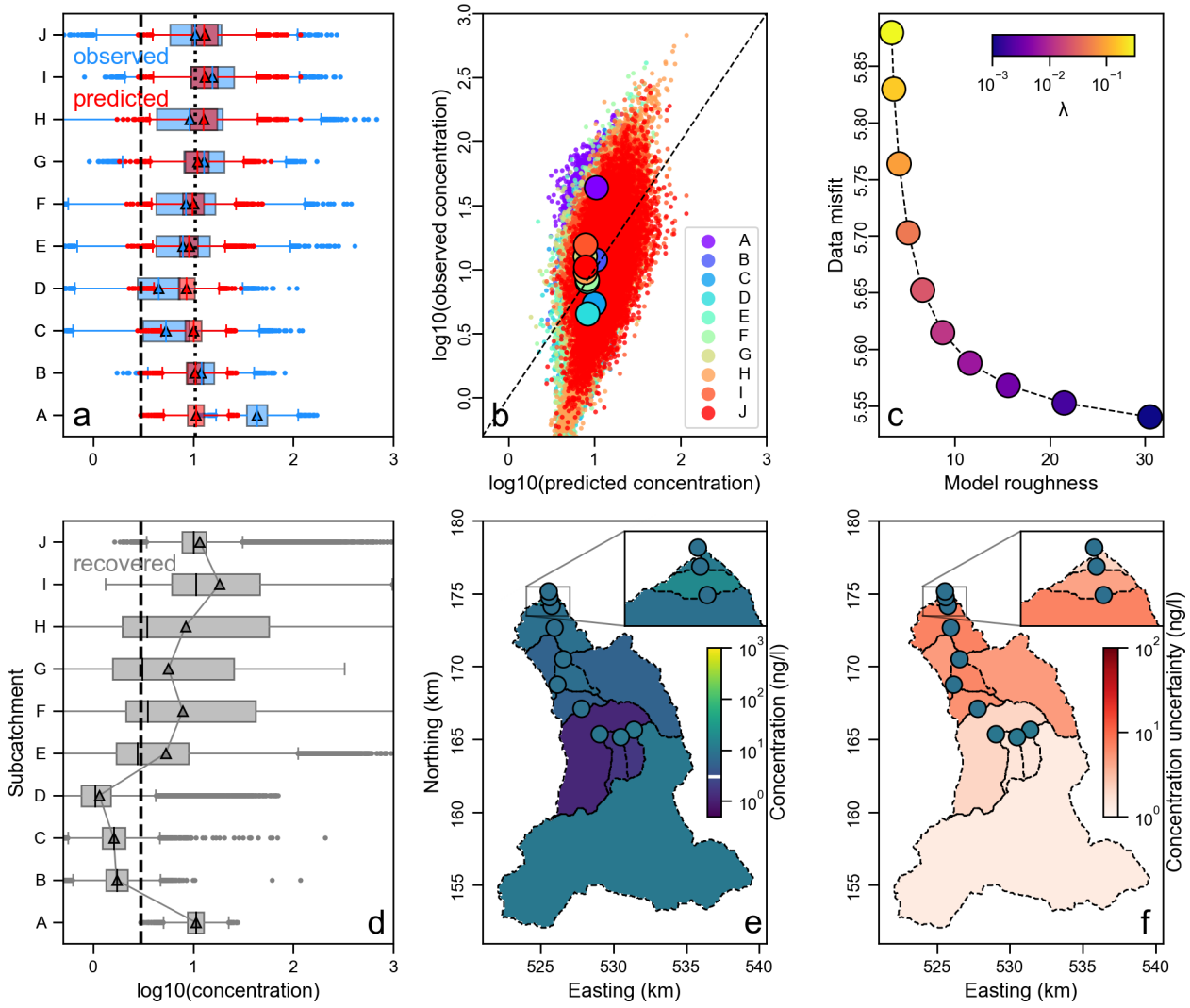

Figure 25: **Objective source apportionment of cocaine.** See caption of Fig. 20 for extended caption and Fig. 12 for description of data. Optimal $\lambda = 10^{-2.2}$.

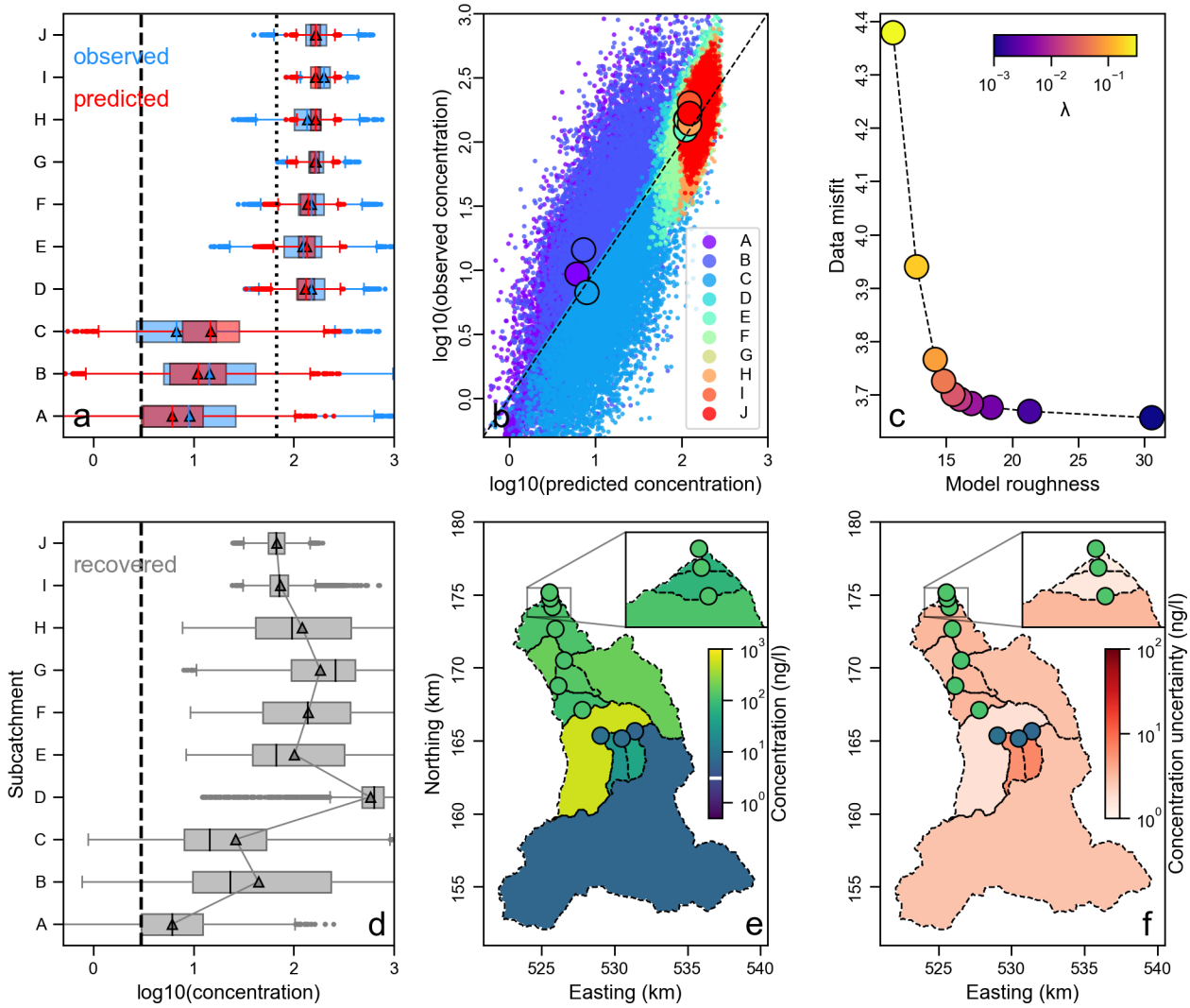

Figure 26: **Objective source apportionment of diclofenac.** See caption of Fig. 20 for extended caption and Fig. 13 for description of data. Optimal $\lambda = 10^{-1.7}$.

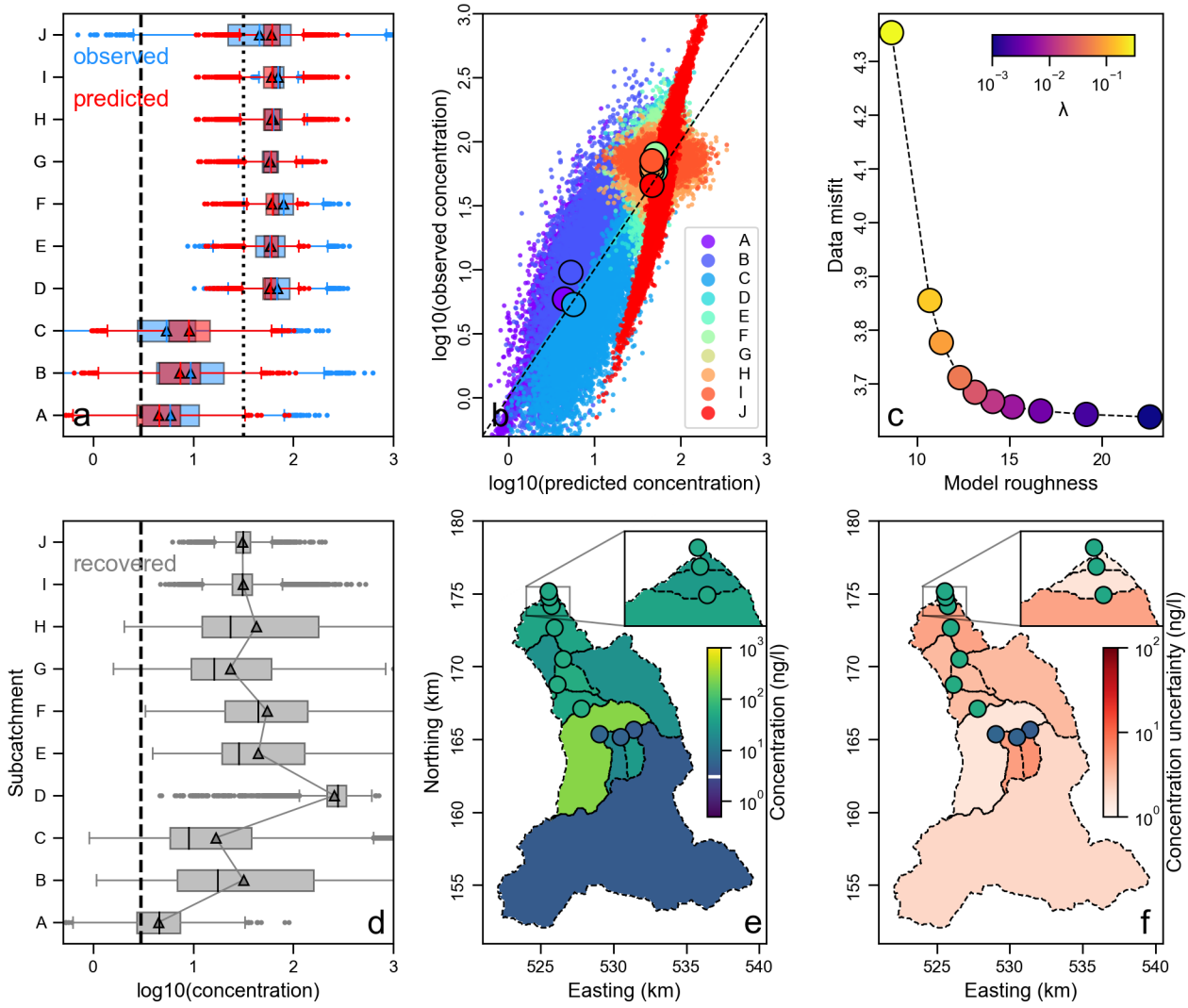

Figure 27: **Objective source apportionment of imidacloprid.** See caption of Fig. 20 for extended caption and Fig. 14 for description of data. Optimal $\lambda = 10^{-1.7}$.

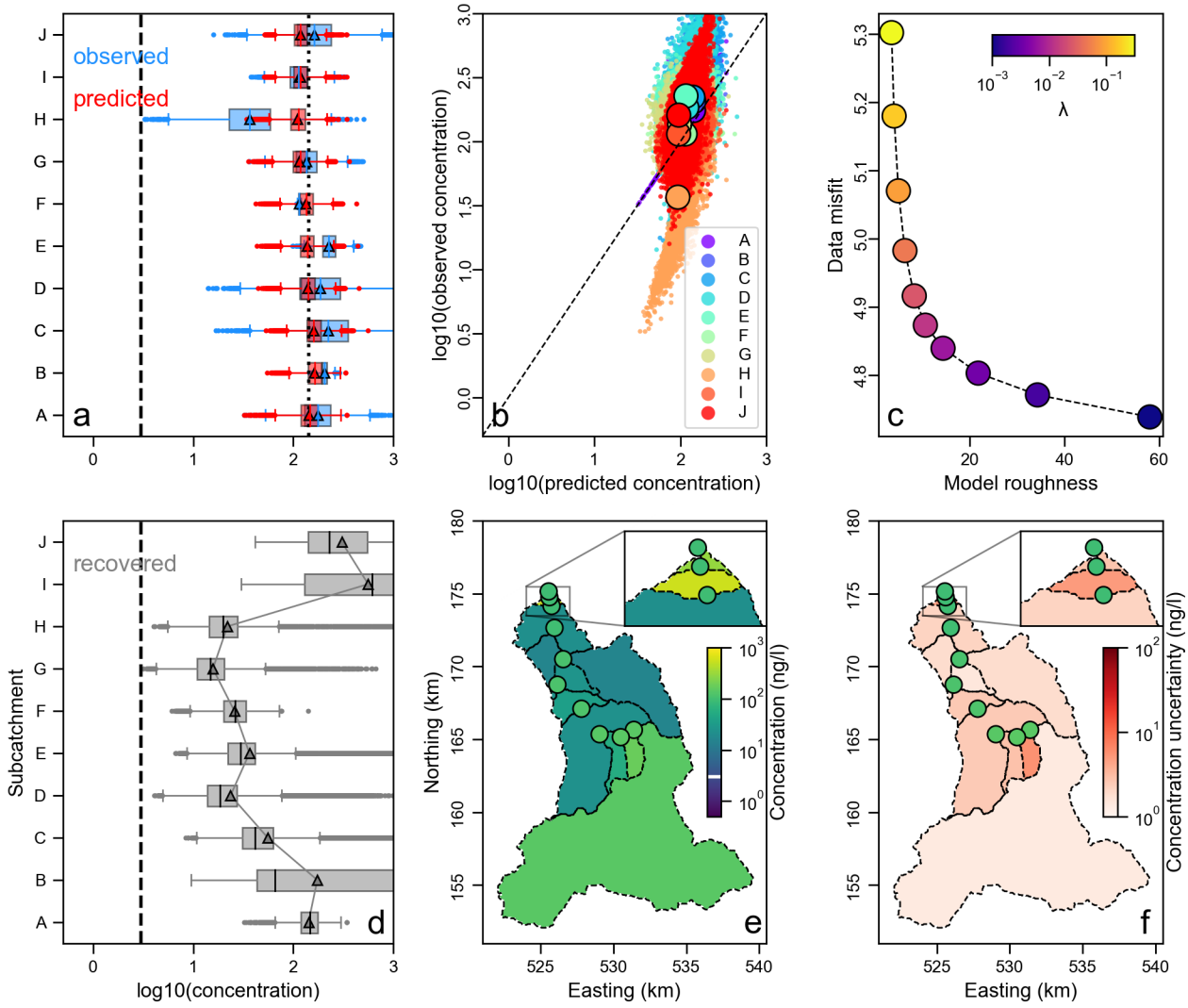

Figure 28: **Objective source apportionment of salicylic acid.** See caption of Fig. 20 for extended caption and Fig. 15 for description of data. Optimal $\lambda = 10^{-2.2}$.

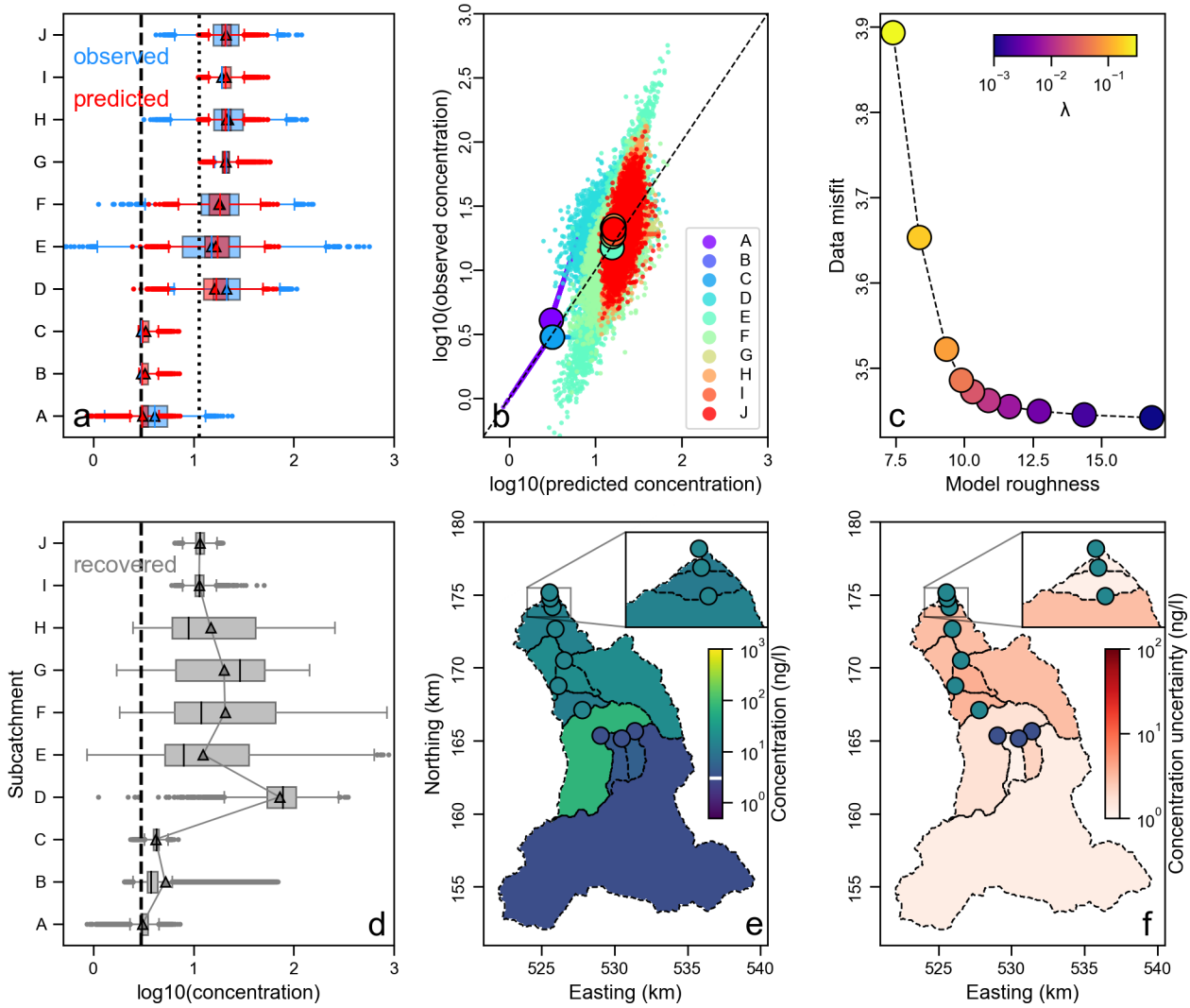

Figure 29: **Objective source apportionment of sulfamethoxazole.** See caption of Fig. 20 for extended caption and Fig. 16 for description of data. Optimal $\lambda = 10^{-1.7}$.

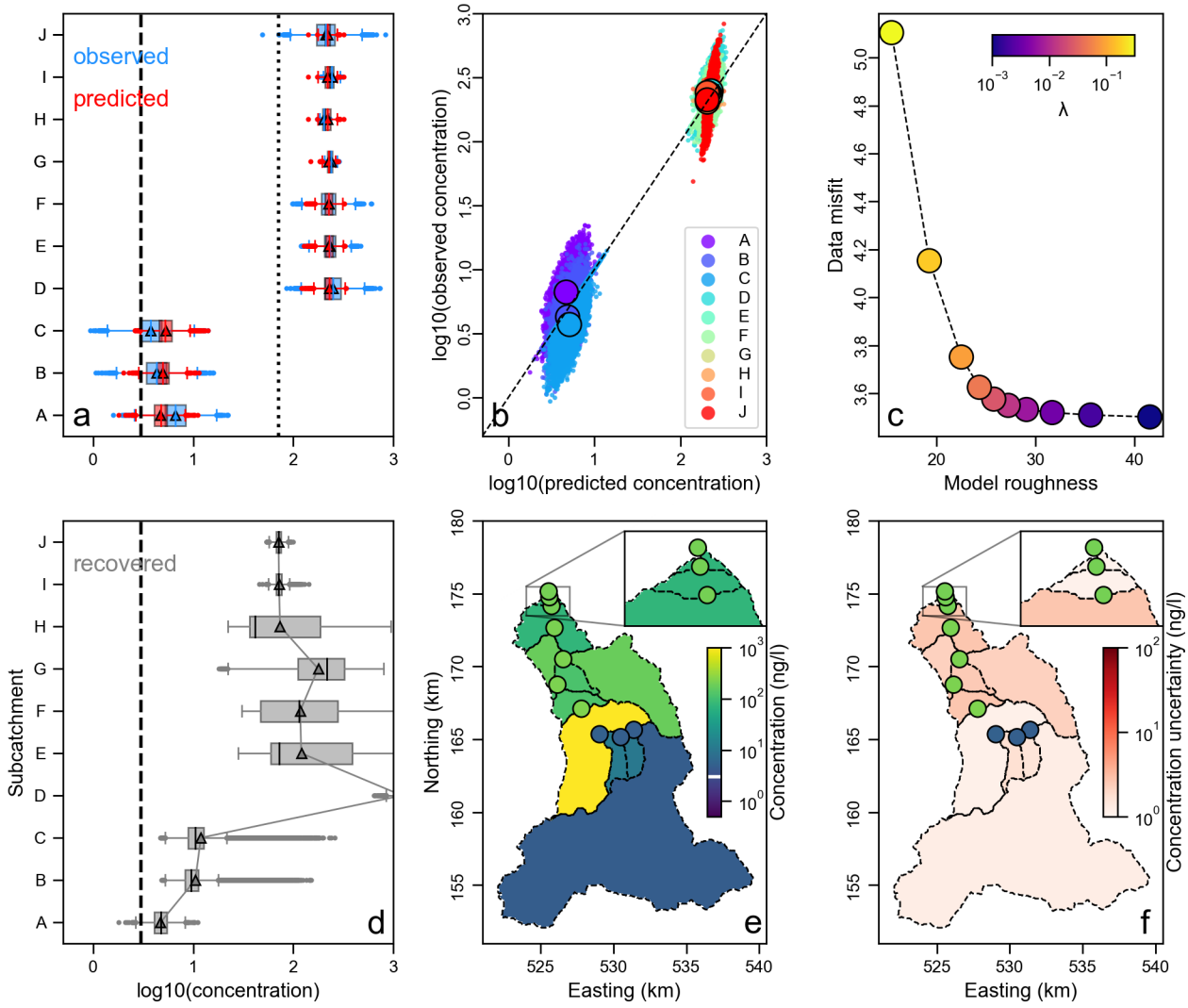

Figure 30: **Objective source apportionment of tramadol.** See caption of Fig. 20 for extended caption and Fig. 17 for description of data. Optimal $\lambda = 10^{-1.7}$.

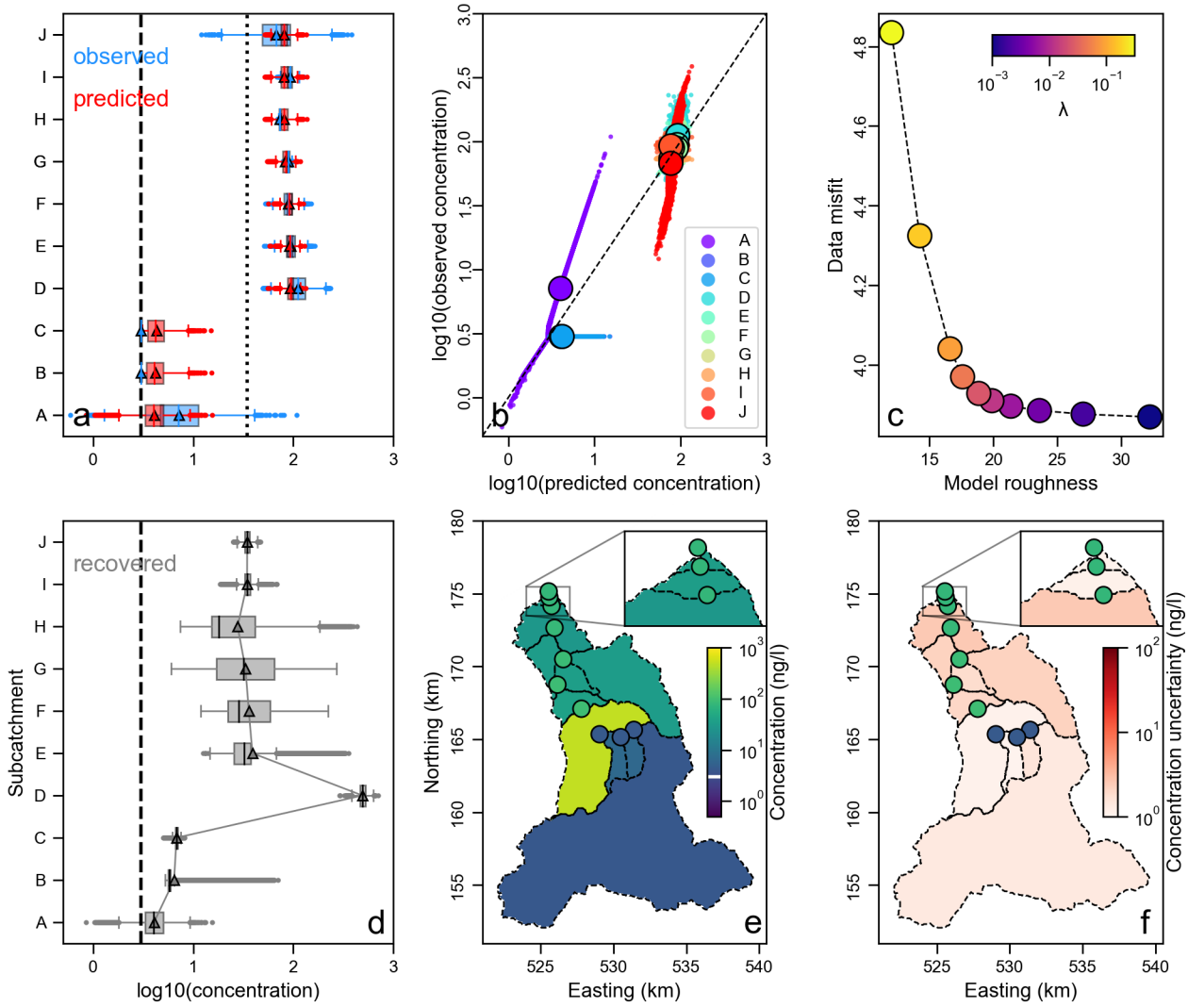

Figure 31: **Objective source apportionment of trimethoprim.** See caption of Fig. 20 for extended caption and Fig. 18 for description of data. Optimal $\lambda = 10^{-1.7}$.

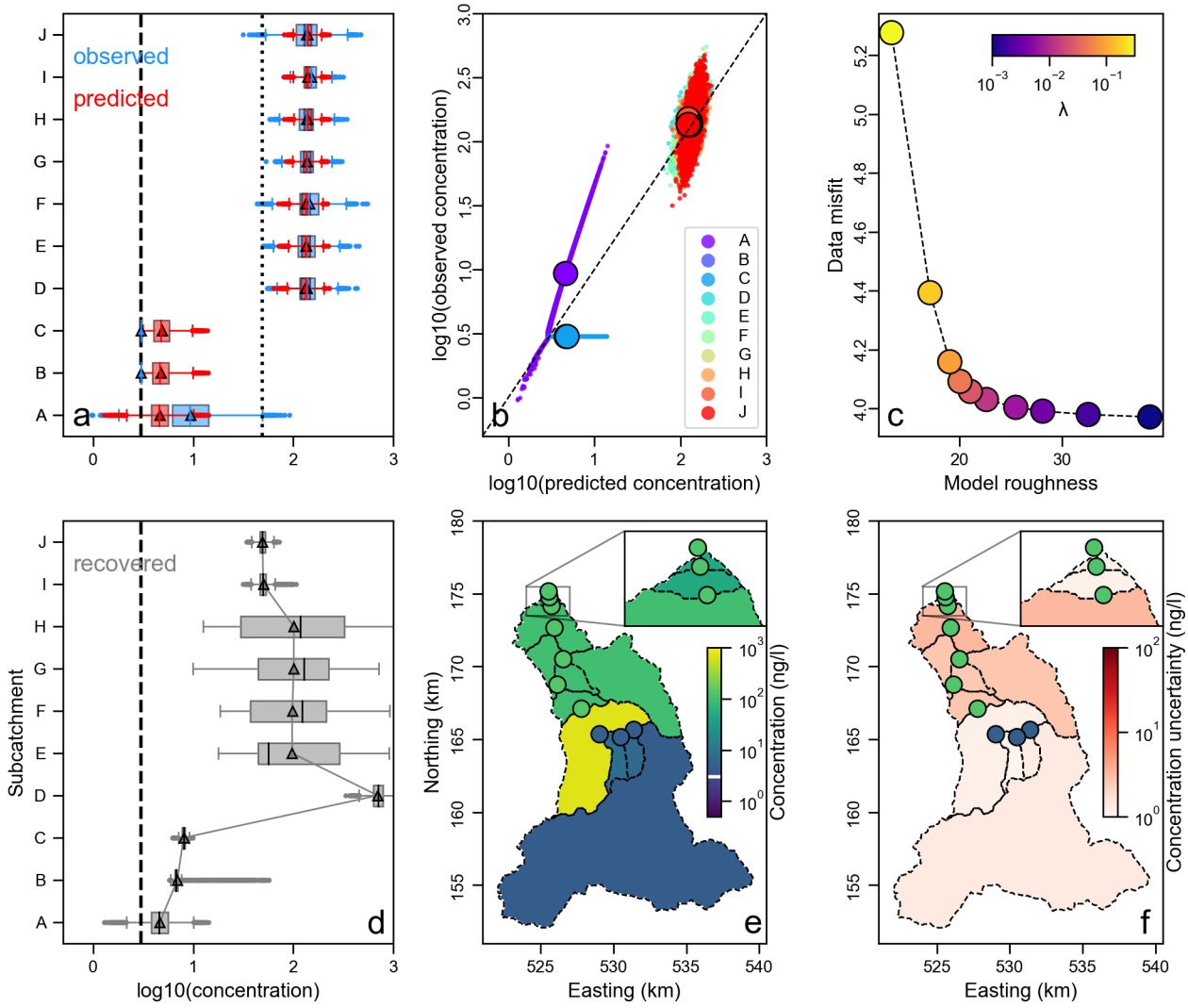

Figure 32: **Objective source apportionment of venlafaxine.** See caption of Fig. 20 for extended caption and Fig. 19 for description of data. Optimal $\lambda = 10^{-1.7}$.

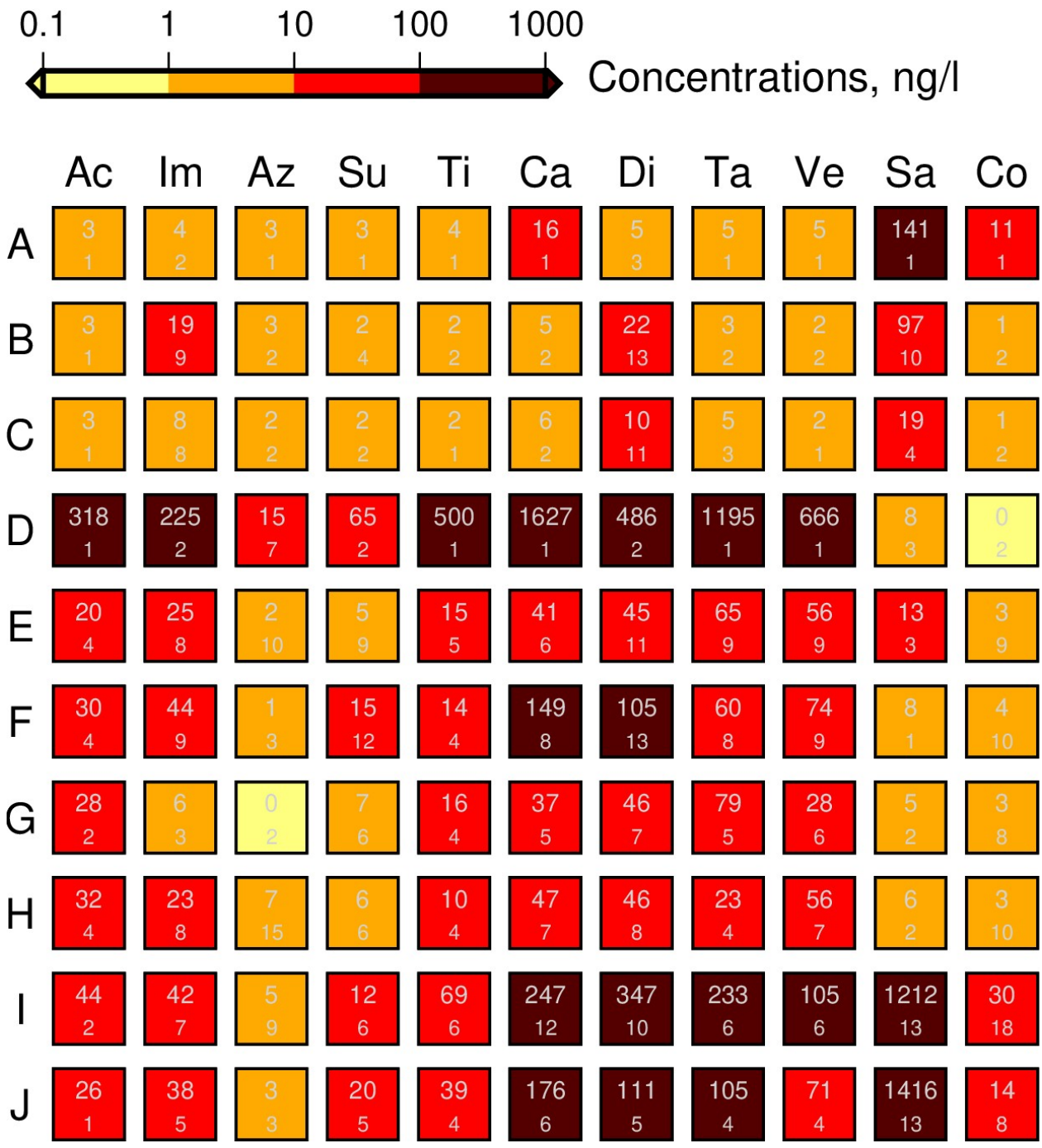

Figure 33: **Summary of source apportionment of contaminants to subcatchments A–J.** Calculated mean concentrations and standard deviations (ng/l) from Monte Carlo inversion (Fig. 20–32); abbreviations—Ac: acetamiprid (24), Im: imidacloprid (13), Az: azithromycin (19), Cl: clarithromycin (-), Su: sulfamethoxazole (600), Ti: trimethoprim (120,000), Ca: carbamazepine (2000), Di: diclofenac (50), Ta: tramadol (8653), Ve: venlafaxine (880), Sa: salicylic acid (18,000), Be: benzoylecgonine (-), Co: cocaine (2456); numbers in parentheses indicate *predicted no-effect concentration* (PNEC; ng/L; NORMAN database; see Discussion in main manuscript). We note that for very low concentrations calculated standard deviations can imply negative concentrations, which is obviously meaningless, they are included here for completeness. See Fig. 4 in main manuscript for associated risk quotients.

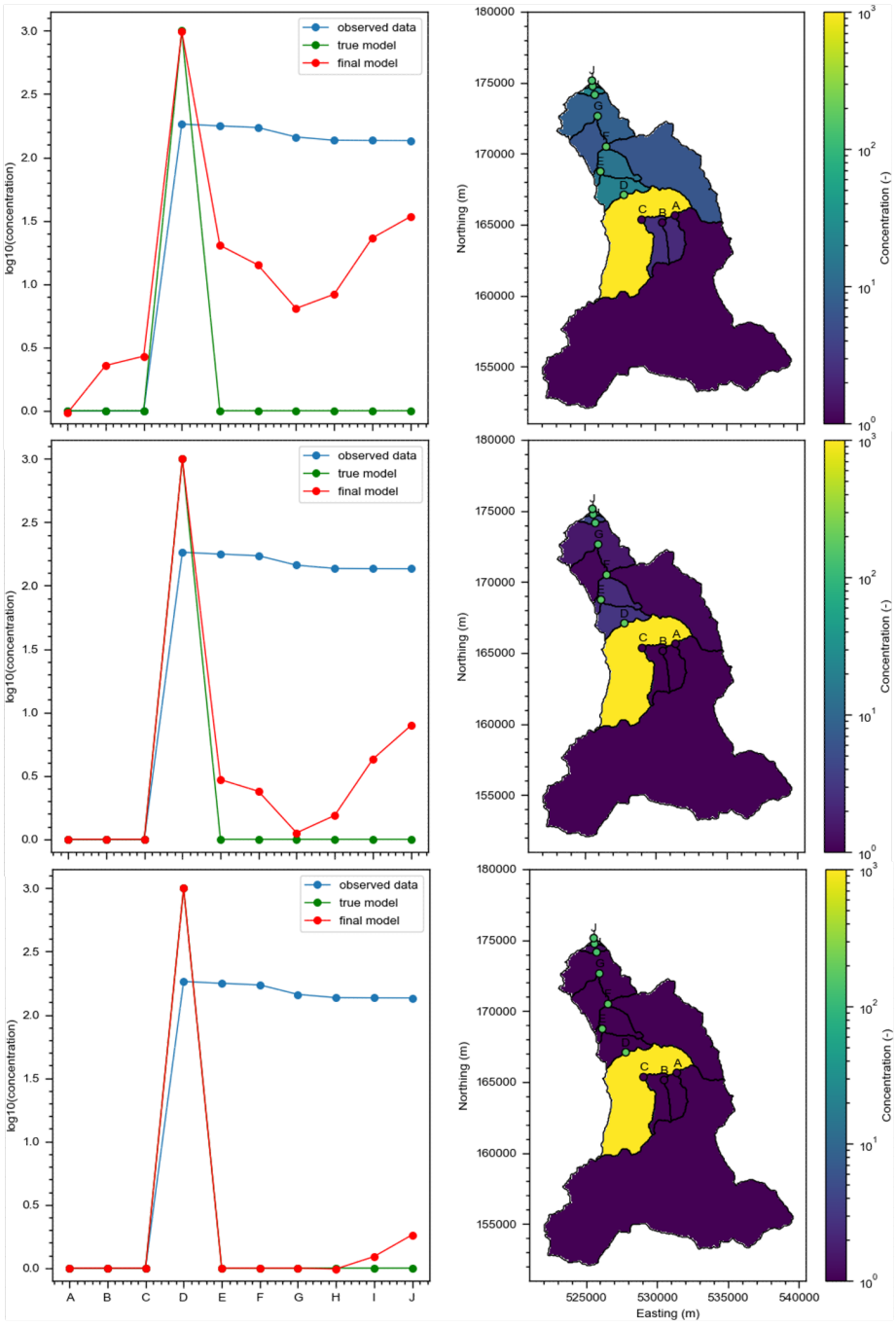

Figure 34: **Assessing impact of regularisation on apportionment using synthetic data.** Value of λ (regularisation 'strength'; see main manuscript) decreases from top to bottom: 10^{-2}, 10^{-4}, 10^{-6}. Green line with points = known source concentrations in subcatchments, blue line = concentrations at localities A–J calculated by forward modelling known subcatchment concentrations, red line = concentrations in source areas calculated by inverting only the concentrations at localities A–J. Note that decreasing λ generates results that more closely match 'observed' known source concentrations; calculated peak source concentration is insensitive to regularisation.

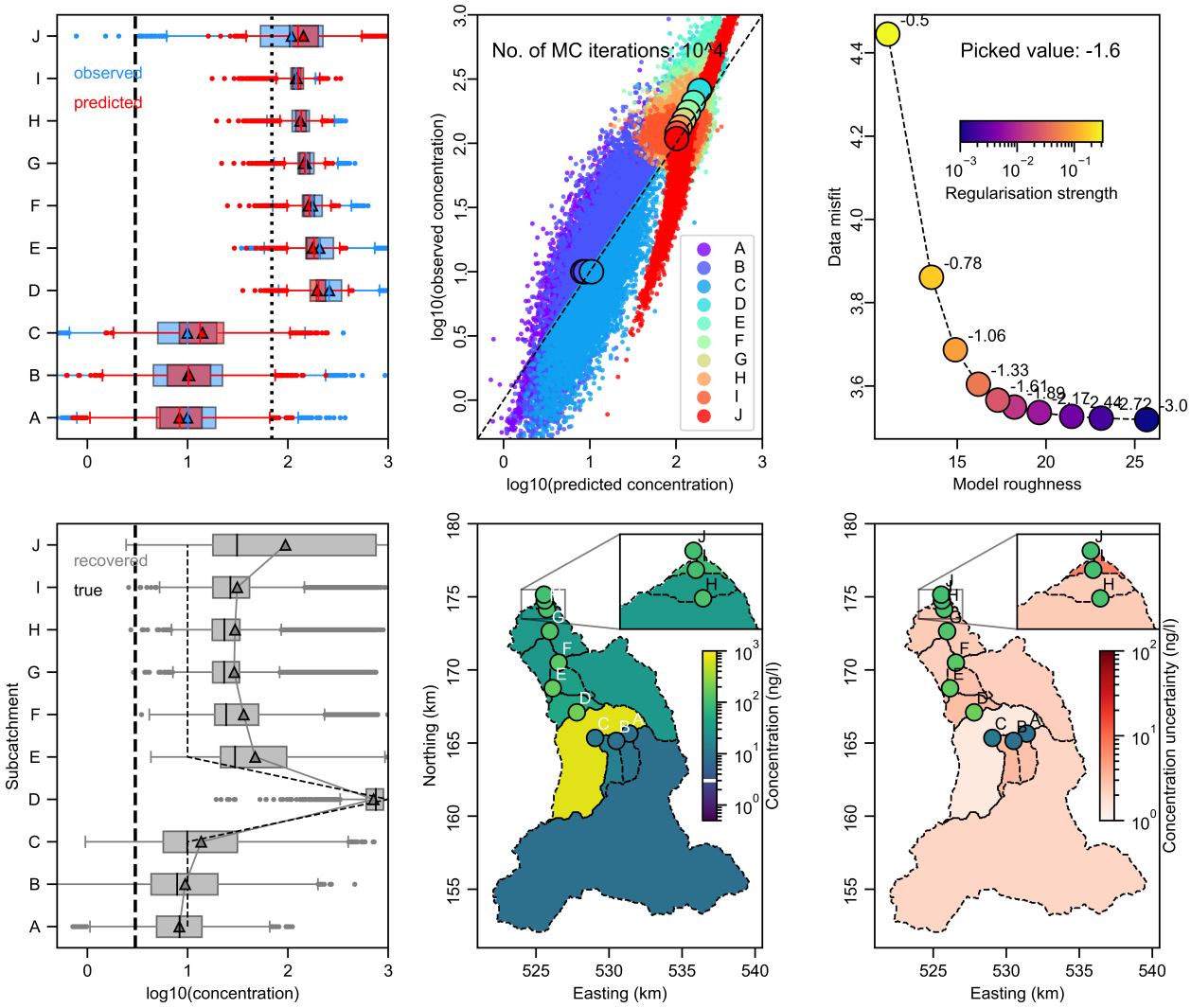

Figure 35: **Monte Carlo experimentation to test impact of noisy data on source apportionment using synthetic data.** 10^4 noisy data sets (blue symbols in panel a; 'observations') were inverted, each with different random noise added to mean concentrations at localities A–J prior to each inversion. Noise was added commensurate with range of values at each locality determined by imidacloprid field data (see grey bars in panel a; and also Fig. S14). Best-fitting predicted concentrations at sample sites from all inverse models are indicated by the red symbols in panel a. (b) Comparison of 'observed' and best-fitting predicted concentrations at localities A–J from the 10^4 inverse models. (c) Identification of optimal regularisation parameter, λ (see Section 2.5 of main manuscript). (d) True (dashed line) and recovered (connected grey triangles) source apportionment from inverse modelling of the 10^4 noisy data sets. (e–f) Mean and standard deviation of calculated source apportionment from the 10^4 inverse models. See caption of Fig. 20 for detailed description of panels.

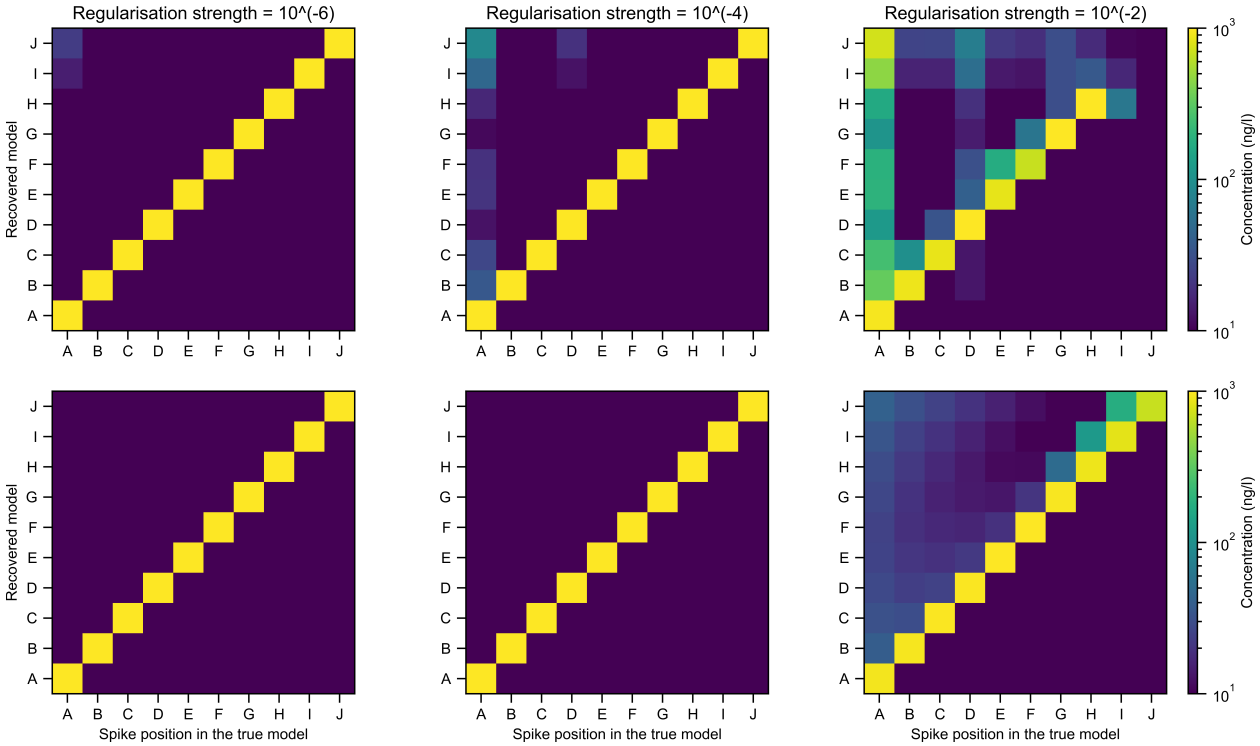

Figure 36: **Resolution matrix for noise-free data.** Top panels—subcatchment areas and export rates that are the same as for inversion of field data. Bottom—fluxes normalised by setting export rates to reciprocal of subcatchment areas.

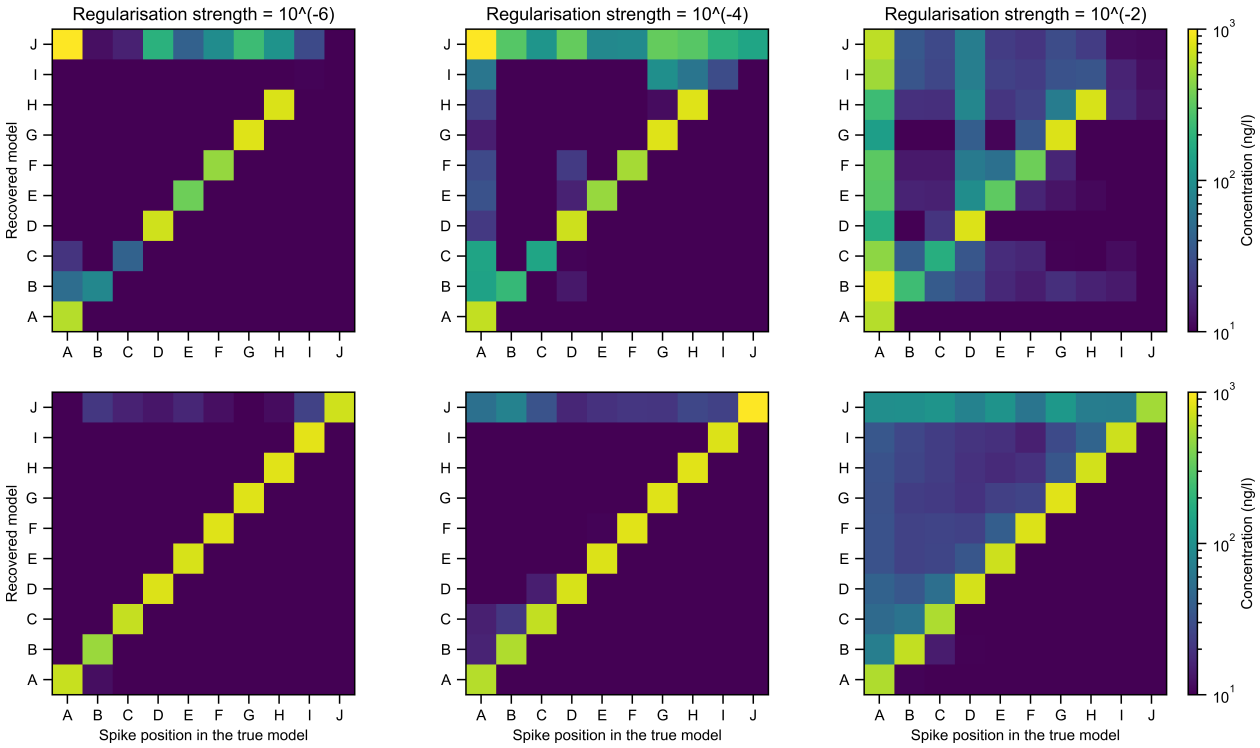

Figure 37: **Resolution matrix for noisy data.** Results were obtained from Monte Carlo inversion. See Fig. 36 for extended caption.

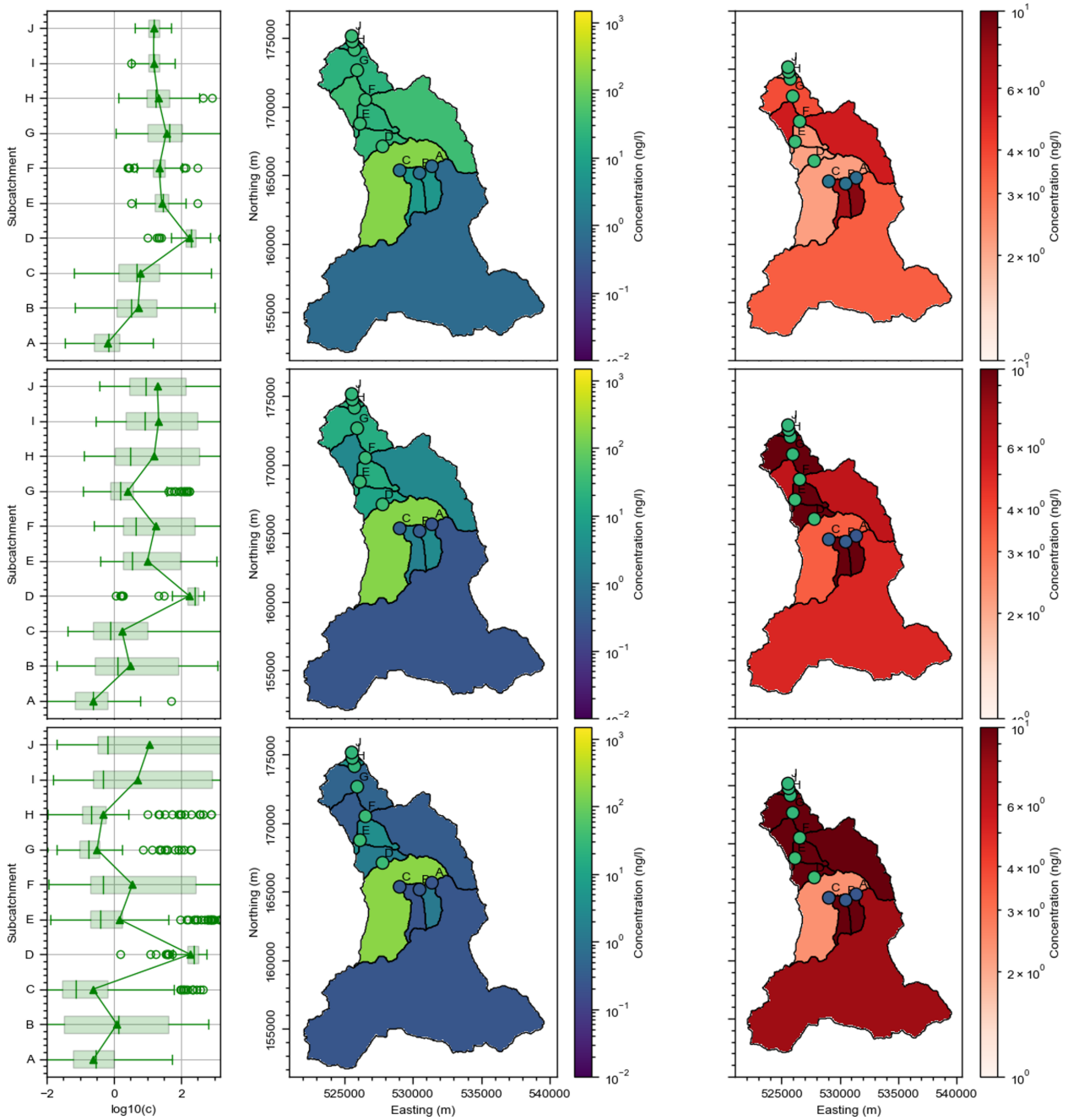

Figure 38: **Testing impact of regularisation on imidacloprid source apportionment.** Regularisation 'strength' λ decreases from top to bottom rows: $10^{-0.8}$, $10^{-2.8}$ (closest to optimal; see Fig. 27) and $10^{-4.8}$. Note that peak concentration (in subcatchment between localities C and D) is relatively insensitive to regularisation. See caption for Fig. 20 for detailed description of panels.

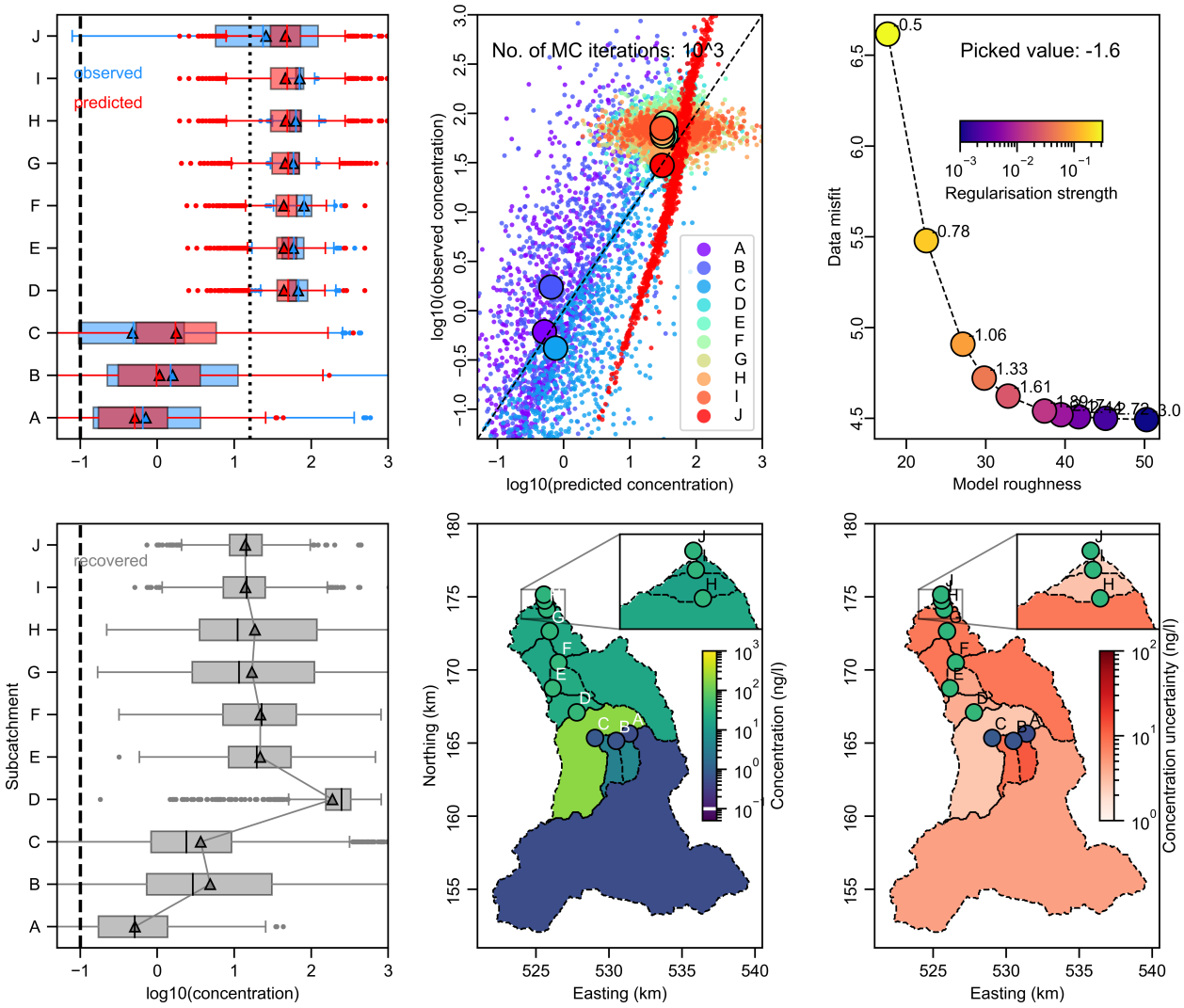

Figure 39: **Sensitivity of inverse model to assumed detection limit (LLOD).** Inversion of field data for imidacloprid source apportionment using LLOD = 0.1 ng/l. See caption of Fig. 20 for extended caption.

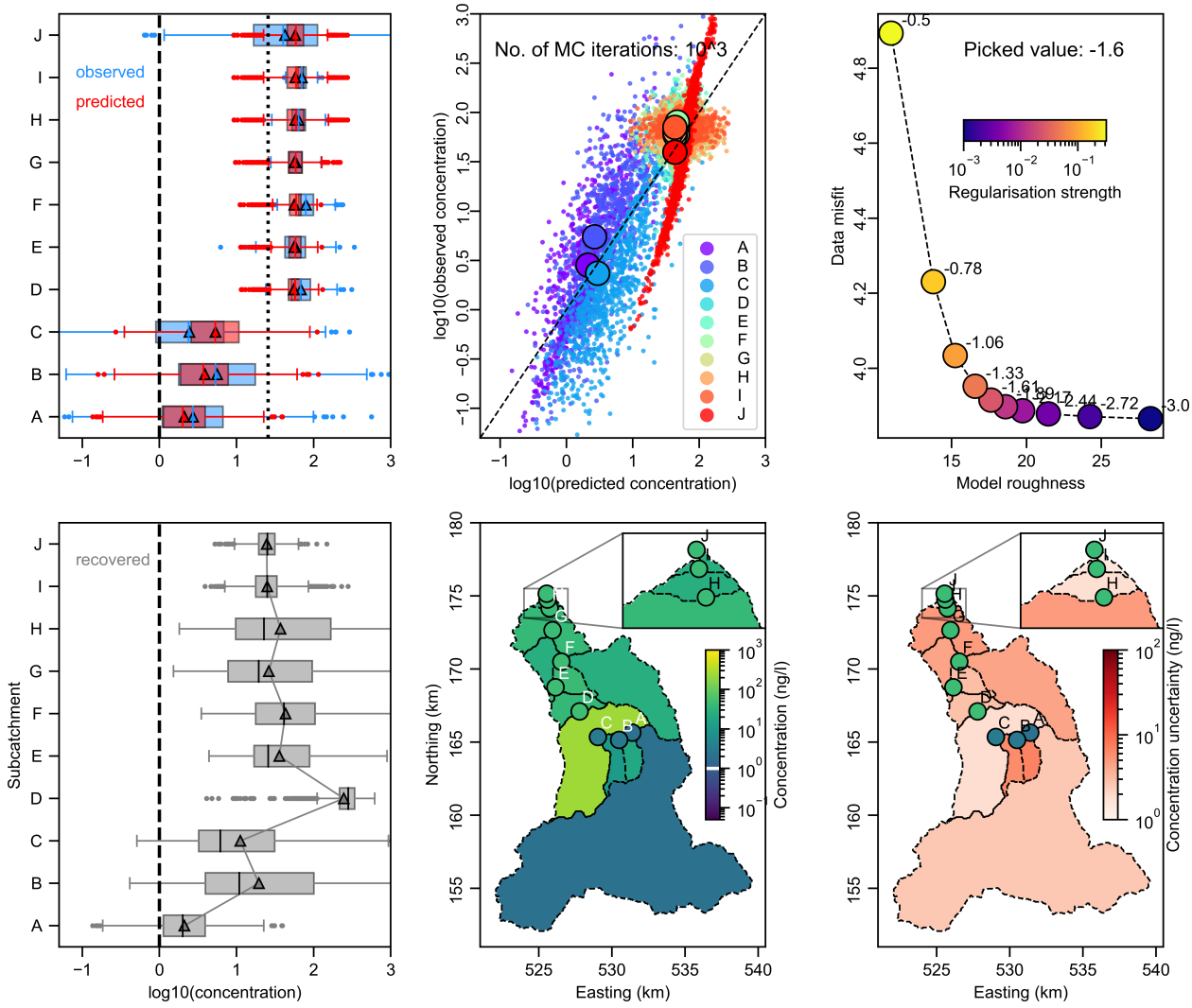

Figure 40: **Same as Fig. 39 but for LLOD = 1 ng/l.**

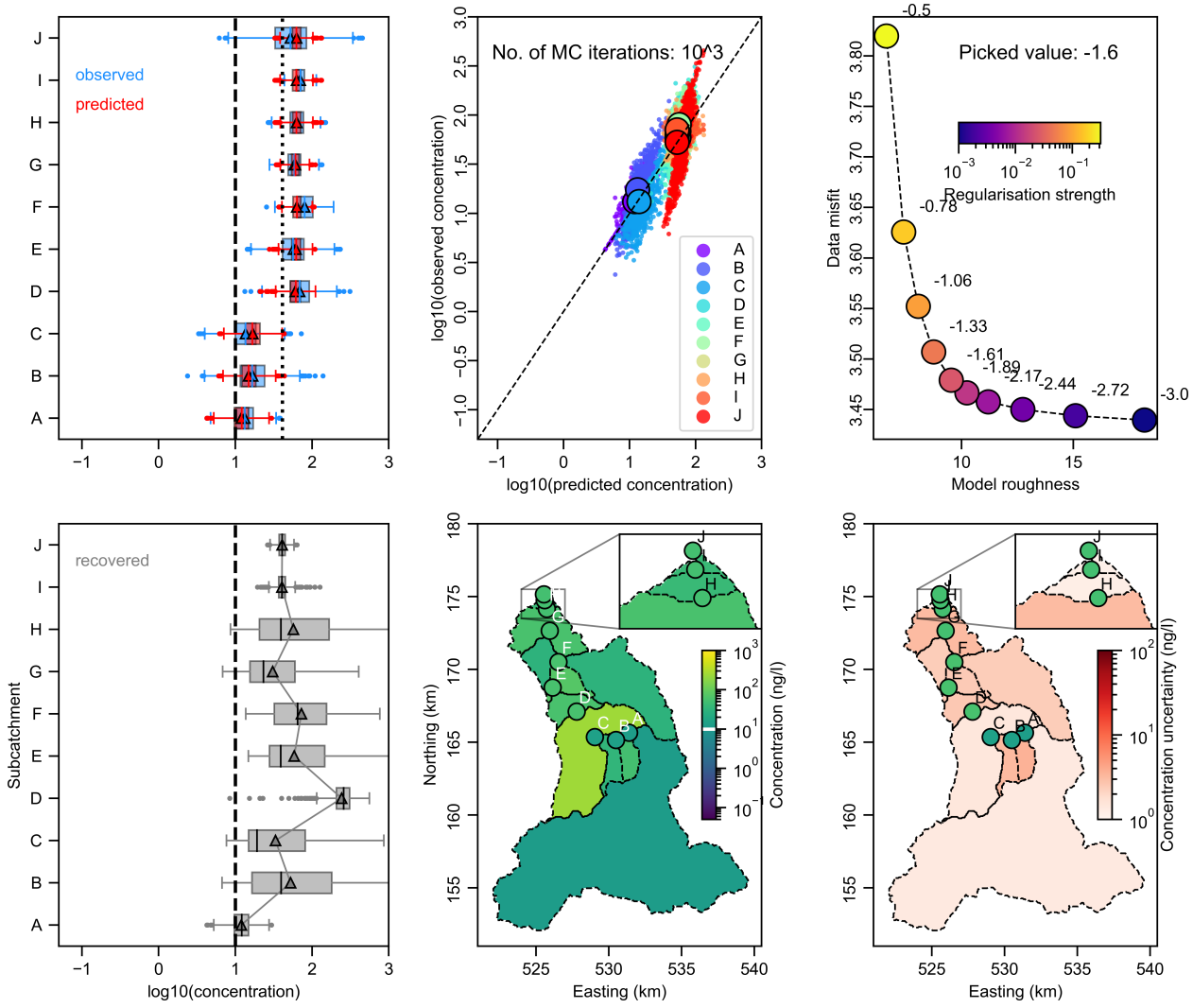

Figure 41: **Same as Fig. 39 but for LLOD = 10 ng/l.**

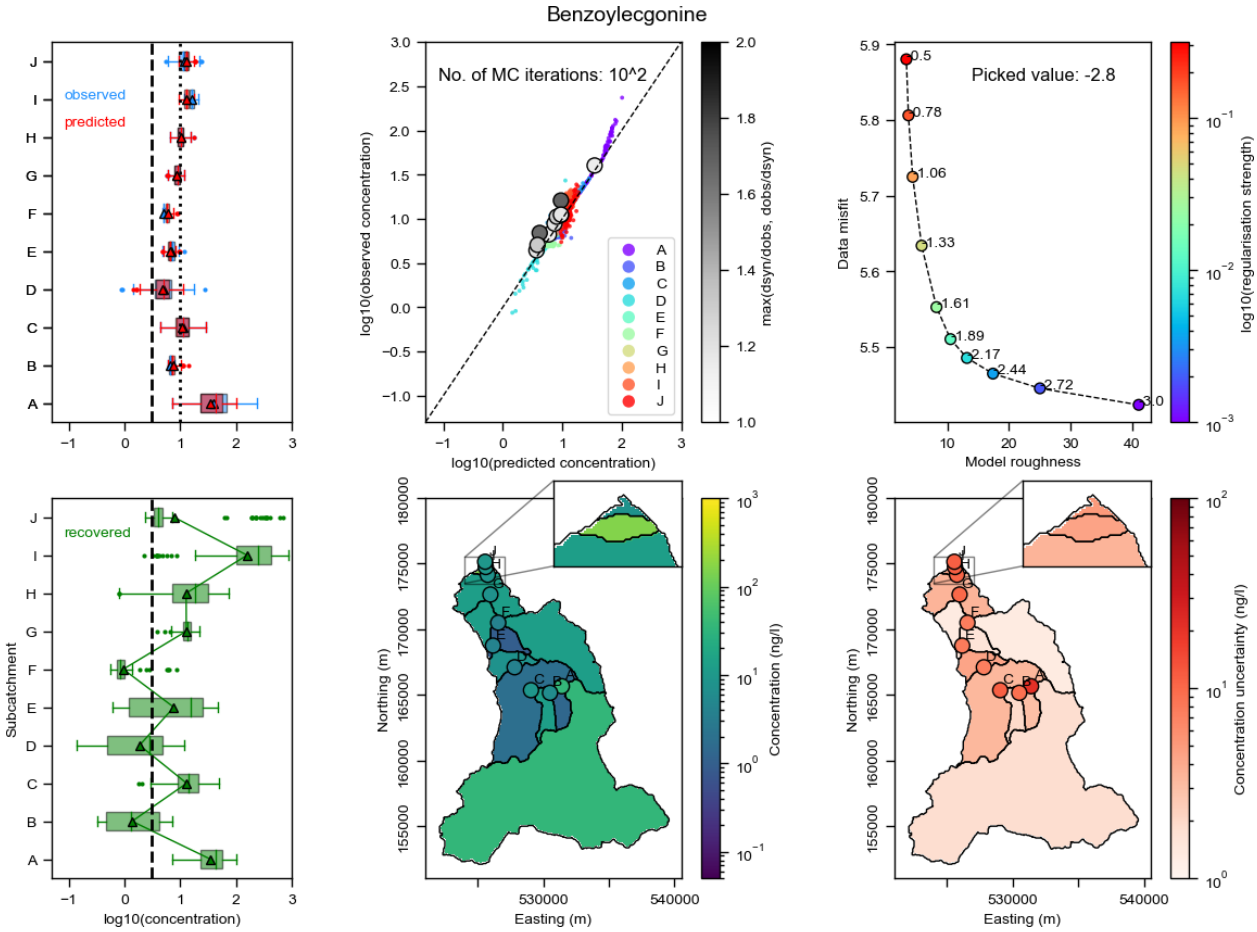

Figure 42: **Testing impact of reducing export rate**. Results from inverting measured benzoylecgonine concentrations assuming export rate in subcatchment A is 100× smaller than the one derived from topography, which was used to produce results shown in Fig. 3c–d of the main manuscript. Note lower residual misfit, and agreement with recovered model shown in Fig. 3d of the main manuscript.